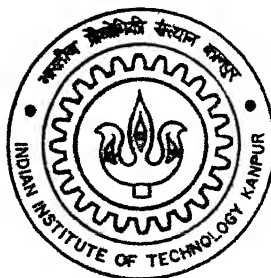


# **EFFECT OF TRANSITION METAL ACTIVATOR ADDITION AND COATING ON THE SINTERING OF W-Cu ALLOYS**

**By**

**Chiradeep Ghosh**

TH  
MME/2003/M  
63432.



**DEPARTMENT OF MATERIALS AND METALLURGICAL ENGINEERING**

**Indian Institute of Technology Kanpur**

**FEBRUARY, 2003**

# **EFFECT OF TRANSITION METAL ACTIVATOR ADDITION AND COATING ON THE SINTERING OF W-Cu ALLOYS**

*A Thesis Submitted*

In Partial Fulfillment of the Requirements

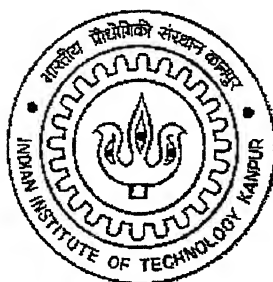
For the degree of

**Master of Technology**

by

**Chiradeep Ghosh**

**(Roll No. Y110603)**



to the

**DEPARTMENT OF MATERIALS AND METALLURGICAL ENGINEERING**

**INDIAN INSTITUTE OF TECHNOLOGY KANPUR**

**FEBRUARY 2003**

3 JUN 2002

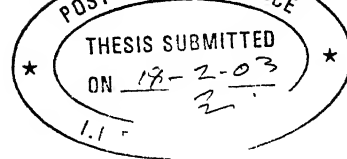
मानव काशीनाथ केरकर पुस्तकालय

विश्वविद्यालयी पुस्तकालय

प्राप्ति क्र० ▲ 123513

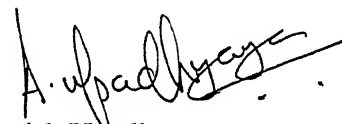


A143513



## CERTIFICATE

It is certified that the work contained in the thesis entitled “**EFFECT OF TRANSITION METAL ACTIVATOR ADDITION AND COATING ON THE SINTERING OF W-Cu ALLOYS**” by **Chiradeep Ghosh (Roll No. Y110603)**, has been carried out under my supervision and to the best of my knowledge this work has not been submitted elsewhere for a degree.

  
Dr. Anish Upadhyaya  
Assistant Professor  
Department of Materials and  
Metallurgical Engineering  
Indian Institute of Technology,  
Kanpur.  
February, 2003.



## ABSTRACT

In the field of thermal management application tungsten copper composite is a potential candidate material. This is due to the fact that tungsten has low coefficient of thermal expansion and copper has high thermal conductivity, which are necessary requirements for such applications. The present study investigates the various sintering aspect of tungsten-copper alloys sintered at temperatures ranging from 1000 to 1400°C. The effect of addition of various transition elements such as Ni, Co and Fe as an activator has also been studied. The tungsten-copper alloys containing 10, 25 and 40 weight percent copper were prepared by two different routes, namely mechanical mixing and chemical coating procedure. Due to the lack of solubility of tungsten in copper, it is very hard to achieve full density even by liquid phase sintering in alloys of starting W powder size greater than 4  $\mu\text{m}$ . The role of transition elements in enhancing the densification during sintering has been critically studied *vis a vis* the solubility effects. Post-sintering characterizations for both macro and microstructures were done. SEM and optical micrographs were taken to characterize the microstructure of the sintered compacts. Mechanical properties of the compacts were also studied, which includes hardness testing. In addition the electrical conductivity of the sintered samples was measured. Characterization of the properties revealed that the coated samples are superior than the uncoated samples.

## Table of Contents

	<b>Page no.</b>
List of Figures	v
List of Tables	ix
Acknowledgements	x
 <b>Chapter 1 INTRODUCTION</b>	 <b>1</b>
 <b>Chapter 2. BACKGROUND</b>	
2.1 Thermal Management System	3
2.2 P/M Processing of W-Cu Alloys	
2.2.1 An Historical Overview	8
2.2.2 Infiltration of Liquid Cu in Sintered Tungsten	8
2.2.3 Powder Injection Molding of W-Cu Composites	8
2.2.4 Solid State Sintering of W-Cu Composites	11
2.2.5 Pressure Assisted Sintering of W-Cu Composites	12
2.2.6 Activated Sintering of W-Cu Composites	13
2.2.7 Liquid Phase Sintering of W-Cu Composites	16
2.2.8 Sintering Atmosphere	24
 <b>Chapter 3. SCOPE OF THE PRESENT STUDY</b>	
3.1 System Selection	27
3.2 Coating the W powder with Cu powder	28
3.3 Addition of Transition Elements	28
 <b>Chapter 4. EXPERIMENTAL PROCEDURE</b>	
4.1 Raw material	
4.1.1 Elemental Tungsten Powder	32
4.1.2 Elemental Copper Powder	32
4.1.3 Copper coated Tungsten powder	32

4.2	Powder Characterization	
4.2.1	Particle Size and Size Distribution	33
4.2.2	Particle Morphology	36
4.3	Composition Preparation	39
4.4	Compaction	40
4.5	Sintering	40
4.6	Densification behavior	
4.6.1	Density and Densification Parameter	44
4.6.2	Linear and Radial Shrinkage	44
4.7	Microstructural Studies	
4.7.1	Optical Microscopy	45
4.7.2	Scanning Electron Microscopy	45
4.8	Electrical Properties	45
4.9	Vickers macro-hardness	46

## **Chapter 5. EXPERIMENTAL RESULTS**

5.1	Densification Behavior	47
5.2	Axial and Radial Shrinkage	51
5.3	Optical Microscopy	51
5.4	SEM Micrographs	64
5.5	Hardness	72
5.6	Compressive Test	72
5.7	Electrical Conductivity	77
5.8	Thermal Conductivity	77

## **Chapter 6. DISCUSSION**

6.1	Densification Behavior	82
6.2	Variation in Radial and Axial Shrinkage	92
6.3	Microstructural Evolution	93
6.4	Variation in Hardness	95
6.5	Variation in Compressive Strength	95

6.6	Variation in Electrical Conductivity and Thermal Conductivity	96
<b>Chapter 7.</b>	<b>CONCLUSIONS</b>	<b>100</b>
	REFERENCES	102
Appendix I:	Experimental data for the green samples	111
Appendix II:	Experimental data for the sintered samples	117
Appendix III.	Axial and radial dimensions of the samples	123
Appendix IV:	Hardness values of the samples, HV <sub>5</sub>	129
Appendix V:	Electrical conductivity of the sintered samples	131
Appendix VI:	Thermal conductivity of the sintered samples	133

## List of Figures

	Page no.
<b>Figure 2.1:</b> Processing steps involved in Powder injection molding [28]	10
<b>Figure 2.2:</b> Idealized binary phase diagram for solid-state activated sintering [25]	18
<b>Figure 2.3:</b> W-Cu equilibrium phase diagram [33]	19
<b>Figure 2.4:</b> Different stages of liquid phase sintering [28]	23
<b>Figure 2.5:</b> Effect of sintering atmosphere on swelling of pure Cu compacts [20]	26
<b>Figure 3.1:</b> Cobalt-Copper Equilibrium Diagram [21]	29
<b>Figure 3.2:</b> Iron-Copper Equilibrium Diagram [21]	29
<b>Figure 3.3:</b> Copper-Nickel Equilibrium Diagram [21]	30
<b>Figure 3.4:</b> Cobalt-Tungsten Equilibrium Diagram [21]	30
<b>Figure 3.5:</b> Iron-Tungsten Equilibrium Diagram [21]	31
<b>Figure 3.6:</b> Nickel-Tungsten Equilibrium Diagram [21]	31
<b>Figure 4.1:</b> SEM micrograph of W powder in as-received condition	34
<b>Figure 4.2:</b> SEM micrograph of Cu powder in as-received condition	34
<b>Figure 4.3:</b> SEM micrograph of W powder coated with Cu (a) W-10Cu; (b) W-25Cu; (c) W-40Cu	35
<b>Figure 4.4:</b> Particle size distribution for coated (a) W-100Cu, (b) W-25Cu, (c) W-40Cu powders	38
<b>Figure 4.5:</b> Sintering cycle when the selected temperature is (a) 1200°C, and (b) 1400°C	43
<b>Figure 5.1:</b> Effect of Cu content and sintering temperature on the density of W-Cu alloys without activator	49
<b>Figure 5.2:</b> Effect of Cu content and sintering temperature on the density of W-Cu alloys (a) with Ni addition; (b) with Co addition; and (c) with Fe addition	50
<b>Figure 5.3:</b> Axial versus. Radial shrinkage of (a) W-10Cu; (b) W-25Cu; and (c) W-40Cu samples in coated and uncoated conditions	53

- Figure 5.4:** Optical micrographs of coated W-10Cu without any activator, sintered at 1000°C (a) 100×; (b) 500× magnification 54
- Figure 5.5:** Optical micrographs of uncoated W-10Cu without any activator, sintered at 1000°C (a) 100×; (b) 500× magnification 54
- Figure 5.6:** Optical micrographs of coated W-10Cu without any activator, sintered at 1400°C (a) 100×; (b) 500× magnification 55
- Figure 5.7:** Optical micrographs of uncoated W-10Cu without any activator, sintered at 1400°C (a) 100×; (b) 500× magnification 55
- Figure 5.8:** Optical micrographs of coated W-10Cu with Ni activator, sintered at 1400°C (a) 100×; (b) 500× magnification 56
- Figure 5.9:** Optical micrographs of uncoated W-10Cu with Ni activator, sintered at 1400°C (a) 100×; (b) 500× magnification 56
- Figure 5.10:** Optical micrographs of coated W-10Cu with Co activator, sintered at 1400°C (a) 100×; (b) 500× magnification 58
- Figure 5.11:** Optical micrographs of uncoated W-10Cu with Co activator, sintered at 1400°C (a) 100×; (b) 500× magnification 58
- Figure 5.12:** Optical micrographs of coated W-10Cu with Fe activator, sintered at 1400°C (a) 100×; (b) 500× magnification 59
- Figure 5.13:** Optical micrographs of uncoated W-10Cu with Fe activator, sintered at 1400°C (a) 100×; (b) 500× magnification 59
- Figure 5.14:** Optical micrographs of coated W-40Cu without activator, sintered at 1400°C (a) 100×; (b) 500× magnification 60
- Figure 5.15:** Optical micrographs of uncoated W-40Cu without activator, sintered at 1400°C (a) 100×; (b) 500× magnification 60
- Figure 5.16:** Optical micrographs of coated W-40Cu with Ni activator, sintered at 1400°C (a) 100×; (b) 500× magnification 61
- Figure 5.17:** Optical micrographs of uncoated W-40Cu with Ni activator, sintered at 1400°C (a) 100×; (b) 500× magnification 61
- Figure 5.18:** Optical micrographs of coated W-40Cu with Co activator, sintered at

1400°C (a) 100×; (b) 500× magnification 62

**Figure 5.19:** Optical micrographs of uncoated W-40Cu with Co activator, sintered at 1400°C (a) 100×; (b) 500× magnification 62

**Figure 5.20:** Optical micrographs of coated W-40Cu with Fe activator, sintered at 1400°C (a) 100×; (b) 500× magnification 63

**Figure 5.21:** Optical micrographs of uncoated W-40Cu with Fe activator, sintered at 1400°C (a) 100×; (b) 500× magnification 63

**Figure 5.22:** SEM micrographs of W-10Cu (C) without activator, sintered at 1000°C (a) 1000×; (b) 3000× magnification 65

**Figure 5.23:** SEM micrographs of W-10Cu (UC) without activator, sintered at 1000°C (a) 1000×; (b) 3000× magnification 65

**Figure 5.24:** SEM micrographs of W-10Cu without activator, sintered at 1400°C (a) and (b) 1000×; (c) and (d) 3000×; (e) and (f) 6000× magnification 66

**Figure 5.25:** SEM micrographs of W-10Cu with Ni activator, sintered at 1400°C (a) and (b) 1000×; (c) and (d) 3000×; (e) and (f) 6000× magnification 67

**Figure 5.26:** SEM micrographs of W-10Cu with Co activator, sintered at 1400°C (a) and (b) 1000×; (c) and (d) 3000×; (e) and (f) 6000× magnification 68

**Figure 5.27:** SEM micrographs of W-10Cu with Fe activator, sintered at 1400°C (a) and (b) 1000×; (c) and (d) 3000×; (e) and (f) 6000× magnification 69

**Figure 5.28:** SEM micrographs of W-40Cu with Fe activator, sintered at 1400°C (a) and (b) 1000×; (c) and (d) 3000×; (e) and (f) 6000× magnification 70

**Figure 5.29:** SEM micrographs of W-40Cu with Ni activator, sintered at 1400°C (a) and (b) 1000×; (c) and (d) 3000×; (e) and (f) 6000× magnification 71

**Figure 5.30:** SEM micrographs of W-40Cu with Co activator, sintered at 1400°C (a) and (b) 1000×; (c) and (d) 3000×; (e) and (f) 6000× magnification 73

**Figure 5.31:** SEM micrographs of W-40Cu with Co activator, sintered at 1400°C (a) and (b) 1000×; (c) and (d) 3000×; (e) and (f) 6000× magnification 74

**Figure 5.32:** Effect of Cu content, coating, and activator addition on the hardness of W-Cu alloys sintered at (a) 1000°C, (b) 1200°C, and (c) 1400°C 76

- Figure 5.33:** Effect of Cu content, coating, and activator addition on the compressive strength of W-Cu alloys sintered at 1400°C 76
- Figure 5.34:** Effect of Cu content, sintering temperature, and coating on the electrical conductivity of W-Cu alloys (a) without activator; (b) with Ni addition; (c) with Co addition; and (d) with Fe addition 79
- Figure 5.35:** Effect of Cu content, coating, and sintering temperature on the thermal conductivity of W-Cu alloys sintered at (a) without activator (b) with Ni addition, (c) with Co addition, and (d) with Fe addition 81
- Figure 6.1:** Effect of activator addition on the sintered density of coated and uncoated W-10Cu and W-40Cu alloys sintered at 1000°C 85
- Figure 6.2:** Schematic representation of the effect of Fe/Co activator addition on the coated and uncoated W-Cu alloy 86
- Figure 6.3:** Schematic representation of the effect of Ni activator addition on the coated and uncoated W-Cu alloy 86
- Figure 6.4:** Effect of activator addition on the sintered density of coated and uncoated W-10Cu alloys sintered at 1200°C and 1400°C 87
- Figure 6.5:** Schematic representation of the dihedral angle and its relationship with grain size and neck size 90
- Figure 6.6:** Schematic representation of the microstructure of coated W-Cu system (a) prior to sintering, and (b) after liquid phase sintering. The high dihedral angle in W-Cu system favors Cu melt retraction, thereby reducing the effect coverage of Cu on to w grains and favoring W-W contacts 91
- Figure 6.7:** Variation in the hardness of W-Cu alloys with and without activator addition plotted against the sintered density 97
- Figure 6.8:** SEM micrograph of W-10Cu compact sintered at 1400°C with Ni activator after compression testing 98
- Figure 6.9:** SEM micrograph of W-40Cu compact sintered at 1400°C with Ni activator after compression testing 98
- Figure 6.10:** Variation in the electrical conductivity of W-Cu alloys with and without activator addition plotted against the sintered density 99



## List of Tables

	Page no.
<b>Table 2.1:</b> Commonly used materials for microelectronic packaging [1]	6
<b>Table 2.2:</b> Two classes of materials based on their thermal properties [1]	7
<b>Table 4.1:</b> Characteristics of the as-received powders	37
<b>Table 4.2:</b> Theoretical densities of various compositions	41

## Acknowledgments

I would like to express my deep gratitude to Dr. Anish Upadhyaya for his expert guidance, support and encouragement throughout my graduate studies at Kanpur. His leadership was immeasurable help to my early identification of an industrially significant area of research.

I am thankful to Mr. R.P. Singh, Dr. Mungole, and Mr. S.C. Soni for providing me with guidance and letting me benefit from their experience during the experimental work.

My time at the P/M lab was enriched by the interaction with my fellow students. Many of them are close friends and I hope to keep for life.

I would also be thankful to Dr. David Houck and Mr. Paul Sedor of Osram Sylvania, Towanda, USA for providing me the powders of the requisite compositions for the experiment. It is needless to say that without this the work can not be done.

I must acknowledge the support provided by my loving parents and my brother. I could not have come this far without their unconditional love and support. This thesis is dedicated to them.

At last but not the least, I extend my special thanks to all the staff of MME and ACMS, who helped me at many occasions.

Chiradeep Ghosh  
IIT, Kanpur  
February, 2003.

# Chapter 1

## INTRODUCTION

In recent years, considerable attention has been directed to the thermal management materials for microelectronic applications [1-5]. The requirement for such high performance materials is necessitated due to the miniaturization of the semiconductor devices, which imposes restriction on the convective cooling media [6,7].

The high heat generated in the limited cross sectional area requires the heat dissipation in a predominantly conductive mode through the surrounding thermal management device. Thus, for better heat dissipation, materials that offer a combination of high thermal conductivity (greater than 200 W/mK) and low thermal expansion coefficient ( $< 7$  ppm/K) matching that of the silicon chips are required [8,9]. It is very difficult to achieve such a combination through monolithic materials and therefore composite/alloy design is desired [10,11]. Tungsten-copper alloys are one such candidate materials for these applications wherein the high thermal conductivity of Cu dissipates heat and the low thermal expansion coefficient of the W skeletal structure provides the hermetic sealing between the microelectronic circuitry and the heat sink [2].

Because of the refractory nature of W (m.p. 3420°C), the W-Cu alloys are fabricated by powder metallurgy (P/M) route. Once such variant involves infiltration of Cu melt into partially sintered W powder compacts having interconnected porosity [12-14]. Alternatively, the W and Cu powders are mixed together and shaped by either pressing the compacts or by powder injection molding (PIM) [3,15]. The latter is employed for complex shape components and/or when finer powders are used, which pose problems during compaction. The as-pressed or as-molded compacts are subsequently sintered. In general, the W-Cu compacts are sintered through liquid phase sintering (LPS) for achieving high sintered density. The relatively lower fusion temperature of Cu (m.p. 1083°C) coupled with its good wetting behavior towards W makes W-Cu alloys amenable to liquid phase sintering [15,16]. Conventionally, rearrangement and solution reprecipitation processes are predominant mechanisms that lead to densification during liquid phase sintering [17]. However, there is no inter solubility between W and Cu in both solid as well as in liquid state [18]. Hence,

achieving full density in W-Cu system. For optimum properties, W-Cu alloy must contain about 20-60 (vol. %) of Cu [7]. A high volume fraction of Cu in turn results in inhomogeneous microstructure and restricts rearrangement, which further limits densification. Another processing difficulty during liquid phase sintering is the sensitivity of the Cu melt wetting W to the oxygen content. Huppmann and Reigger [19] have shown that the wetting angle of Cu melt in the W-Cu system may vary from  $0^\circ$  to  $5^\circ$ . Consequently, densification in the W-Cu system through capillary stress induced rearrangement is highly dependent on the purity of the powders and of the atmosphere [16,20]. To achieve full densification, the W-Cu alloys are milled or very small W-particle size is used to enhance the solid state densification, and thereby achieving full density [21,22]. Researchers have used sub-micron to nano sized W powders for this [20,23]. Another variant of the P/M processing involves using  $\text{WO}_3$  and CuO as starting powders, which are milled together. Subsequently, the powders are co-reduced and sintered to near full density [23-25].

An alternate approach for attaining full density in W-Cu alloys is by adding small quantities of transition elements, such as Ni, Fe, Co, and Pd [26,27]. These additives either segregate at the W-W grain boundary, forming intermetallic phases at the grain boundaries, or dissolve in the Cu melt, thereby providing a short circuit diffusion path.

One of the objectives of this research is to investigate the effect of Cu content on the densification behavior of W-Cu alloys both during solid state as well as liquid phase sintering condition. The sintering response of both uncoated and coated W-Cu alloys was investigated in the presence of Fe, Ni, and Co additives. The variations in mechanical and electrical properties with the addition of activators were also studied. For the coated samples homogeneous melt formation can lead to more capillary induced rearrangement phenomenon to take place.

## Chapter 2

### BACKGROUND

#### 2.1 Thermal Management System

Thermal management materials are those which surround the semiconductors, microelectronic circuitry, computer chips etc. The semiconductor devices are achieving enhanced speed and computational performance through miniaturization. A similar feature in logic and memory chip integration has been occurring. There is a tremendous computing cost reduction and speed increase with this progression. With such progress there arise problems with heat generation on the computer chip. So thermal management materials are needed to dissipate heat associated with these chips and circuitry. Challenges arise both with the material selection and the component fabrication. Powder metallurgy techniques provide a means of fabricating high quality composite systems with tailored thermal properties. Never the less it is a new application area for P/M with major implications since over  $10^9$  microelectronic circuits are fabricated each year [1].

In the past, extruded aluminum was an acceptable thermal management material. But with higher power densities, the demands can not be satisfied by Al. Moreover, thermal cycles induced large stress because of mismatched coefficient of thermal expansion (CTE). Aluminum alloys have CTE in the range of 22-27 ppm/°C; whereas for Si it is in the range of 3-5 ppm/°C and for Ga-As it is close to 6 ppm/°C. Ceramic substrates used to mount the semiconductor are often made from alumina (7.6 ppm/°C), beryllia (8 ppm/°C) or aluminum nitride (5.8 ppm/°C) [1]. These circuits require contacts with high thermal conductivity, controlled thermal expansion package materials to remove heat while avoiding stresses due to thermal cycling.

Thermal fatigue is one of the major failure modes in electronic circuitry. For instances, failures have been reported in as few as 100 cycles with a CTE difference of 12 ppm/°C between the contacting materials. The combination of Al and substrate ceramics is unacceptable, because of the 15 ppm/°C CTE difference between them. Accordingly, the new heat dissipation materials must be thermally compatible with the semiconductor and the substrate materials. The target CTE is the range of 7 ppm/°C. This is a problem since most of the high thermal conductive materials have high CTE [1].

Other requirements for the heat dissipation materials vary with the applications. For example, density of the material is of major concern for the aerospace application, and cost is a concern for personal computers and work-stations. There may be other additional criterion like strength, microwave absorption, and electroplating compatibility depending on design and assembly procedure. These are largely associated with device performance, especially in high frequency and military environments. Many of the devices will operate under conditions where they must protect from atmospheric oxidation. Thus, the design window for thermal management materials in micro-electronic packaging emerges with a desired CTE in the range of 7 ppm/°C from a high thermal conductivity system (300 W/mK). The ability to fabricate these articles in an economical manner is an important attribute offered by powder metallurgy [6].

Table 2.1 lists several common microelectronic packaging materials, giving the density, CTE, thermal conductivity, and elastic modulus. The properties are for pure materials. Contamination may have a major effect on the properties like thermal conductivity, which can be reduced by as much as can 50% of the tabulated value in commercial materials. Table 2.1 includes invar, silica, and cordierite as low CTE but

with also low thermal conductivity. The material with high thermal conductivities (Cu, Ag, and Au) has high CTE. The elastic modulus is also important in understanding the interfacial stresses deflection that occurs between components. Aluminum is generally acceptable in all aspects except for its high CTE [1]. On the other hand, low CTE materials such as invar lack the desire thermal conductivity and can be difficult to fabricate. At the extreme, stainless steel lacks both the thermal conductivity and CTE, but proves easy to fabricate. Analysis of the options for heat dissipation application leads to consideration of combinations from two generic material classes; the high thermal conductivity and low CTE. Table 2.2 groups typical materials selected for one or the other of these attributes. Silicon carbide, aluminum nitride, and diamond/graphite are the only materials that appear on both lists. These are difficult to fabricate as pure materials and have inherent chemistry control and assembly problem as well as low electrical conductivities [1]. Thus a composite consisting of a high thermal conductivity matrix phase and low thermal expansion filler metals (such as W-Cu, SiC-Al, Mo-Cu etc.) provides a means to tailor thermal properties [6]. In some applications, there may be additional constrain relating to microwave absorption or dielectric behavior.

Powder metallurgical approaches are suitable possible routes to the fabrication of devices from these materials. W-Cu is highly desirable for thermal management applications because of its combination of high thermal conductivity and low thermal expansion coefficient.

**Table 2.1:** Commonly used materials for microelectronic packaging [1].

MATERIAL	DENSITY (g/cm <sup>3</sup> )	CTE (ppm/°C)	THERMAL CONDUCTIVITY (W/m.K)	ELASTIC MODULUS (GPa)
Alumina	3.96	7.60	39	360
Aluminum nitride	3.29	5.80	270	345
Aluminum alloys	2.70	24.00	177	71
Beryllium	1.85	12.00	194	318
Boron carbide	2.52	3.50	39	448
Boron nitride	2.10	2.00	15	78
Cobalt	8.90	13.00	96	211
Copper	8.96	17.00	403	145
Corderite	2.58	2.30	1	118
Epoxy	1.20	60.00	0	0.10
Gallium arsenide	5.32	6.00	46	100
Gold	19.3	14.00	316	79
Invar	8.04	0.40	11	144
Iron	7.86	12.00	75	196
Kovar	8.36	6.00	17	131
Mo	10.20	5.00	138	326
Nickel	8.90	13.00	95	214
Silica	2.30	1.00	2	70
Silicon	2.34	4.00	139	113
Silicon carbide	3.21	5.00	270	414
Silver	10.50	19.00	431	76
Stainless steel	8.00	15.00	14	216
Tungsten	19.30	4.50	174	411



**Table 2.2:** Two classes of materials based on their thermal properties [1].

HIGH THERMAL CONDUCTIVITY	LOW THERMAL EXPANSION
Aluminum	Aluminum nitride
Aluminum nitride	Boron nitride
Copper	Corderite
Diamond	Graphite
Gold	Invar
Silver	Osmium
Silicon carbide	Silica
	Silicon carbide
	Silicon nitride
	Tungsten
	Tungsten carbide

## **2.2 P/M Processing of W-Cu Alloys**

### **2.2.1 An Historical Overview**

The evolution of the powder metallurgy industry originated as a means of fabricating refractory metals (W, Nb, Mo, Zr, Ti, and Re) otherwise not feasible due to their high melting points. In fact, tungsten has an historical link with powder metallurgy and there is continued progress in expanding the available compositions and processing options. The literature based in W processing is expanding and includes new alloys, microstructures, and processing routes [28]. In this section few examples will be emphasized here including the options for complex shaping using powder injection molding, solid sintering mechanisms for W-Cu, pressure assisted sintering, activated sintering, and liquid phase sintering advances.

### **2.2.2 Infiltration of Liquid Cu in Sintered Tungsten**

Manufacturing of products by the infiltration method consists of two basic stages, i.e. forming of porous material with defined properties and infiltration of a liquid into them. To make infiltration process effective, a high degree of filling of product pores (low porosity) should be achieved [12].

Experimental investigations of sintered tungsten of various porosities which were infiltrated with liquid copper had been carried out by J. Lezanski and W. Rutkowski [12]. The Cu infiltration in sintered W in gaseous atmosphere proceeds in three stages. This course of infiltration is related to the mechanical influence of gas upon an infiltrant liquid. These stages may overlap to some extent. It is also possible that some of the stages do not occur [12].

### **2.2.3 Powder Injection Molding of W-Cu Composites**

Powder injection molding (PIM) is an emerging technique for producing

outline of the PIM process. It was the best way to solve the difficulty of complex shaping of conventional P/M technologies. In particular, this process is characteristic of near net shaping of the precision P/M parts by using a thermo-plastic binder [29]. However, one of the most serious problems in the PIM technology is a dimensional change of the parts (volume shrinkage) during sintering which is unavoidable for obtaining a full density. But the infiltration process hardly accompanies the size change of the P/M parts. Thus it was thought that the near net shaped P/M parts with full density can be produced by the new production route consisting of two combined technologies, i.e., the PIM and the infiltration process. This production route for P/M parts had been investigated on the W-Cu system by Kim *et al.* [29].

In the process, starting powder was prepared in the form of the Ni-doped W powder in order to give strength to the W-skeleton. The binder system used for the near net shaping of the W powders by extrusion process was a mixture of carnauba wax (CW), low density polyethylene (PE) and stearic acid (SA) of which mixing ratio was CW (45)-PE (45)-SA (10) by weight [29]. The extrusion of the W powder binder mixtures was done in the rod form. The extruded rod specimen was inserted immediately into a water bath which is located directly under the nozzle of the extrusion apparatus. Finally W binder mixture rod having enough strength for handling and smooth surface was obtained. The debinding sequence was having two optimum isothermal temperatures (180°C/450°C). It consists of two isothermal processes; the first stage corresponding to wicking process of the binder was the isothermal heating at 180°C for 4h in N<sub>2</sub> and the second one contributing to the elimination of residual binder by evaporation was also the isothermal heating at 450°C for 4h in H<sub>2</sub>. Under this debinding sequence, the binder contained in the

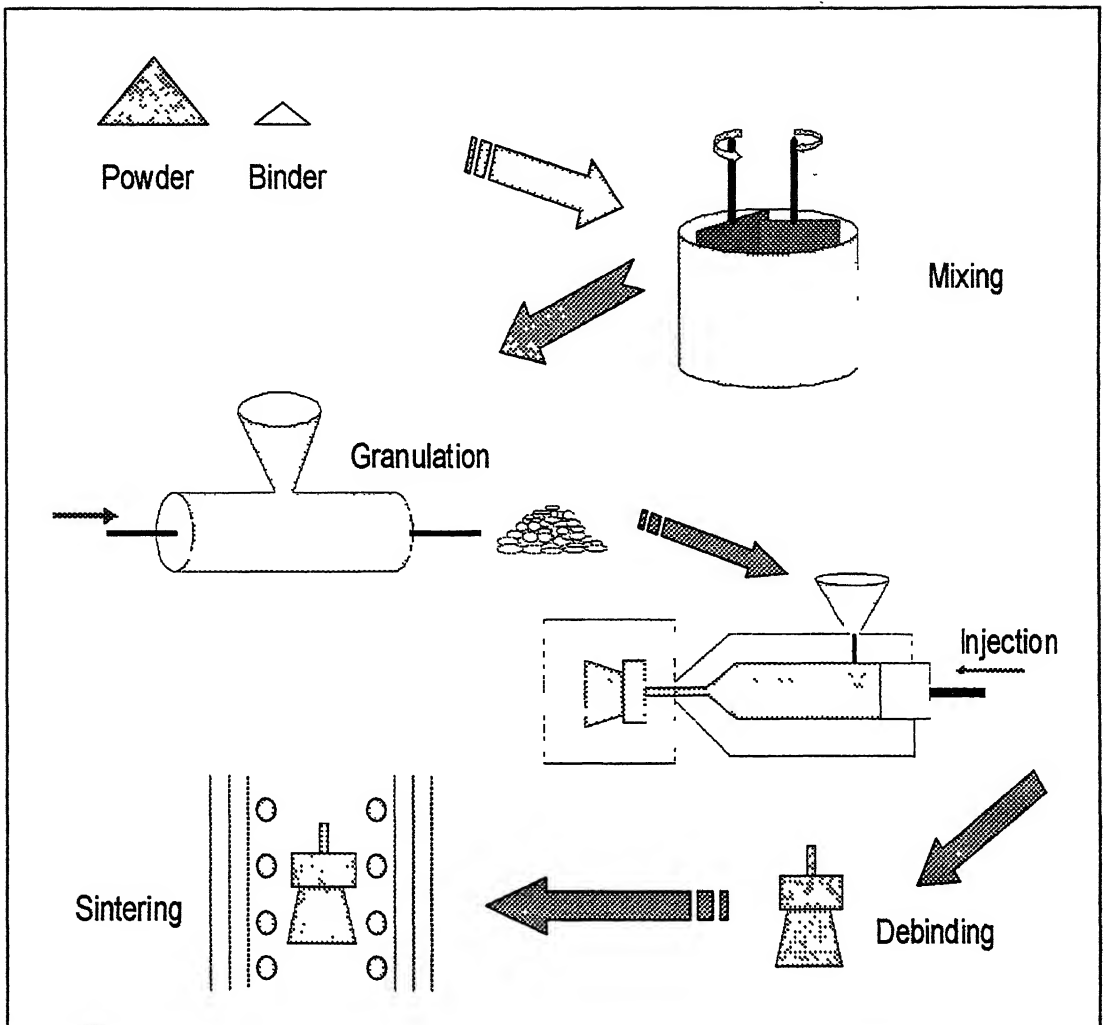


**Figure 2.1:** Processing steps involved in Powder injection molding [28].

extruded specimen being embedded in 3  $\mu\text{m}$  alumina powders was eliminated. After debinding, the rod specimens were sintered at 1150°C for 30 min in  $\text{H}_2$  to form a strong structure of the W skeleton. The infiltration of Cu into the W rod specimens was performed at 1150°C for 5 min in  $\text{H}_2$  in which W rod was embedded in Cu powders [29].

#### 2.2.4 Solid State Sintering of W-Cu Composites

During heating a powder compact up to the temperature where liquid phase forms, sintering is known as solid state sintering [30]. In systems having solubility in the binder phase, such as W-Ni-Fe or WC-Co, significant densification occurs in the solid-state. In systems without solubility, such as W-Cu, the densification is small in both the solid and liquid states. Densification in the solid state has been observed for classic mixtures [31] and is very important in the case of nano-scale mixtures, either for mechanically alloyed [32-34] or for co-reduced powders [35]

In spite of some negative aspects of solid-state sintering, such as formation of a W-skeleton [36], the solid state spreading of Cu is expected to have positive effects. Lee *et al.* [31] have suggested that first spreading of Cu mono-layers induces the rapid densification, but have also evidenced long time spreading of thick layers between W particles. As suggested by Sebastian and Tendulkar [37] Cu spreading tends to homogenize the W-Cu mixture, which is known to improve densification by rearrangement in liquid phase sintering of W-Cu [28].

The fundamental sintering behavior of the system is well understood and can be accurately predicted using multiple mechanism computer simulations [28]. Initial solid state sintering is dominated by surface diffusion. The initial neck growth occurs without densification because sintering is dominated by this particular diffusion mechanism. Densification does not initiate until grain boundary diffusion becomes

active [28]. The activation energy for surface diffusion is 326 kJ/mole, which is lower than the activation energies for either grain boundary or lattice diffusion, which are 378 and 585 kJ/mole, respectively. This agrees with the extensive surface smoothing evident in partially sintered compacts and explains the pore enlargement often observed in solid-state sintering. Neck growth by surface diffusion does not give densification, but leads to the formation of grain boundaries at the particle contacts. Hence, at high temperatures the increased grain boundary area, decreased surface area, and increased thermal energy combined to promote a greater sintering contribution from grain boundary diffusion [28]. Such a mixture of sintering mechanisms (surface and grain boundary diffusion) was observed by Kothari [38] using powders between 0.5 and 15  $\mu\text{m}$ . He indicated that grain boundary diffusion was favored by as smaller particle size, which seems the opposite from expectations with the higher surface area. Since the densification is due to grain boundary diffusion, accordingly there is a great sensitivity to grain growth during sintering. As grain growth occurs the diffusion distances for pore elimination increase and the rate of densification declined. Accordingly it is very important to give attention to heating path ways that control grain growth during sintering to aid in densification.

### **2.2.5 Pressure Assisted Sintering of W-Cu Composites**

The densification of the W-Cu compacts can be enhanced during sintering by the application of stress on the powders. The strength of the W drops rapidly with temperature. So at high temperatures an external stress or pressure supplements the basic diffusional flow with plastic deformation and creep processes. The densification is largely controlled by Nabarro-Herring creep [28].

Hot isostatic compaction has been employed in the consolidation of W with the presence of a liquid phase. However, the resulting properties were not

significantly improved to make such additional processing steps attractive. This is particularly due to pressure induced preferential flow of the liquid into the pores, creating in-homogeneities in the final microstructure. The greatest promise for the hot isostatic compaction is in healing defects and removal of large pores using high pressures and short processing times. Interestingly, the use of a post HIP liquid phase sintering treatment eliminated the agglomeration and inhomogeneity [28].

### **2.2.6 Activated Sintering of W-Cu Composites**

The addition of small amounts of an element or any special process that results in an increase in the rate of densification is termed as activated sintering [28]. Figure 2.2 is an example phase diagram for an activated sintering system. A liquid phase often forms at temperatures slightly above the activated sintering range.

Since W and Cu are not mutually soluble in each other, which is evident from their phase diagram (Figure 2.3) solid-state sintering is not an effective means to produce W-Cu alloys. Furthermore the difference in atomic weight between these two elements is very large so that it is very difficult to mix them in uniformly for liquid phase sintering. Hence the infiltration method as described earlier, in which a skeleton of cold pressed W powder is filled with Cu melt, is widely used in practice for applications, such as, high power electrical contacts and heat sink materials. The infiltration method however can not be employed to fabricate complicated parts of low Cu content W-Cu alloys [27].

Investigators have studied the effects of group VIII transition element additions on the sintering of W powder at temperatures below those at which a liquid phase would be predicted [27]. In fact, in the case of W, temperature as high as 2800°C are needed to achieve 99% densities for untreated powder. The role of additive is to lower the activation energy for bulk transport of W by providing a high

diffusivity transport path. Consequently, the additive forms a phase with a much lower melting point than tungsten. On one hand, W has some solubility in the additive, while on the other hand, at high solubilities, the net-inter atomic bond strength may be changed resulting in higher diffusional activation energy. The additives increase the diffusivity by creating a weaker bonding segregated layer for rapid transport as compared with the pure structure [27]. The Ni-W system is perhaps the best documented activated sintering system. Early studies by Kurtz [39] showed a significant decrease in the sintering temperatures with Ni additions up to 0.2 wt%. Vacek [40] included other additives in his investigation of the process. A more detailed study by Brophy *et al.* [41] on the effects of Ni on the densification of W concluded that one monolayer coating on the W particles is sufficient to promote high diffusion of W through or on the Ni, thereby forming the interparticle necks. Gessinger and Fischmeister [42-43] suggested Ni segregation to the W grain boundary and successfully constructed a geometric and kinetic model for activated sintering assuming a hetero diffusion controlled process. German and Munir [44] studied the effects of different dopants on the sintering of W. Pd and Ni are the most effective dopants. They also have found that the activation energies for the shrinkage processes agree with the activation energies calculated for the hetero diffusion process. Parameters that enhance the activated sintering of W are:

- 1) Fine particle size (in the submicron range).
- 2) High green density to promote higher densification.
- 3) Homogeneous dopant distribution where Pd is the most effective followed by Ni, Fe, Co, Pt, and Rh.
- 4) Solubility of W in the activator.
- 5) An optimum sintering temperature and time to minimize grain growth [45].



In the case of heavy alloys, activated sintering is usually coupled with liquid phase sintering to promote high densification. This is achieved by either a one step or a two-step process. In the two step case, activated sintering is used to form a W skeleton and subsequently infiltrated by the liquid phase Lee and coworkers [46] investigated the effects of Ni-P additions on the formation of a W skeleton which enhanced the infiltration of Cu melt into the pre-form. The coupling of both processes was used by Moon and Lee [47] in their study of the effect of Co addition to the W-Cu alloy system. They have showed that Co is more effective than Ni in activating the liquid phase sintering of W-Cu compacts, which is the converse of their effect on the solid state sintering of pure W compacts. The activated liquid phase sintering and the increased wettability mechanisms are suggested to explain the cause of the effectiveness of Co addition. In the case of the activated liquid phase sintering mechanisms, the sintering of W-Cu alloy is accelerated by the volume diffusion of W through the activated intermetallic compound ( $W_6Co_7$ ) formed. Whereas, in the case of increased wettability mechanism it is proposed that the increased sinterability is due to the fact that the  $W_6Co_7$  formed on the surface of W promotes the rearrangement of W particles. However, since these mechanisms were based on the results obtained after sintering, it appears to not exactly explain the role of additive elements in the densification of W-Cu alloy [47].

It has been reported that Ni can be added to improve the mechanical properties of W-Cu alloys. It has also been found that a small amount of Co addition can improve the electrical properties of W-Cu alloys [27]. However, the detailed sintering behavior of W with additions of group VIII transition metals has not yet been systematically studied, in particular for the case of the liquid phase sintering W-Cu alloys.

### 2.2.7 Liquid Phase Sintering of W-Cu Composites

Sintering in the presence of a liquid can accelerate the rate of densification more than possible through activated solid state sintering [28]. During microstructural evolution in liquid phase sintering (LPS), three stages are observed; 1) particle rearrangement, during this period the liquid forms and wets the solid particles, 2) solid dissolution and reprecipitation resulting in grain shape accommodation and pore elimination, and 3) microstructure coarsening, causing an increase in the mean grain size with time to achieve a minimum surface energy per volume ratio [46]. The driving force for these three processes is the reduction in surface energy. The surface energy acts on the microstructure to achieve a minimum energy configuration. Good wetting is also a major concern in liquid phase sintering. A low solid-liquid surface energy, compared to the solid-vapor and liquid-vapor surface energies, enhances the final densification. Another aspect associated with interfacial energies is capillarity. When the liquid forms, it can penetrate along the W particle contacts and grain boundaries such that strong attractive forces are exerted on the solid to cause rearrangement, densification, and particle contact flattening [46]. Flow of W in the liquid results in homogenization, pore elimination and strengthening. In the case of W-Cu system the liquid phase persists through out the sintering cycle as opposed to the transient liquid phase sintering.

#### *Rearrangement*

Due to limited inter-solubility in the W-Cu system, factors which affect rearrangement are especially important [17]. During this first stage of liquid phase sintering, capillary forces due to the wetting liquid act on the particles and pool the particles into close proximity. The particles repacked closely as successive cluster of particles form and pores are eliminated by viscous flow. The presence of the liquid

phase aid in smoothing the particle surface, there by lubricating particle rearrangement [28]. The liquid further enhances the packing by attacking and disintegrating cluster of particles and repacking follows through redistribution of the small fragments between the big particles [46-50] as shown in Figure 2.2. The wetting behavior of W by molten Cu is greatly affected by the sintering atmosphere. A contact angle of zero degrees can be obtained with a pure dry hydrogen atmosphere. Wetting behavior becomes poorer with increasing oxygen content of the Cu powder [17].

The powder characteristics significantly affect the kinetic of liquid phase sintering. In the W-Cu system, a smaller W particle size increases the initial homogeneity, results in larger capillary forces during rearrangement, increases the solubility in the liquid phase, and increases the overall driving force for sintering. So small particle size enhances shrinkage. The W particle shape is also important for small volume fraction of Cu. Rough particle surfaces result in mechanical interlock and hence retard and/or inhibit rearrangement resulting in a porous structure. Smooth, round particles result in greater densification since they tend to pack more homogeneously and are more easily rearranged. For mixed elemental powders, densification behavior increases with decreasing particle size due to improved initial homogeneity and easier rearrangement. Higher initial homogeneity can be obtained through milling the powders; however, Cu coated W powders provide best results [17].

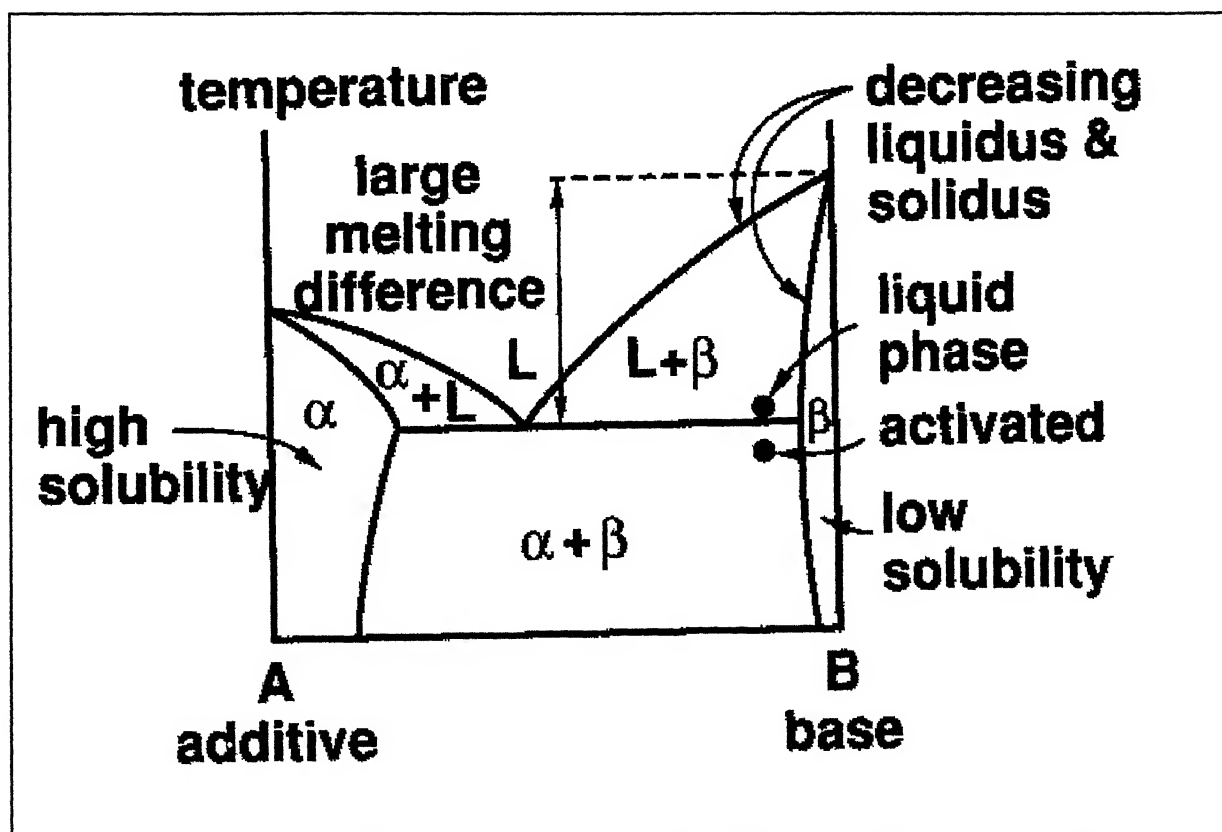


Figure 2.2: Idealized binary phase diagram for solid-state activated sintering [25].



At low dihedral and contact angles, high shrinkage rates are observed [28]. Rearrangement processes are hindered by high compaction pressures due to more W-W contacts which lock the particle into place [17]. The effect of green density on the rearrangement phenomenon is very complicated. In fact, at high green densities, the particles are not free to move and capillary forces contribute little to rearrangement. At low green densities, the structure is porous and long time and/or higher temperatures are needed to achieve high densities. This is not as noticeable in systems in which the solid is soluble in the liquid since solution reprecipitation is generally the dominant densification mechanism. Greater densification and higher densification rates can be obtained through rearrangement with a higher liquid phase volume fraction; however, the composition of W-Cu structure is often fixed by electrical or thermal property requirements [17].

Pore formation is due to inhomogeneous rearrangement and liquid flow from large to small capillaries resulting in a lower pore density with a higher mean porosity [58]. In the W-Cu system, Huppmann and coworkers [51] showed that the uniformity of the particle packing and mixing are major parameters in the rearrangement stage. This has been further extended to W-Ni-Cu [52-60] alloys. They also observed that rearrangement is a discontinuous process. After formation of a rigid W-skeleton, only a fraction of single or small groups of particles are free to rearrange. Schatt *et al.* [61] suggested in his study of the W-Ni system that dislocation pile up at the grain boundary during compaction results in an increase of the grain boundary energy which favors the penetration of the melt. At high liquid content (30 to 35 volume fraction), full densification can be achieved during the rearrangement stage. As the liquid content is decreased other sintering phenomenon are involved such as, solution reprecipitation. However, in heavy alloy systems such as, W-Ni-Fe where W is

soluble in Ni-Fe matrix and in the case of low heating rates, considerable solid state sintering takes place prior to rearrangement stage.

Slow heating is detrimental to rearrangement since solid state sintered bonds form before liquid phase formation. Dissolution of these sintered bonds by the liquid phase is necessary before rearrangement can take place, however, the heating rate has little effect on the sintering of W-Cu, since the solid state sintering of W is a very slow process below the melting point of Cu. Additives that enhance the solid state sintering of W may allow significant shrinkage before liquid phase formation, resulting in substantial solid state sintered bonds which hindered rearrangement [17]

### ***Solution Reprecipitation***

During the rearrangement stage, solution reprecipitation is also active. However, it does not become dominant until the end of the first stage. Kingery [54] treated this phenomenon as case of thin film completely wetting spherical particle. He showed that the driving force for this process is the difference in chemical potential arising from the pressure difference between the thin melt and surrounding melt. Subsequent work by Gessinger and coworkers [62] considered the case for contact angles greater than zero and showed that it can be treated in the same manner. Hence for solution reprecipitation to occur, solid should have some solubility in the melt, such as in the case of W-Ni-Fe system, and therefore the arte of densification in this stage is dependant on mass flow through the liquid. Shatt *et. al* [61] relates the solution reprecipitation process to dissolution pile up at the grain boundary giving a pressure gradient with respect to the surrounding liquid rather than capillary effect. He observed more distinct contact flattening and shape accommodation in the case of mechanically activated W powder. The net surface energy decreases due to the elimination of pores by liquid filling [28]. Particle coalescence in this stage has been

observed in the W heavy alloy systems followed by neck formation. The growth of neck proceeds by mass transfer from small particles in the surrounding matrix and with a lesser extent from the redistribution of mass over the curved grain surface. The grain growth in systems with little or no solubility in the liquid such as W-Cu is attributed to coalescence [28].

### ***Microstructural Coarsening***

In this stage, a solid skeleton forms. However, solution reprecipitation still proceeds in systems where W is soluble in the liquid phase. As a consequence, grain growth, grain shape accommodation, and final stage pore removal follow [63] because a solid skeleton exists between the solid grains; any remaining pore elimination is dependant on diffusional relaxation of the skeleton. During the final stage of liquid phase sintering, grain coalescence contributes to grain growth. The effect of coalescence on grain growth is best seen in W-Cu system, where no mutual solubility exists between W and Cu. Coalescence and Ostwald ripening result also in pore coarsening [63]. The elimination of pores in this stage is dependant on this processing atmosphere and the nature of the vapor entrapped within [28].



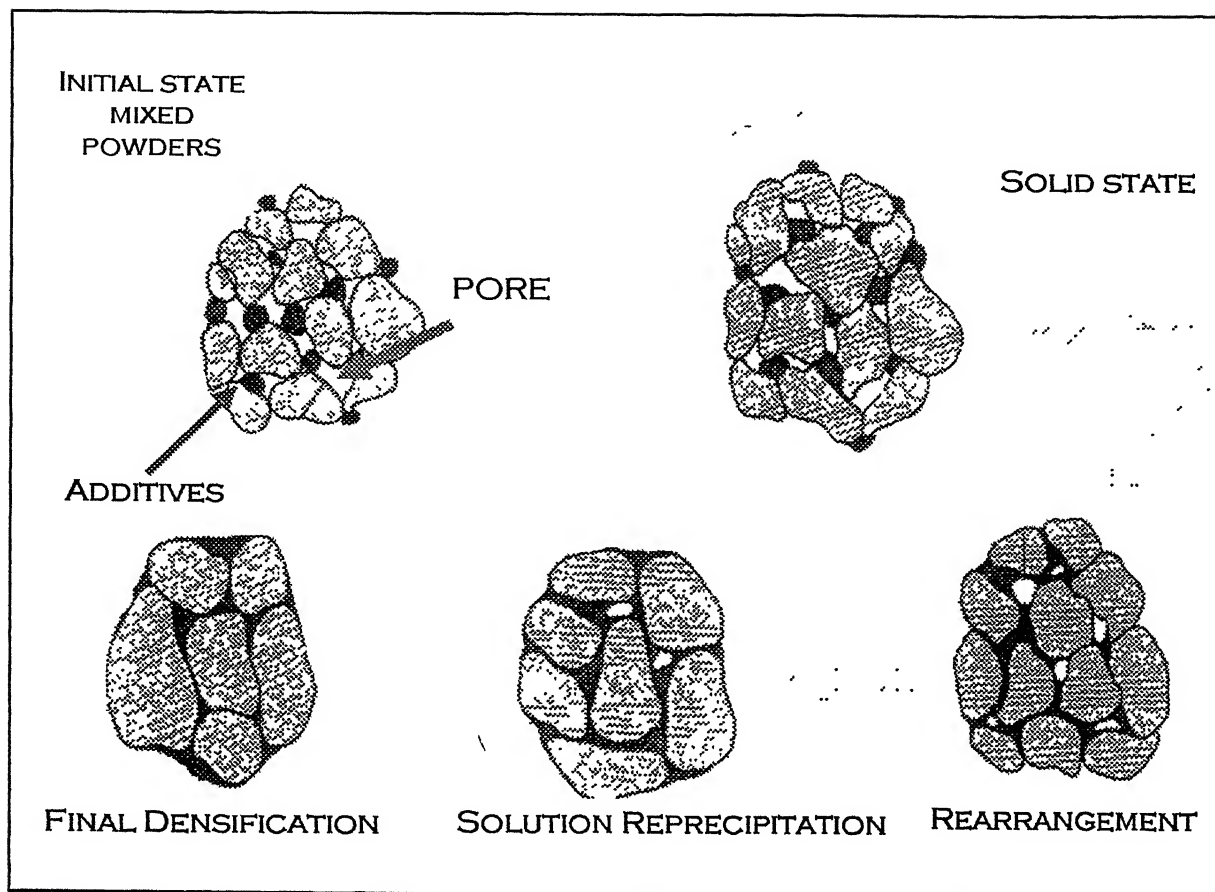


**Figure 2.4:** Different stages of liquid phase sintering [28].

### 2.2.8 Sintering Atmosphere

The sintering atmosphere has a direct effect on the residual porosity of W alloys. Insoluble or low diffusivity gases such as argon or nitrogen result in entrapped pores in the microstructure. These pores persist during final stage sintering and collapse due to pressurization [28]. The use of vacuum or high diffusivity gases, coupled with optimum sintering time, inhibit the formation of such pores [28]. In general, hydrogen is used as a sintering atmosphere because vacuum sintering does not aid in oxide dissociation and removal. However, residual porosity can also result from the reaction of hydrogen with dissolved oxygen in W alloys, forming water bubbles which cause swelling. A post reduction cycle followed by sintering in high dew point hydrogen prevents this reaction. Reduction cycle prior to liquid formation allows the water vapor to diffuse through the open pores [40] and sintering at high dew point hydrogen renders the formation of water vapor thermodynamically unfavorable. German and coworkers [59] related the effect of initial oxygen content in heavy alloy powders with the dew point on the formation of residual porosity. They concluded that oxygen segregation to the grain boundary is insignificant and a pre-reduction cycle is an effective means of controlling the porosity formed by the entrapment of water vapor. The use of hydrogen in heavy alloy systems, such as, W with a Ni to Fe ration of 7:3, results in embrittlement in leading to a decreasing ductility. Ekbom [56] has indicated that even at 1 ppm hydrogen, there is segregation of hydrogen to the matrix-W interface. The hydrogen, like most impurities in heavy alloys, is preferentially concentrated in the matrix. The result in an apparent embrittlement since under deformation the hydrogen accumulates (via dislocation transport) at the interface, resulting in a decreased interfacial cohesion. This model is supported by other observation on hydrogen partitioning. Hence an annealing cycle in

an inert gas or vacuum after sintering is appropriate [28]. German and Churn [48] observed an increase in ductility and strength attributed to pore degassing and removal of hydrogen embrittlement by switching from hydrogen to argon after 30 minutes of sintering in the presence of liquid phase. Nitrogen gas is also effective to avoid hydrogen embrittlement. As pointed out by several studies, post-sintering heat treatment is needed for high ductility W heavy alloys [39,43-46]. Low temperature anneals (near 600°C) after swaging deformation result in increased strength and hardness, but decrease ductility. Residual contamination from the hydrogen sintering atmosphere can be removed by annealing in the 800 to 1200°C range in vacuum, argon, or nitrogen. Water quenching further improves the properties by freezing impurities into solution, thereby avoiding the detrimental condition of segregation to the matrix/tungsten interface [46]. When an optimum cooling rate is used, homogenization of impurities occurs which leads to superior mechanical properties resulting from cleavage of the W grains. In the other hand, a high cooling rate can result in entrapped pores due to differential shrinkage between the matrix and the W grains [28].

Figure 2.5 shows the effect of sintering atmosphere on swelling in pure Cu compacts; the compacts were heated at 10°C/min.

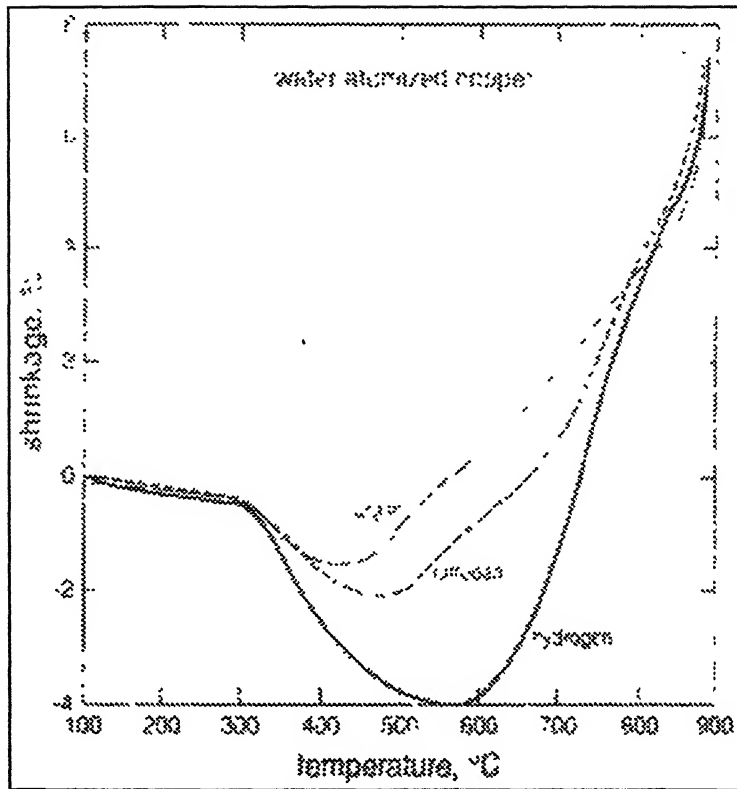


**Figure 2.5:** Effect of sintering atmosphere on swelling in pure Cu compacts [20].

## Chapter 3

### SCOPE OF THE PRESENT WORK

#### 3.1 System Selection

From the previous chapter, it is evident that W-Cu system is an important thermal management material. The only route of making the products is powder metallurgy technique. W-Cu system exhibits good wetting behaviour but almost negligible inter solubility, which is evident from the phase diagram (Figure 2.3) This system can be prepared by liquid phase sintering (LPS). The thermal conductivity of this composite is extremely sensitive to processing, while the thermal expansion coefficient shows much less variation.

The combination of a refractory material such as W, which has a low thermal expansion coefficient and a high thermal conductivity material such as Cu, is one approach to tailoring material for thermal management applications. The final thermal properties can be controlled by adjusting the relative amount of matrix and reinforcement. Clearly, a trade-off exists between the high conductivity of the matrix and the low thermal expansion coefficient of the reinforcement, so the relative amount of components depend on the specific application. To select the composition of these thermal management materials, it is necessary to know how much the thermal conductivity will decrease from that of the pure matrix as increasing amounts of reinforcement are added. Likewise, the amount by which the thermal expansion coefficient decreases as reinforcement is added needs to be quantified. Numerous models for the prediction of the thermal conductivity and thermal expansion coefficient of composites from the properties of their constituent have been derived over the couple of years [1].

Liquid phase sintering (LPS) of W-Cu is an attractive processing route, but is hindered by the low solubility of the base material in the liquid phase. The densification behaviour can be enhanced by the use of submicron powders or by the addition of transition element with specific phase diagram characteristics. The cost of these submicron nano-sized powders is exorbitantly high and also is very prone to oxidation due to their high surface to volume ratio.

In the present study the densification behaviour of the W-Cu alloys are investigated with powder modification i.e. coating the W powder with Cu and with the addition of transition element as an activator.

### **3.2 Coating the W powder with Cu powder**

Chemical coating procedure is used to coat the W- powder with Cu powder. Three compositions are taken for the present investigation, namely W-10Cu, W-25Cu, and W-40Cu. The compositions are optimal for the present work. To compare with the coated powder, in another set the same compositions are prepared by taking elemental W and Cu powder, and mix them mechanically.

### **3.3 Addition of Transition Elements**

In the present study the transition elements, namely Ni, Co, and Fe are added. They are added individually to the selected system with 1 wt. %. Figure 3.1 to 3.6 show the equilibrium phase diagram for Co-Cu, Fe-Cu, Cu-Ni, Co-W, Fe-W, and Ni-W respectively. The role of these activators is to increase the densification of the W-Cu system. The mechanism by which they enhanced the densification is different for different activators. But as a whole they increase the diffusivity of the solid particles by providing a short circuit diffusion path.

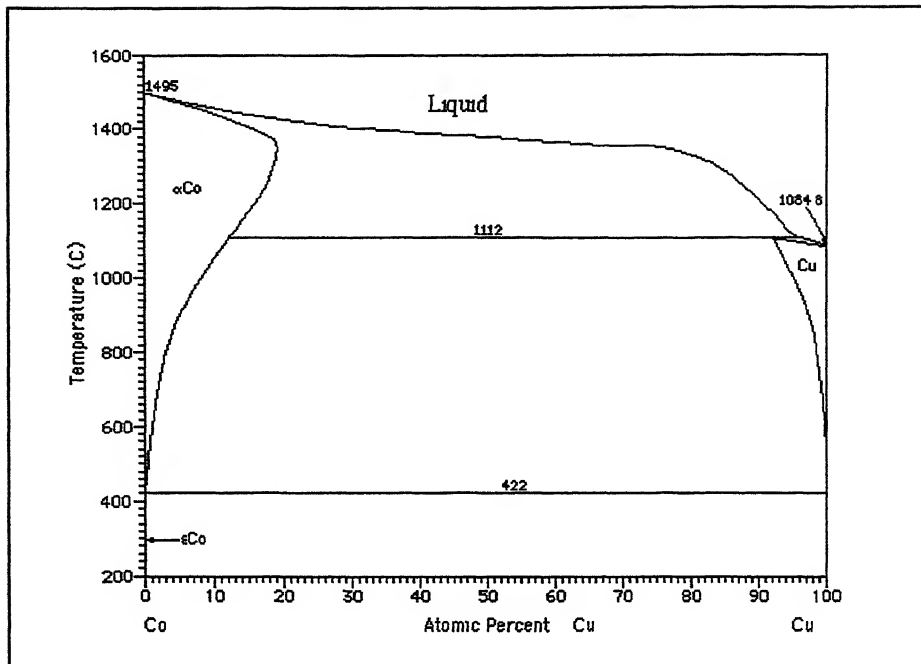


**Figure 3.1.** Cobalt-Copper Equilibrium Diagram [21].

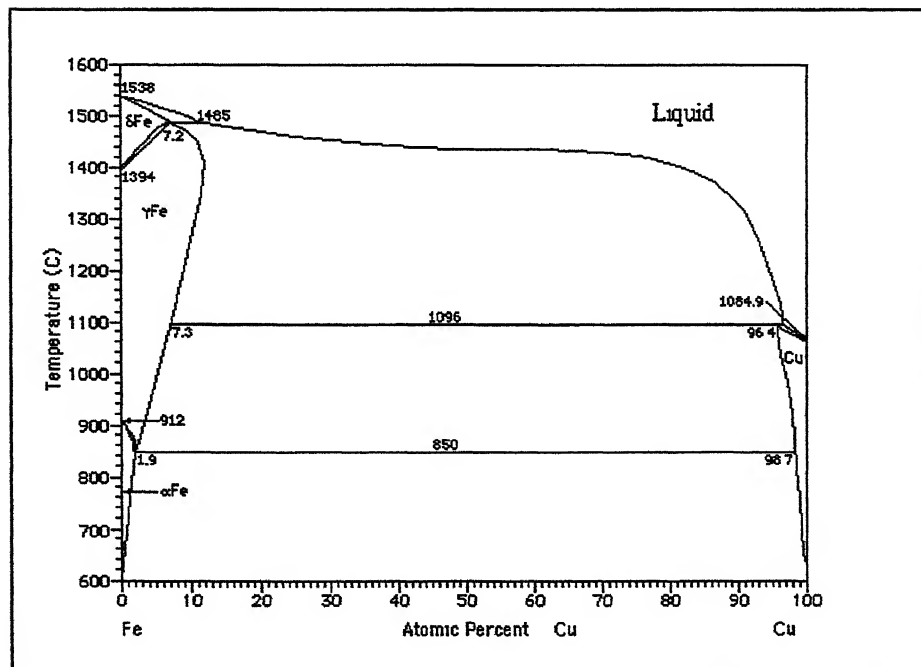


**Figure 3.2:** Iron-Copper Equilibrium Diagram [21].

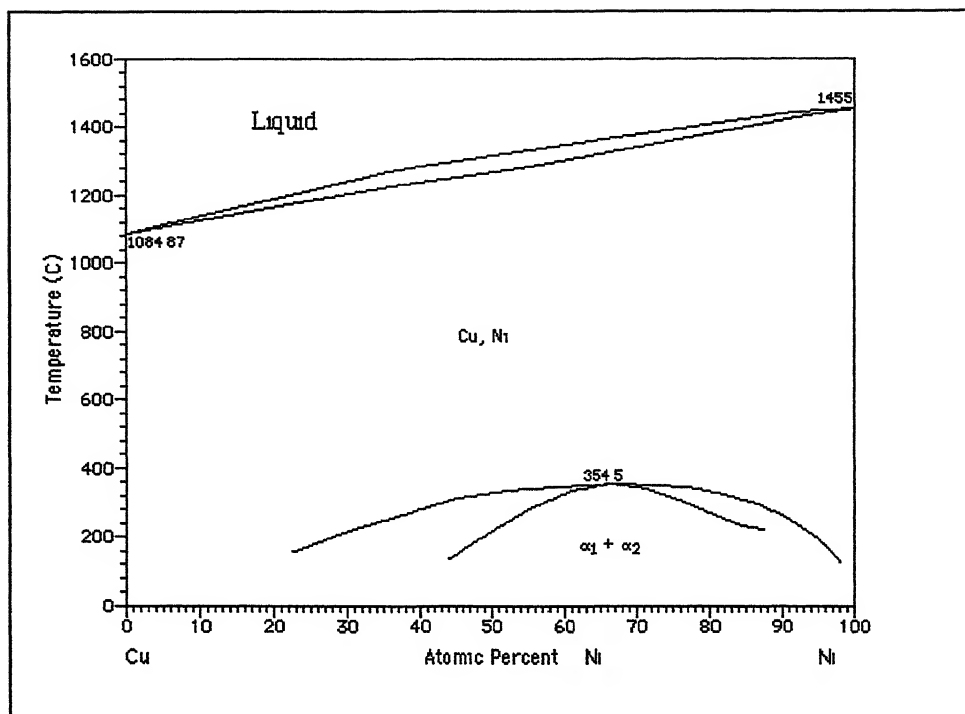


Figure 3.3: Copper-Nickel Equilibrium Diagram [21].

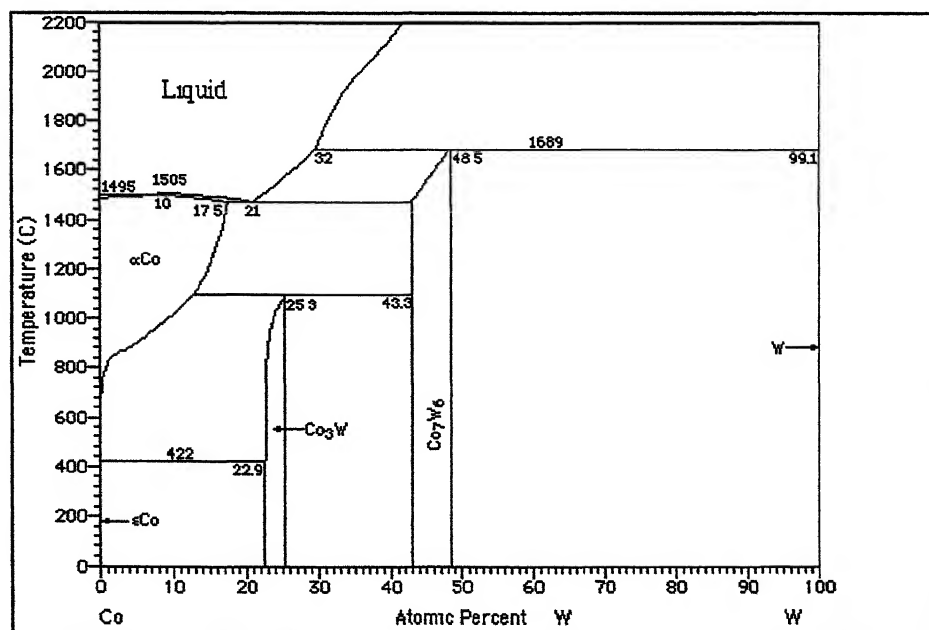


Figure 3.4: Cobalt-Tungsten Equilibrium Diagram [21].



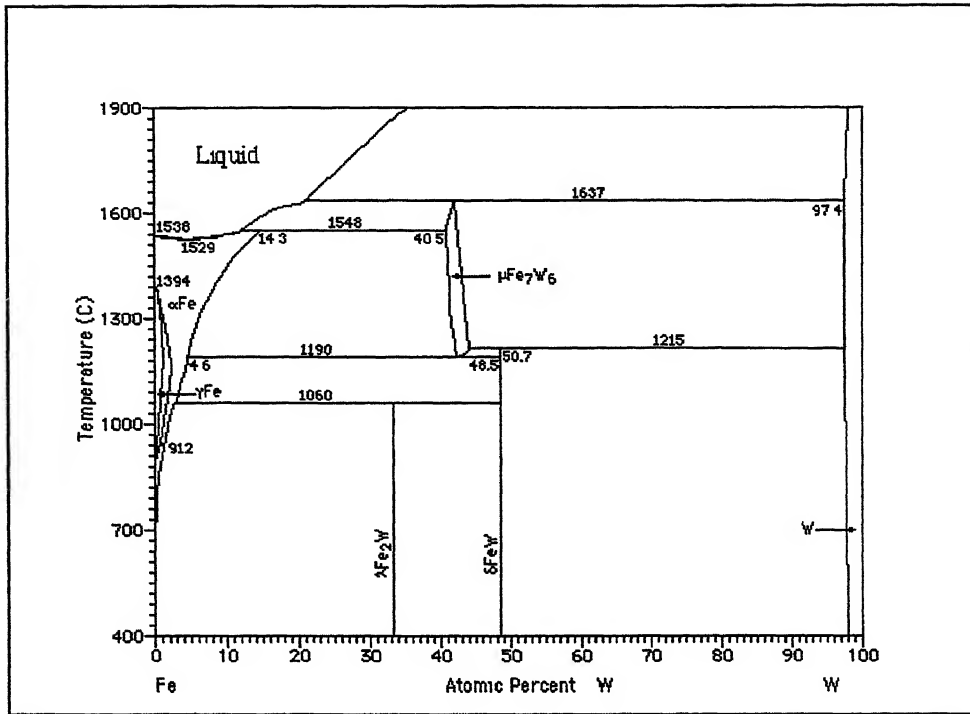


Figure 3.5: Iron-Tungsten Equilibrium Diagram [21]

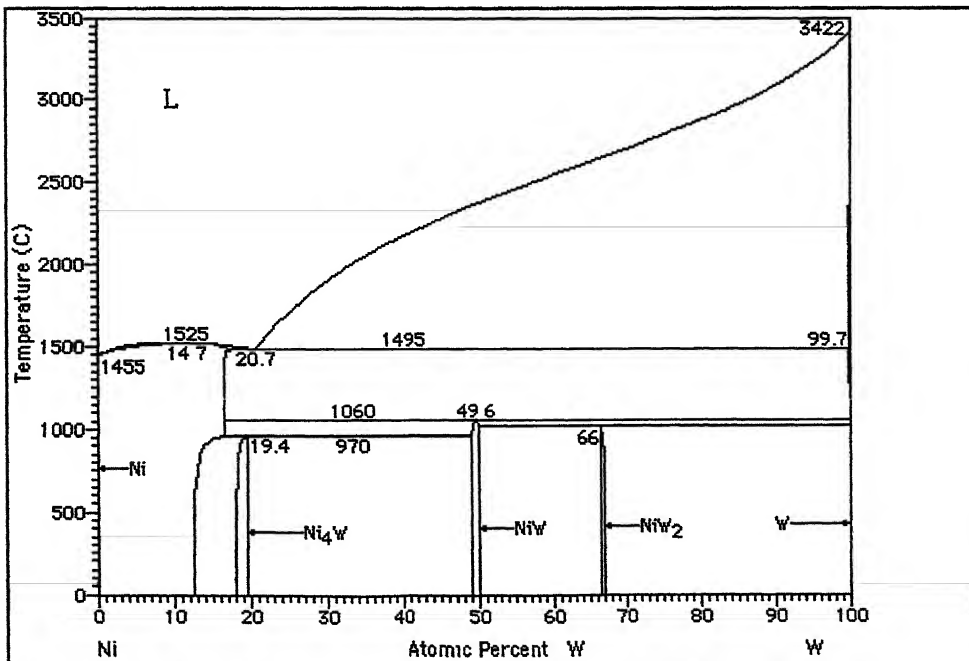


Figure 3.6: Nickel-Tungsten Equilibrium Diagram [21].

## Chapter 4

### EXPERIMENTAL PROCEDURE

The present chapter deals with various experimental techniques used in the present study. Those are a) raw materials; b) powder characterization; c) composition preparation; d) compaction; e) sintering; f) densification behavior; g) microstructural studies; h) mechanical properties; i) electrical properties.

#### 4.1 Raw Materials

##### 4.1.1 Elemental Tungsten Powder

The tungsten-powder (Grade: M55), supplied by Osram Sylvania (Towanda, PA, USA) was manufactured by reduction and had an average size of  $5.4\mu\text{m}$  with minimum and maximum size of  $4.3$  and  $5.7\mu\text{m}$ , respectively. Figure 4.1 shows the SEM micrograph of elemental W powder.

##### 4.1.2 Elemental Copper Powder

The copper powder (Grade: 635) was supplied by ACuPowder International (Union, NJ, USA). The Cu powder was prepared by gas atomization and had a rounded shape with the average size of  $13\mu\text{m}$  in as received condition. The Figure 4.2 shows the SEM micrograph of Cu powder.

##### 4.1.3 Copper Coated Tungsten Powder

The Cu coated W powders were prepared by chemically coating Cu onto the W powders so as to yield the required composition. The coated powders were supplied by Osram Sylvania Ltd. The W powders are first coated with  $\text{CuCl}_2$  to the requisite requirement. The solution was then dried by baking. The  $\text{CuCl}_2$  coated W

micrographs of W-10Cu, W-25Cu, and W-40Cu (coated powders) The W powder show a faceted, polygonized morphology, whereas that coated with Cu shows a relatively a more rounded surface.

## **4.2 Powder Characterization**

The characteristics of the starting powders greatly affect the densification behavior during sintering. Establishing the relationship between the sintering behavior and powder characteristic requires quantitative information regarding the particle size, size distribution, and morphology. Most of the characterization technique requires only a small quantity of the sample powder; it is therefore assumed that the powder sample is representative of the bulk.

### **4.2.1 Particle Size and Size Distribution**

Powder size was analyzed using a laser-scattering size analyzer (model Economy, Laser Klasse 1; supplier: Fritsch, Germany). Low angle Fraunhofer light scattering using monochromatic (laser) light and dispersed particles are used in this case. Particles are suspended in a moving fluid. The suspension was made using 1 to 3g of powder in approximately 60 ml of distilled water with 10% sodium metaphosphate. The particles are passed through a laser beam in a circulating water stream. The light is scattered after the interaction with the particles, and strategically placed detectors measure the intensity. Particle size affects both the intensity and angular extent of scattering. With coherent light the angle of scattering varies inversely with the particle diameter. The scattering depends on the refractive index of the particle in the suspending medium, the wavelength of light, and the particle size and shape.

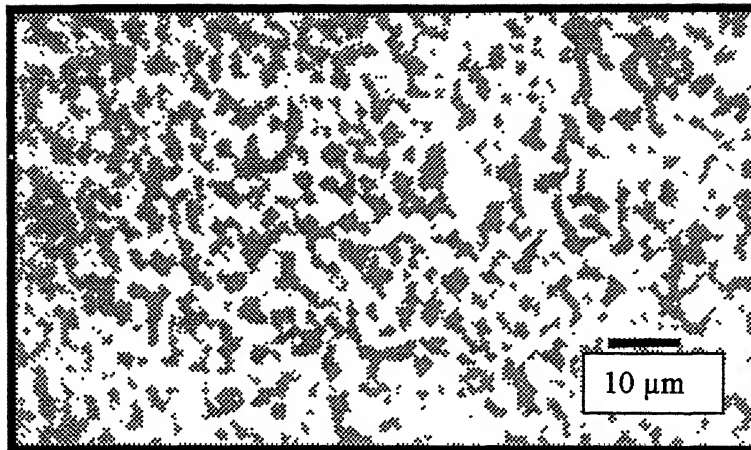


**Figure 4.1:** SEM micrograph of W powder in as-received condition.

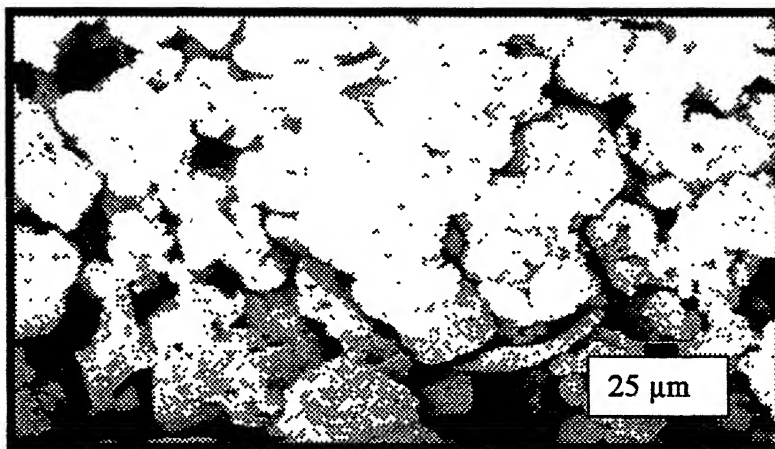
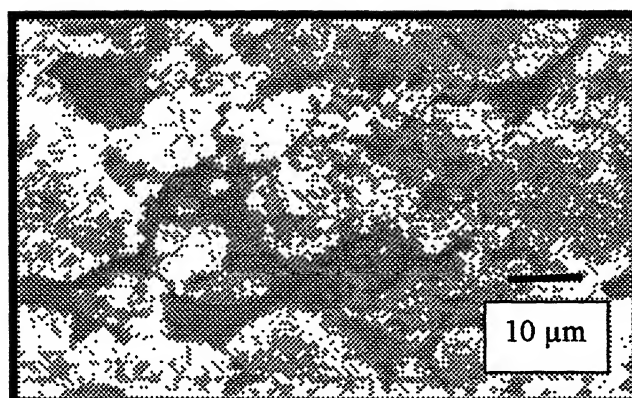
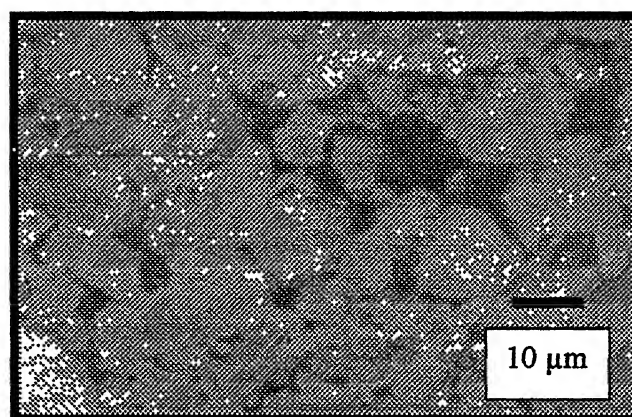


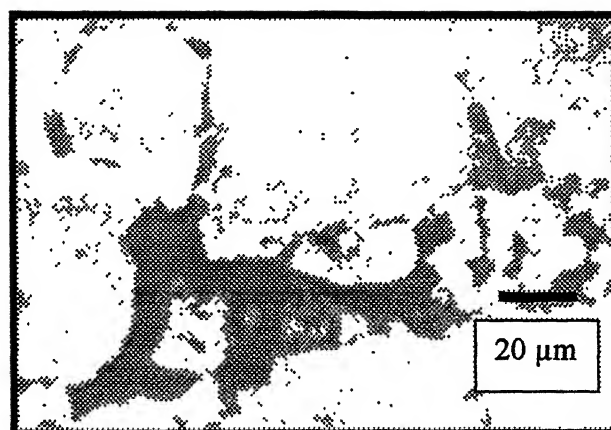
**Figure 4.2:** SEM micrograph of Cu powder in as-received condition.



(a)



(b)



(c)

**Figure 4.3:** SEM micrograph of W powder coated with Cu (a) W-10Cu; (b) W-25Cu; (c) W-40Cu.

From the particle size analysis it is evident that the W-10Cu and W-25Cu (coated) powder particles are having bimodal size distribution. Figures 4.4a and 4.4b shows the size distribution curve for these two powder particles, respectively. Maximum particles for W-10Cu (coated) retained in the range of 30-38  $\mu\text{m}$  and that for W-25Cu (coated) is in 30-35  $\mu\text{m}$ . On the other hand we got the unimodal size distribution of the W-10Cu (coated) powder particles. Figure 4.4c shows the size distribution curve for W-40Cu (coated) powder particles. From the graph it is clear that maximum particles are in the range of 30-35  $\mu\text{m}$  size.

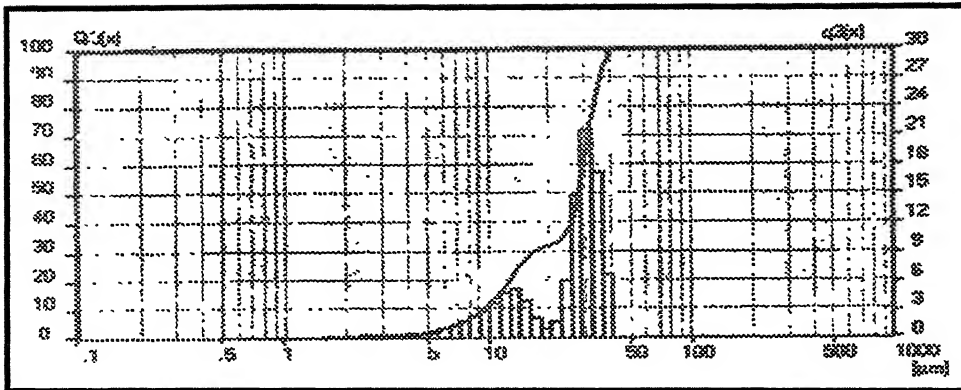
Table 4.1 summarizes the particle size distribution of the as-received powders.

#### **4.2.2 Particle Morphology**

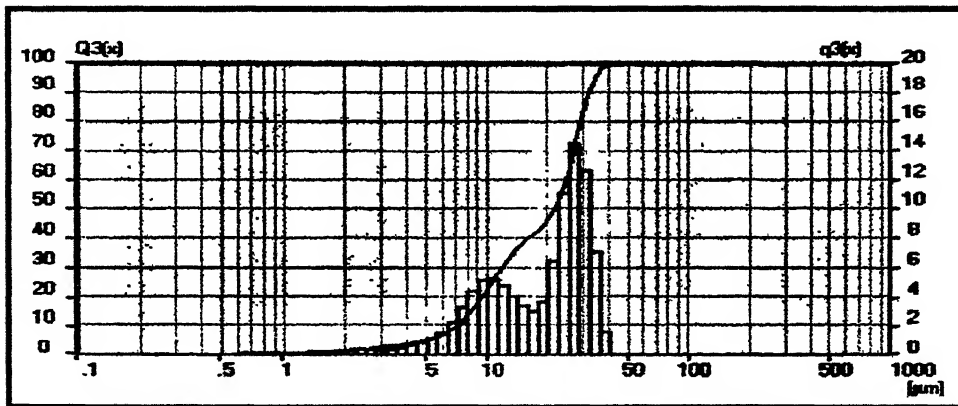
A qualitative measure of particle shape was obtained using a JEOL, JSM – 840 A, Scanning Electron Microscopy, in the secondary electron (SE) mode. The SEM permitted far greater viewing magnification than optical equipment. The W powders were produced by the reduction of ammonium para-tungstate. This process produces a faceted polygonized morphology, which can be seen clearly from Figure 4.1. The Cu powders were prepared by gas atomization and had a rounded shape. Figure 4.2 shows the SEM micrograph of the gas atomized Cu powder. The morphology of the Cu coated W powder shows a more rounded surface than that of the pure W powder. Figure 4.3 shows the SEM micrographs of the copper coated W powders.

**Table 4.1:** Characteristics of the as-received powders.

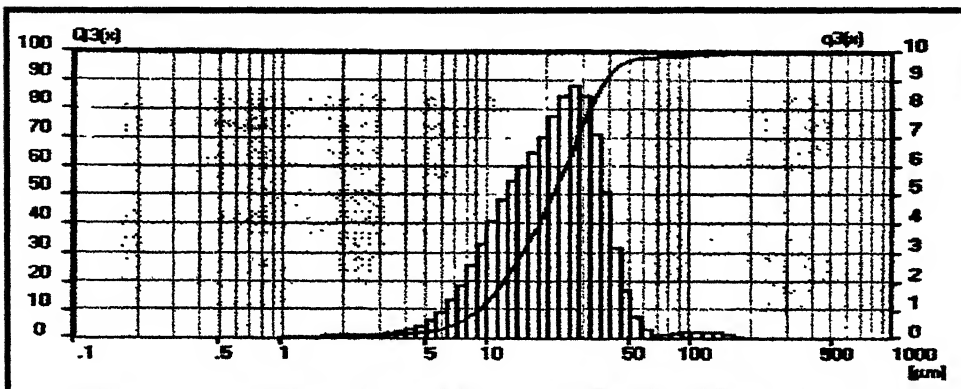
Powder Designation	D <sub>10</sub> ( $\mu\text{m}$ )	D <sub>50</sub> ( $\mu\text{m}$ )	D <sub>90</sub> ( $\mu\text{m}$ )
W-10Cu (coated)	9.52	28.10	35.86
W-25Cu (coated)	7.21	21.81	32.24
W-40Cu (coated)	9.28	21.57	38.98



(a)



(b)



(c)

**Figure 4.4:** Particle size distribution for coated (a) W-100Cu, (b) W-25Cu, (c) W-40Cu powders.



### 4.3 Composition Preparation

In the present study, W Cu alloys containing 10, 25 and 40 wt. % Cu were investigated. In one set of experiment, the compositions were prepared by mixing the constituents W and Cu powders in requisite proportion. Elemental W and Cu were weighed to 0.001 g accuracy using an electronic balance (supplier: Mettler, AE 200, USA). The balance was calibrated using a series of standard weights. The alloy compositions were then placed in a 1litre capacity glass jar and mixed in a Turbula mixer (type: T2C, supplier: Bachofen AG, Switzerland) for 30 min. Mixing ensures complete homogeneity in the powder mixture. To prevent segregation, due care was taken to make that the powders were not shaken after mixing.

In the second set, the same compositions were prepared by chemically coating the Cu on to the W powders so as to yield the required composition. The coating procedure was described in the previous paragraph. In a separate set of experiment, Ni, Fe, and Co was added to both the coated and the uncoated (as mixed) powders. The activator amount was restricted to 1 wt. %. The Ni, Fe, and Co was blended with W-Cu powder mixture using Turbula mixer.

After the mixing of the powders to make the desire composition, the density of the selected composition was determined by the inverse rule of mixing. Inverse rule of mixing can be written as:

$$\frac{w}{\rho_{th}} = \frac{w_1}{\rho_1} + \frac{w_2}{\rho_2} \quad (4.1)$$

where,  $w_1$  and  $w_2$  are the weight fraction of the powders to be mixed. Their respective densities are represented by  $\rho_1$  and  $\rho_2$ .  $\rho_{th}$  is the theoretical density of the mixture. The rule is applicable for the non-interactive system only.

## 4.4 Compaction

The powders were compacted at 200 MPa pressure using a manually operated uniaxial hydraulic press (Apex Construction Ltd, UK) of 20 tons capacity. The compacts were pressed in cylindrical pellet form with diameter of 12.7 mm and height of about 5 mm. The die was made of high chromium high carbon steel, was cleaned with acetone and was lubricated with zinc-stearate prior to each powder fill. Lubrication facilitates compaction and subsequent removal of the green compacted samples. Both coated and uncoated compositions resulted in similar green density. The green density of W-Cu compacts was found to increase slightly with increasing Cu content. The W-10Cu compacts had a green density of 57% of the theoretical, whereas the W-40Cu compacts were pressed to 62% of the theoretical density. W-25Cu had a green density of 59% of the theoretical.

## 4.5 Sintering

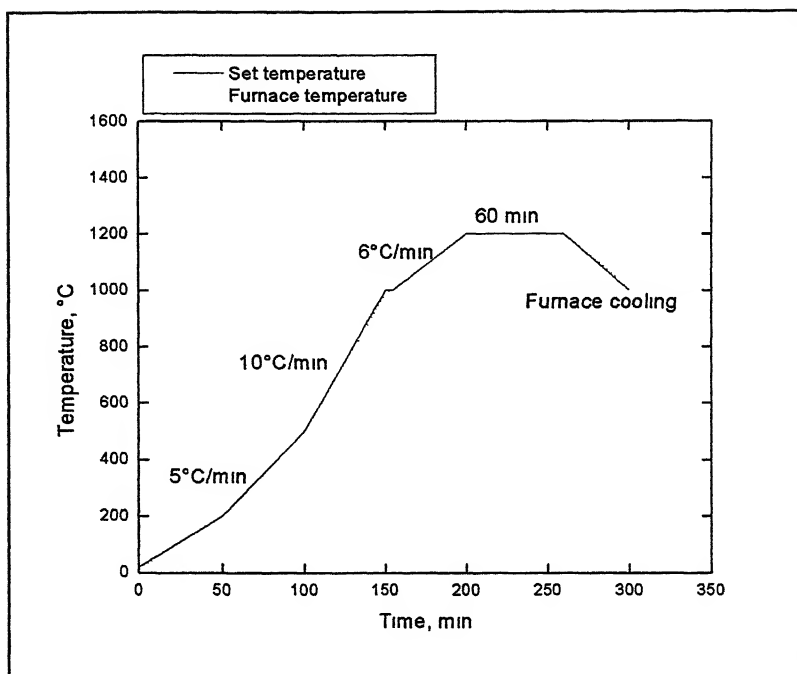
Sintering was carried out in a super-Kanthal heated horizontal tubular furnace (model: OKAY 70T-4) supplied by Bysakh and Co., Kolkata, India. The furnace had an alumina tube of diameter 7.5 cm and length 98 cm. The sintering was done in commercially pure hydrogen (dew point  $-35^{\circ}\text{C}$ ) atmosphere. The flow rate of hydrogen was maintained at 1 l/min. The furnace had a heating zone of approximately 10.5 cm in the temperature range of  $1500\text{--}1650^{\circ}\text{C}$  with an accuracy of  $\pm 5^{\circ}\text{C}$ .

In the present work three different temperatures were selected for sintering. The temperatures were 1000, 1200, and  $1400^{\circ}\text{C}$ . Requisite number of the green cylindrical compacts of coated and uncoated W-Cu powder were placed over a graphite boat and transferred in the heating zone of the tubular furnace. To avoid diffusion of graphite into the samples, alumina padding was placed in between the

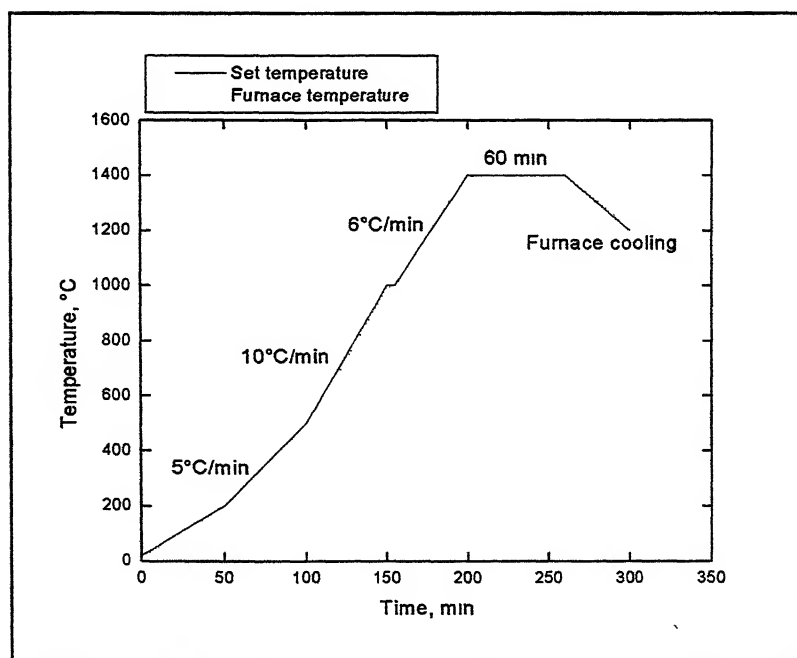
**Table 4.2:** Theoretical densities of various compositions

Composition, (wt. %)	Theoretical density, $\rho_{th}$ , g/cm <sup>3</sup>
W-10Cu	17.24
W-25Cu	14.92
W-40Cu	13.16
W-10Cu-1Fe	17.08
W-10Cu-1Ni	17.12
W-10Cu-1Co	17.12
W-25Cu-1Fe	14.81
W-25Cu-1Ni	14.84
W-25Cu-1Co	14.84
W-40Cu-1Fe	13.07
W-40Cu-1Ni	13.1
W-40Cu-1Co	13.1

boat and the green compacts. Graphite has got higher melting point than the present maximum sintering temperature. So, there should be no sticking problem of the samples with the boat. Both ends of tubular furnace were sealed with SILASTIC (RTV 700) adhesive/sealant to prevent any leakage. Heating rates were same for all the sintering operations ( $5^{\circ}\text{C}/\text{min}$ ). The samples were heated to the final sintering temperature without intermittent holding. Holding time was 60 min at final sintering temperature for each case. Automatic temperature controller was used to control the temperature within  $\pm 5^{\circ}\text{C}$ . In all cases cooling was done in  $\text{H}_2$  atmosphere at an average rate of  $2 - 3^{\circ}\text{C}/\text{min}$ . Figure 4.5 shows the sintering cycle in the above mentioned furnace. Note that the observed thermal cycle closely follows the set cycle.



(a)



(b)

**Figure 4.5:** Sintering cycle when the selected temperature is (a) 1200°C, and (b) 1400°C.

## 4.6 Densification Behavior

### 4.6.1 Density and Densification Parameter

Densities of green and sintered cylindrical compacts were calculated from the mass and the physical dimension measurements of the samples. Densification parameter was also a way to determine the amount of densification occurred after sintering. Densification parameter ( $\psi$ ) was expressed as follows

$$\psi = \frac{SD - GD}{TD - GD} \quad (4.2)$$

where SD is the sintered density, GD is the green density, and TD is the theoretical density.

Theoretical densities of various compositions were determined from the inverse rule of mixture taking the theoretical density of various elements at room temperature.

### 4.6.2 Linear and Radial Shrinkage

Linear dimensions of the sintered samples were measured using vernier callipers and screw gauge. Average of four measurements of each dimension is reported. The formula used for calculations are as follows,

$$\delta h = \left( 1 - \frac{h_s}{h_g} \right) \times 100\% \quad (4.3)$$

$$\delta r = \left( 1 - \frac{r_s}{r_g} \right) \times 100\% \quad (4.4)$$

Where,

$h_g, r_g \rightarrow$  height and radius of the green compact

$h_s, r_s \rightarrow$  height and radius of the sintered compact.

$\delta h \rightarrow$  % linear shrinkage in height

$\delta r \rightarrow$  % radial shrinkage

## 4.7 Microstructural Studies

### 4.7.1 Optical Microscopy

As the height of the cylindrical samples was enough for holding, no mounting was done. The compacts were wet polished on the Lunn Major Unit made in Struers, Denmark make 220, 320, 500 and 1000 grit silicon carbide emery papers followed by fine wheel polishing with suspended 0.03  $\mu\text{m}$  size alumina in distilled water. Due to the high contrast between the W and Cu phases, no etchant was required. The samples were then examined under the optical microscope

### 4.7.2 Scanning Electron Microscopy

The microstructures of selected samples were also observed using JEOL, JSM – 840 A, scanning electron microscopy. Operating voltage was 10 – 15 kV and probe current ranged from  $1 \times 10^{-10}$  to  $5 \times 10^{-8}$  Amp in secondary electron imaging mode.

## 4.8 Electrical Conductivity

The electrical conductivity of the sintered samples was measured using conductivity meter (model: 757) supplied by Technofour Ltd., Pune, India. Initially

the conductivity was measured relative to that of an international anneal copper standard (%IACS) Then they were expressed in the practical unit  $\text{m}/\Omega \cdot \text{mm}^2$ .

#### **4.9 Vickers Macrohardness**

Vickers Macrohardness of the polished specimens were measured on Leco V-100-C1, Hardness Tester, manufactured by Akashi Corporation, Japan. The machine was automatic and time for indentation was pre-programmed The load of 5 kg and indentation time of 15 s was maintained The diagonal length of the impressions was measured and the hardness was obtained directly in HV scale on the monitor



## Chapter 5

### EXPERIMENTAL RESULTS

The experimental results of the present investigation are described in this chapter. The most promising systems for thermal management are those which can be densified *via* liquid phase sintering. Liquid phase sintering of compacts made from mixed powders is a low cost fabrication route. However, achievement of the properties required for electronic packaging applications require an understanding of the relationships between processing, microstructure, and thermal properties. These links are experimentally investigated for the W-Cu system. A list of the specific compositions in weight percent is given in Table 5.1. The first section of this chapter presents the result of the sintering parameters and properties of the coated and uncoated W-Cu powder. In this section densification behavior of the samples are discussed. Second section deals with axial and radial shrinkage behaviors. Optical and SEM microscopy, hardness testing, electrical conductivity, and thermal conductivity, results are given in the subsequent sections.

#### 5.1 Densification Behavior

As described in the earlier chapters, the present work had been carried out with two different approaches. One of them was premixed route, which means the compositions were prepared by mechanically mixing the elemental W and Cu powders in requisite proportion. The other route was chemically coating Cu onto the W powders so as to yield the required composition. Appendices I and II give the experimental data before and after sintering for all the samples used in the present study.

Figures 5.1 and 5.2 show the variation in sintered density with varying Cu content and sintering temperature for coated as well as uncoated W-Cu alloys without activators, and with Ni, Co, and Fe as activators, respectively.

From the Figures it is obvious that an increase in Cu content and an increase in sintering temperature enhance the density of W-Cu alloys. In addition, for both solid state (1000°C) as well as liquid phase sintering conditions (1200 and 1400°C), Cu coated W compacts give marginally higher densification.

Figure 5.1a shows the sintered density variation with Cu content, coating, and temperature in W-Cu alloys with Ni addition. Ni enhances the sintered density in W-Cu alloys irrespective of the Cu content. As compared to the uncoated samples, the Ni containing coated W-Cu alloys undergo higher densification during sintering.

From Figure 5.1b, it can be inferred that 1 wt % Co addition has limited effect on densification enhancement in solid state sintering condition (1000°C) for W-Cu system. However, Co acts as a potent activator in enhancing the densification of W-Cu alloys during liquid phase sintering at 1200 and 1400°C. The density enhancement due to Co addition is more in coated samples and increase with increasing Cu content and temperature.

The effect of Fe as an activator is similar to that of Co which can be very well observed from Figure 5.1c.

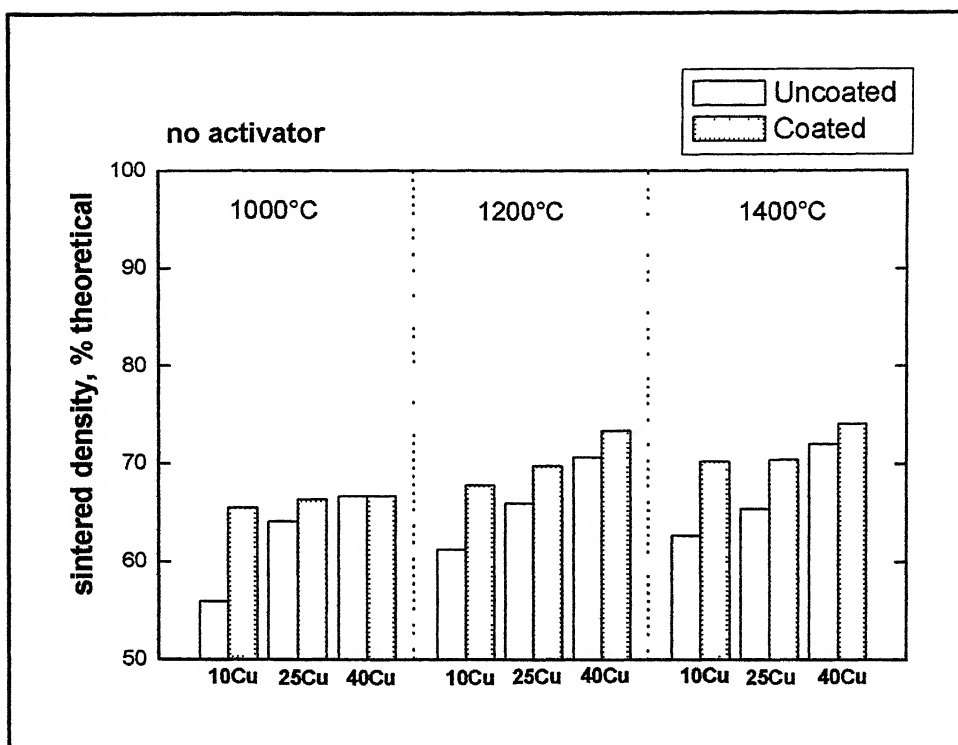
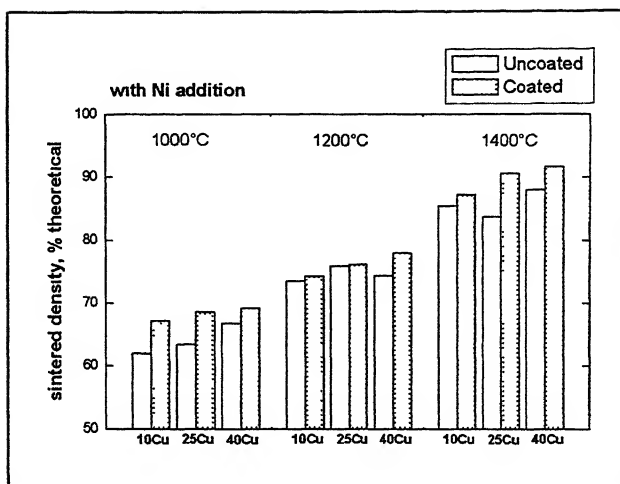
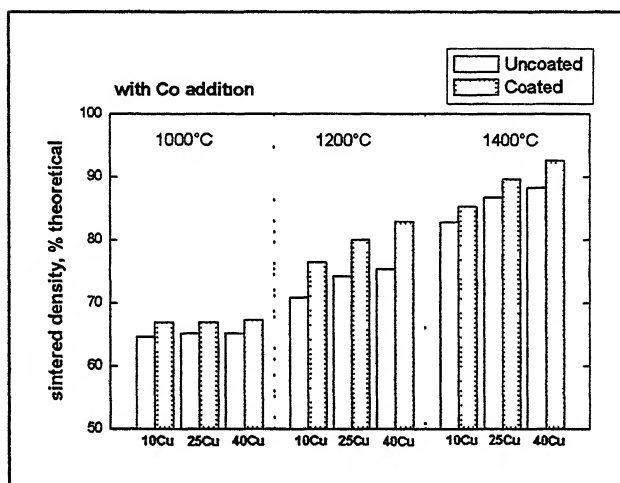


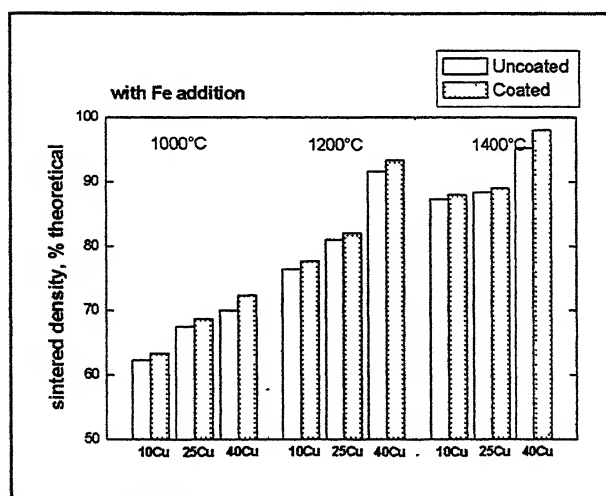
**Figure 5.1:** Effect of Cu content and sintering temperature on the density of W-Cu alloys without activator



(a)



(b)



(c)

**Figure 5.2:** Effect of Cu content and sintering temperature on the density of W-Cu alloys (a) with Ni addition; (b) with Co addition; and (c) with Fe addition.

## 5.2 Axial and Radial Shrinkage

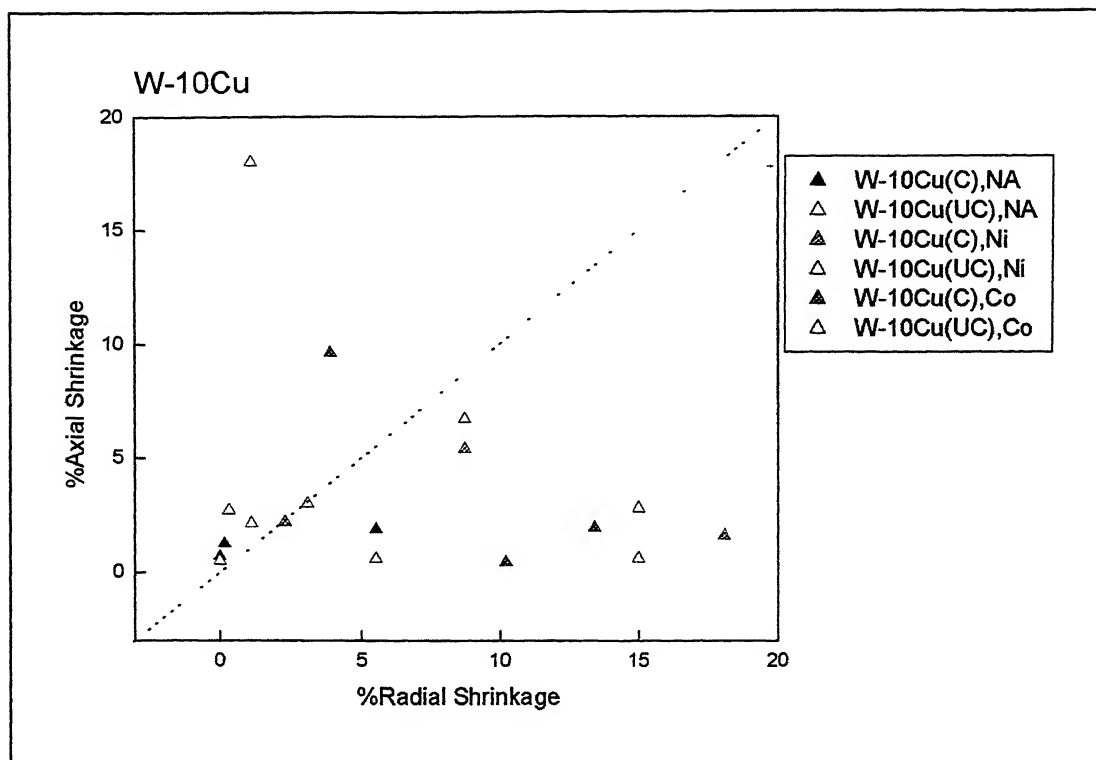
Figures 5.3a to 5.3c is the graphical representation of the axial versus radial shrinkage for the sintered samples. Appendix III represents the axial and radial shrinkage data for the samples after sintering same. Careful observation of the Figure reveals that all the samples have undergone shrinkage on both axial and radial directions; no swelling has taken place in any of the samples. As sintering temperature increases, the amount of shrinkage also increase. In most of the samples, the shrinkages in both directions are uniform. Ni addition leads to more shrinkage on axial direction than radial direction. On the other hand, Co addition leads to more shrinkage on radial direction than that of the axial direction.

## 5.3 Optical microscopy

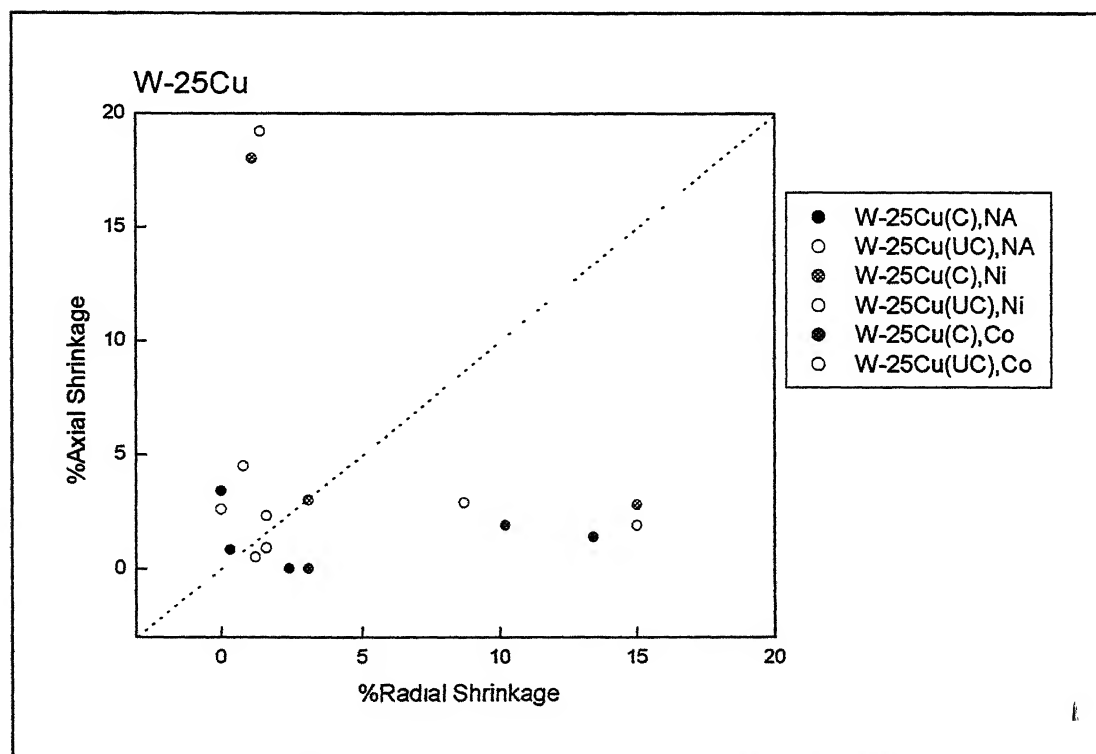
Figure 5.4 shows the optical micrographs of the coated W-10Cu samples. The samples are sintered at 1000°C. Figure 5.5 shows the same microstructure of the uncoated samples. The presence of pore is more in the second case than that of the first one. The black portions in the microstructure are the possible positions of the pores. The distribution of Cu is more homogeneous in coated samples than that of the uncoated one.

Figure 5.6 shows the micrographs of the coated W-10Cu compacts, sintered at 1400°C, without any activator addition. Figure 5.7 is the micrographs of the uncoated W-10Cu compacts sintered at same temperature and conditions. The pores are more in the uncoated samples compared to coated one.

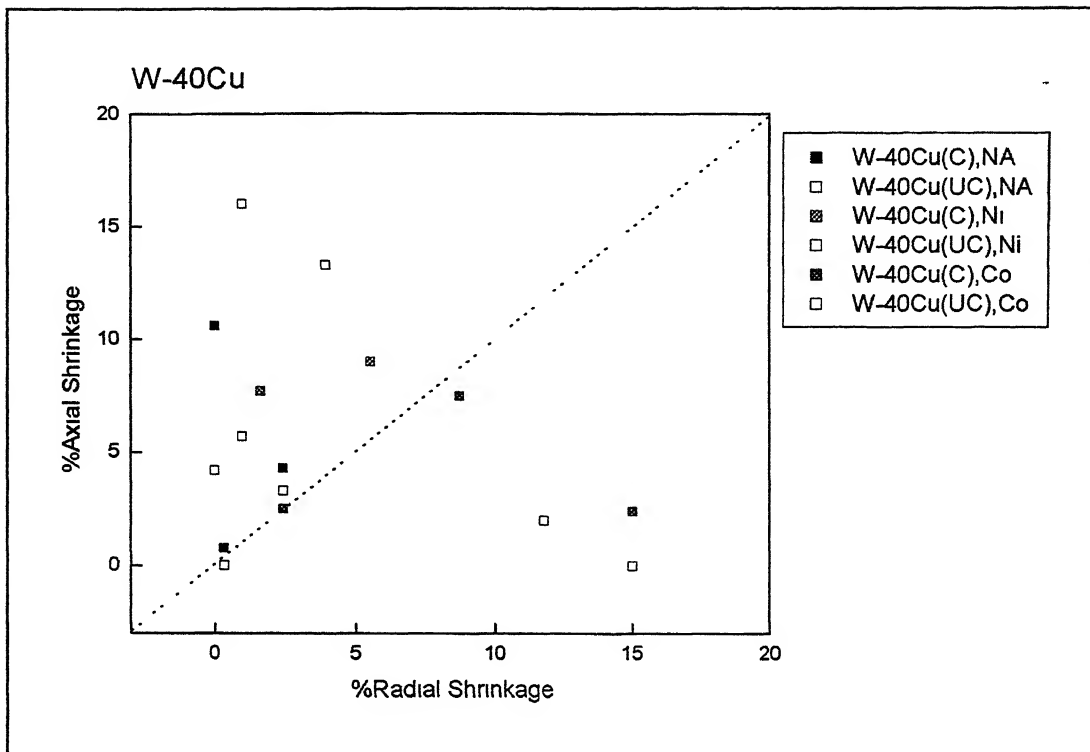
Figure 5.8 shows the micrographs of the coated W-10Cu compacts, sintered at 1400°C, with Ni activator addition. Figure 5.9 is the micrographs of the W-10Cu compacts sintered at same temperature and conditions. The porosity is more in the uncoated samples compared to coated one, which is seen from the micrographs.



(a)

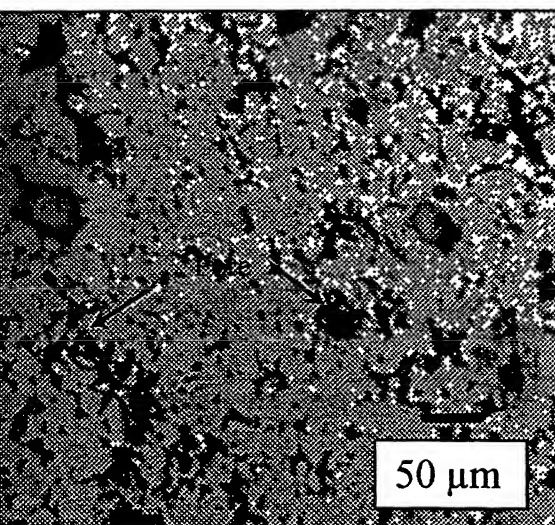


(b)

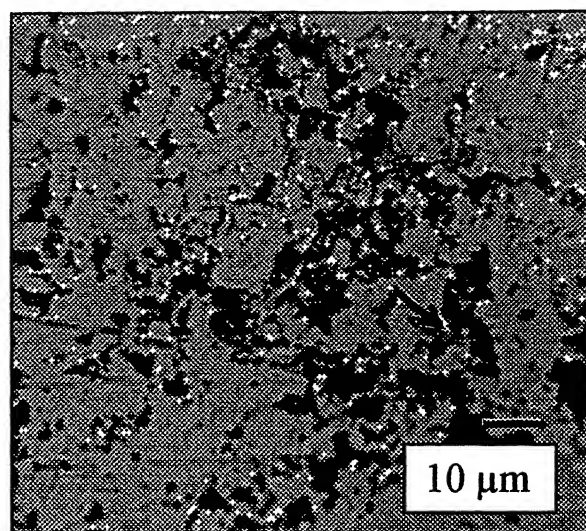


(c)

**Figure 5.3:** Axial versus. Radial shrinkage of (a) W-10Cu; (b) W-25Cu; and (c) W-40Cu samples in coated and uncoated conditions.

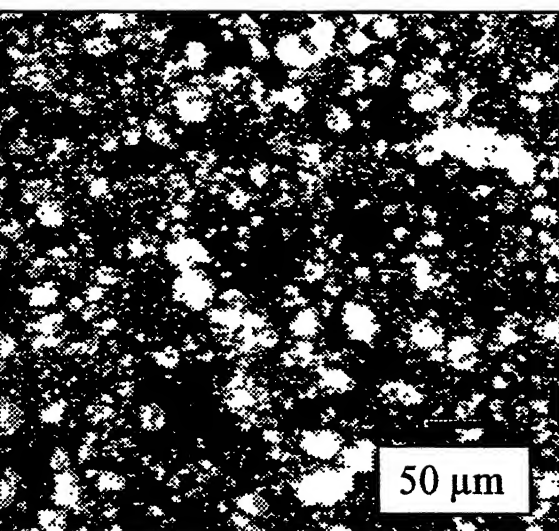


(a)

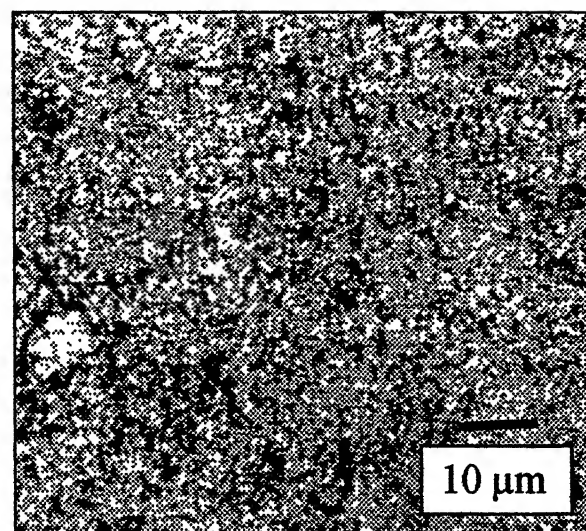


(b)

**Figure 5.4:** Optical micrographs of coated W-10Cu without any activator, sintered at 1000°C (a) 100 $\times$ ; (b) 500 $\times$  magnification.



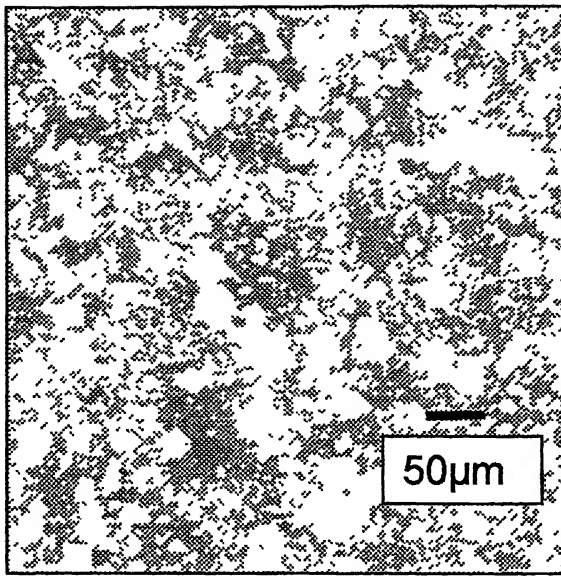
(a)



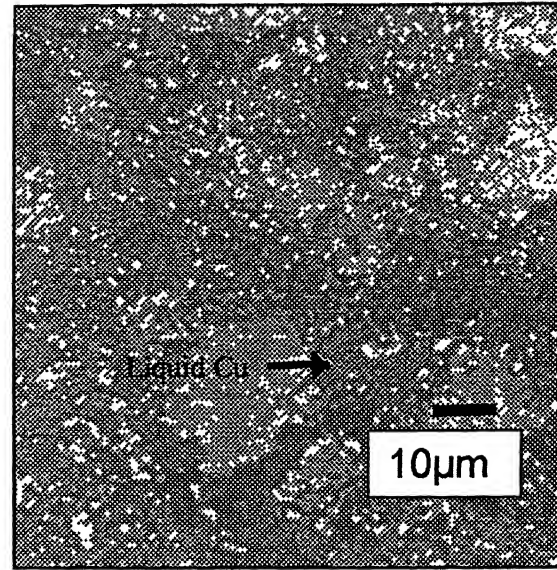
(b)

**Figure 5.5:** Optical micrographs of uncoated W-10Cu without any activator, sintered at 1000°C (a) 100 $\times$ ; (b) 500 $\times$  magnification.



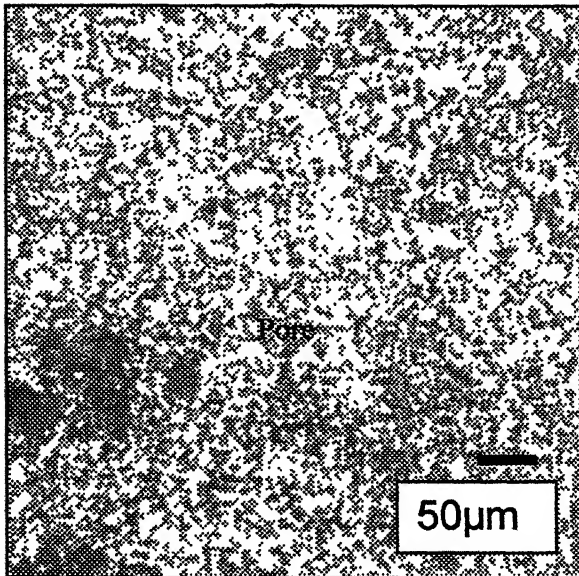


(a)

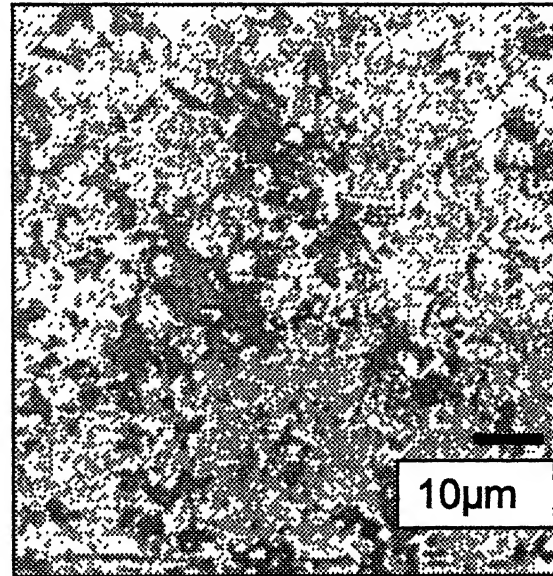


(b)

**Figure 5.6:** Optical micrographs of coated W-10Cu without any activator, sintered at 1400°C (a) 100×; (b) 500× magnification.

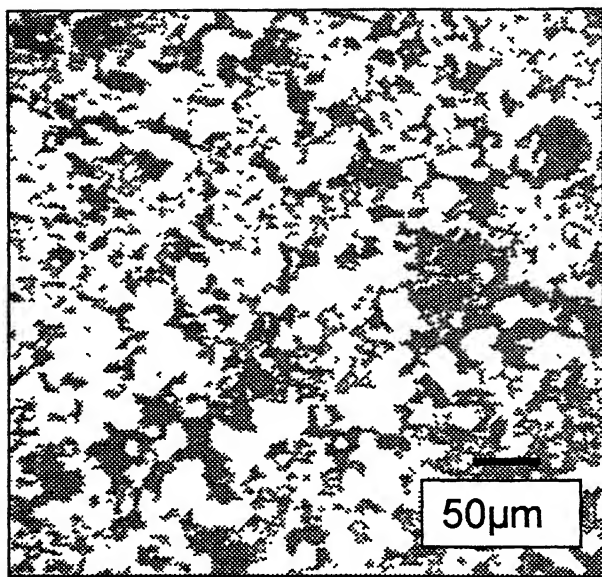


(a)

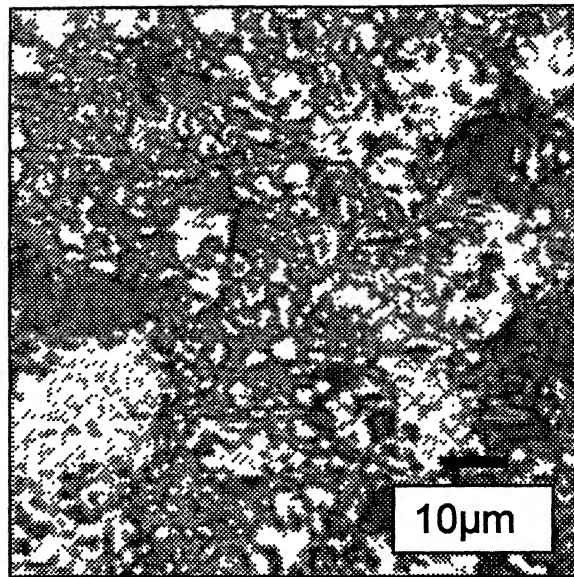


(b)

**Figure 5.7:** Optical micrographs of uncoated W-10Cu without any activator, sintered at 1400°C (a) 100×; (b) 500× magnification.

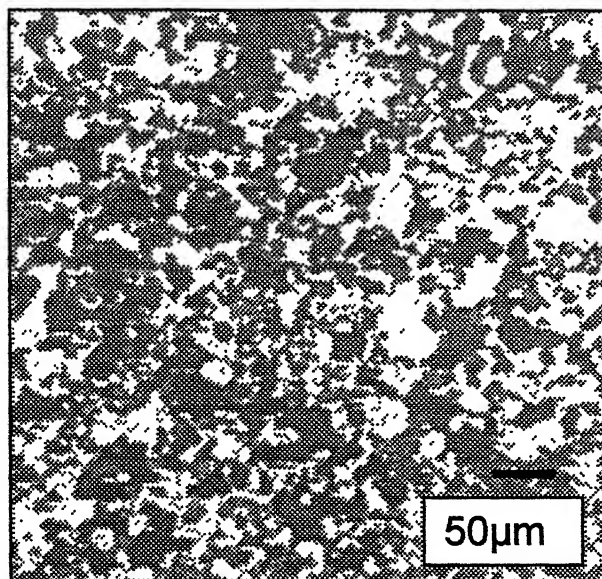


(a)

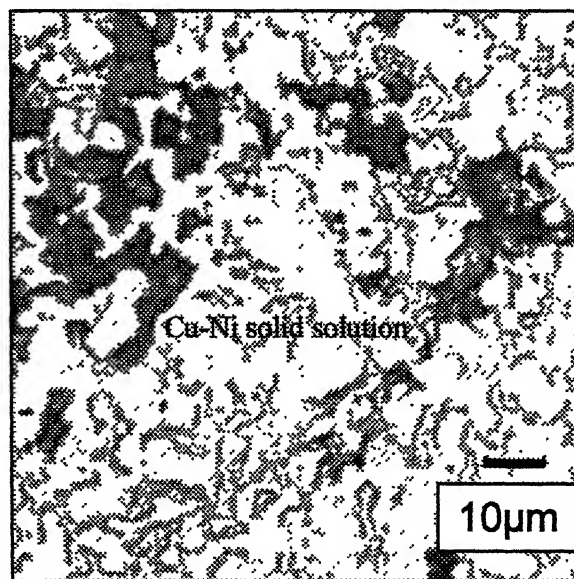


(b)

**Figure 5.8:** Optical micrographs of coated W-10Cu with Ni activator, sintered at 1400°C (a) 100×; (b) 500× magnification.



(a)



(b)

**Figure 5.9:** Optical micrographs of uncoated W-10Cu with Ni activator, sintered at 1400°C (a) 100×; (b) 500× magnification.

Figure 5.10 shows the micrographs of the coated W-10Cu compacts, sintered at 1400°C, with Co activator addition. Figure 5.11 is the micrographs of the uncoated W-10Cu compacts sintered at same temperature and conditions. It is well known that Co is immiscible in Cu. So in both the samples we get the true color of the Cu melt.

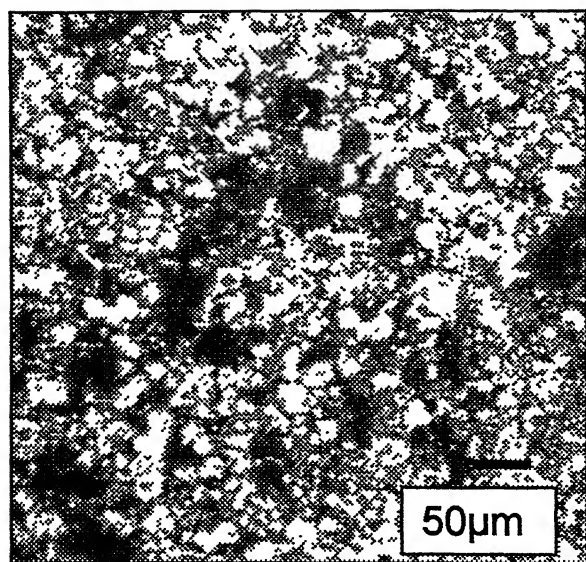
Figure 5.12 shows the micrographs of the coated W-10Cu compacts, sintered at 1400°C, with Fe activator addition. Figure 5.13 is the micrographs of the uncoated W-10Cu compacts sintered at same temperature and conditions. Here the amount of porosity is substantially less than that of the samples which are sintered at 1000°C.

Figure 5.14 shows the micrographs of the coated W-40Cu compacts, sintered at 1400°C, without activator addition. Figure 5.15 is the micrographs of the uncoated W-40Cu compacts sintered at same temperature and conditions. Here the amount of Cu melt is more than the W-10Cu compacts. Clearly the W-W grain contacts are visible in the microstructure.

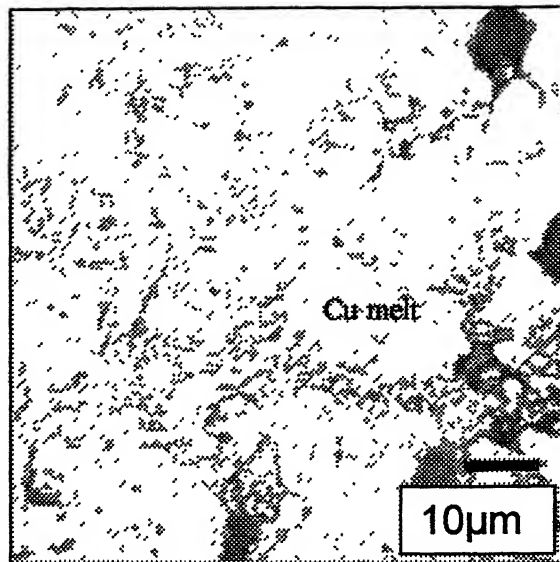
Figure 5.16 shows the micrographs of the coated W-40Cu compacts, sintered at 1400°C, with Ni activator addition. Figure 5.17 is the micrographs of the uncoated W-40Cu compacts sintered at same temperature and conditions.

Figure 5.18 shows the micrographs of the coated W-40Cu compacts, sintered at 1400°C, with Co activator addition. Figure 5.19 is the micrographs of the uncoated W-40Cu compacts sintered at same temperature and conditions.

Figure 5.20 shows the micrographs of the coated W-40Cu compacts, sintered at 1400°C, with Fe activator addition. Figure 5.21 is the micrographs of the uncoated W-40Cu compacts sintered at same temperature and conditions.

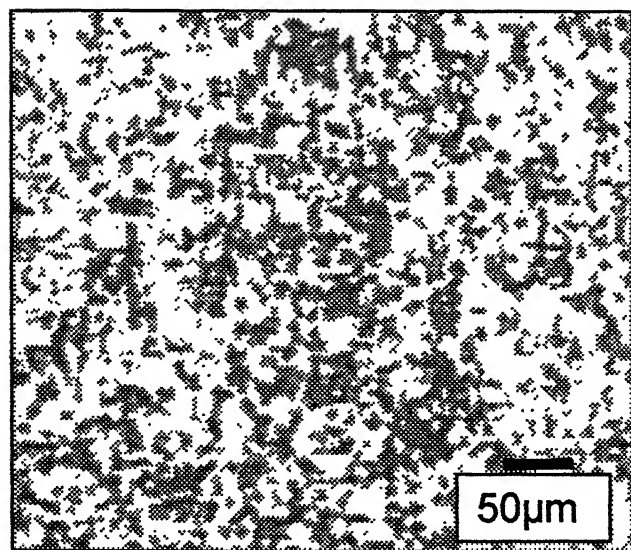


(a)

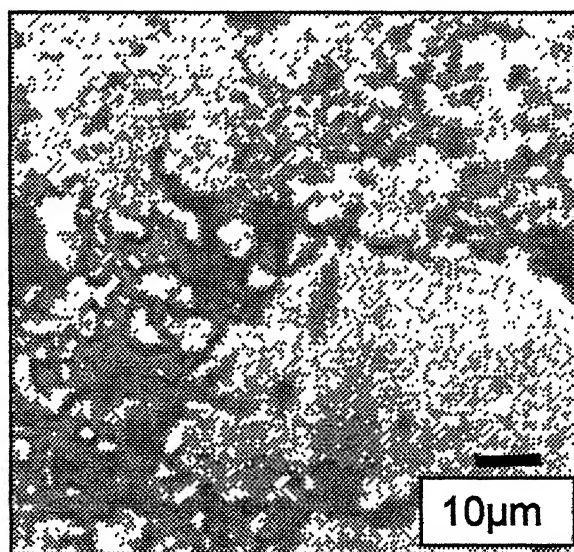


(b)

**Figure 5.10:** Optical micrographs of coated W-10Cu with Co activator, sintered at 1400°C (a) 100×; (b) 500× magnification.



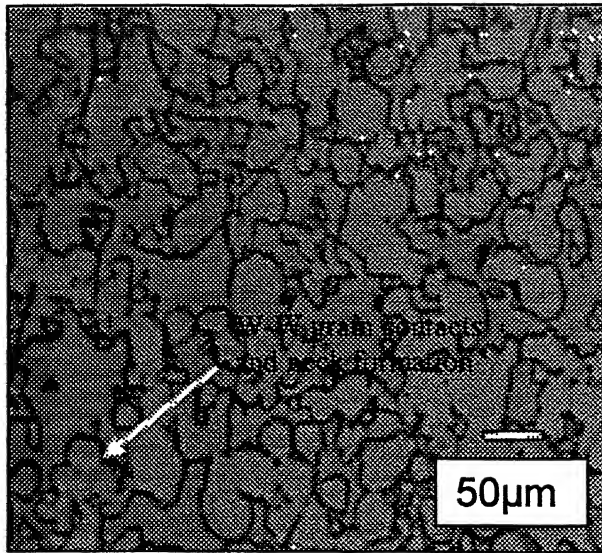
(a)



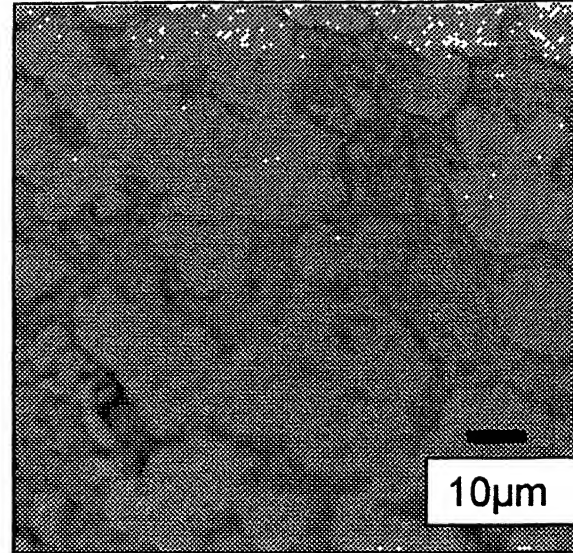
(b)

**Figure 5.11:** Optical micrographs of uncoated W-10Cu with Co activator, sintered at 1400°C (a) 100×; (b) 500× magnification.



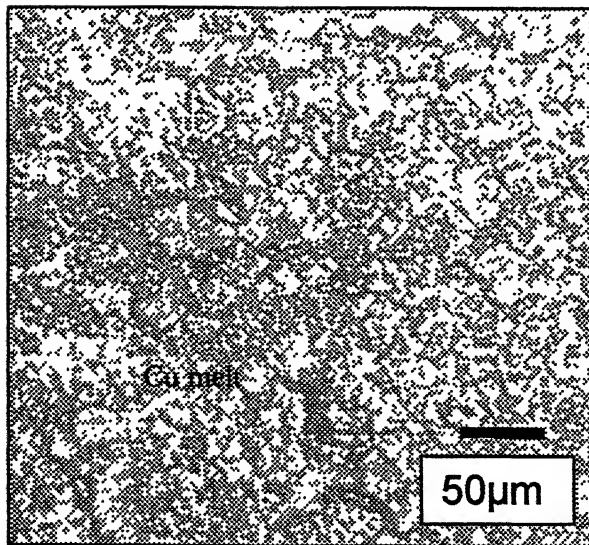


(a)

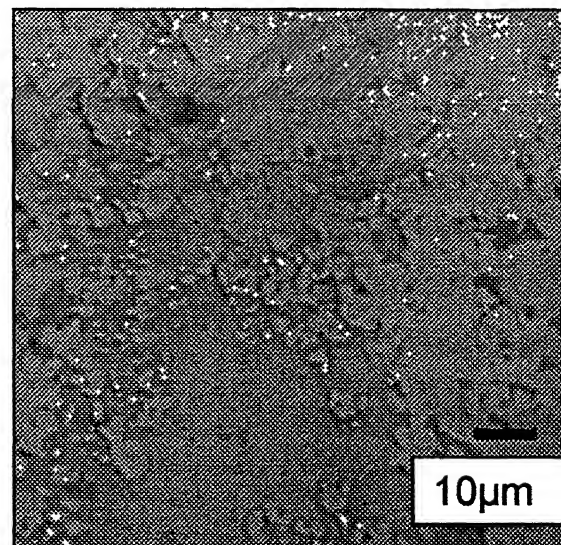


(b)

**Figure 5.14:** Optical micrographs of coated W-40Cu without activator, sintered at 1400°C (a) 100×; (b) 500× magnification.

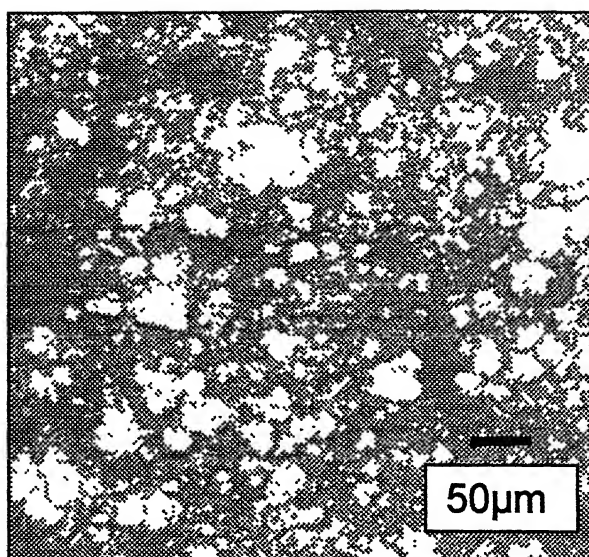


(a)

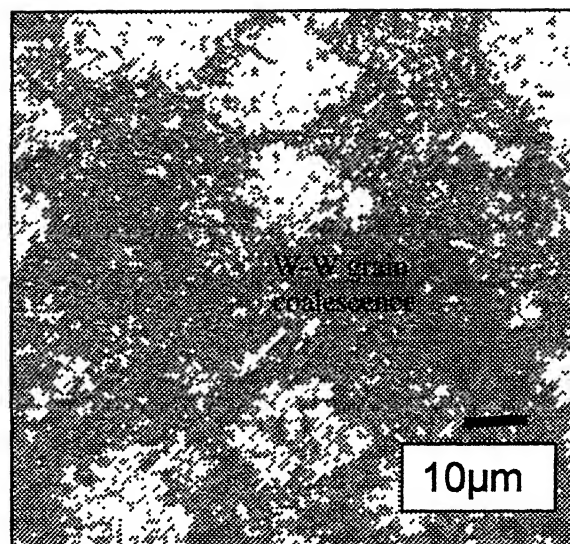


(b)

**Figure 5.15:** Optical micrographs of uncoated W-40Cu without activator, sintered at 1400°C (a) 100×; (b) 500× magnification.

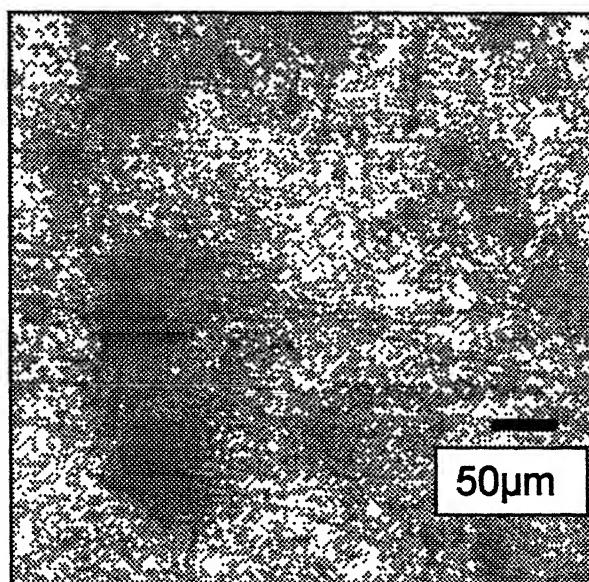


(a)

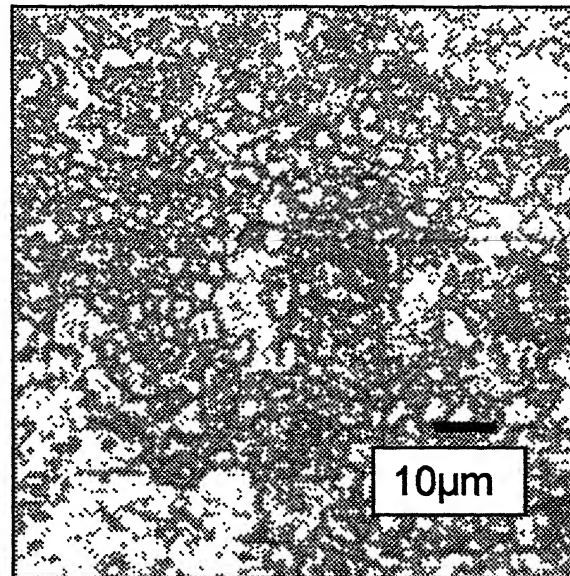


(b)

**Figure 5.16:** Optical micrographs of coated W-40Cu with Ni activator, sintered at 1400°C (a) 100×; (b) 500× magnification.

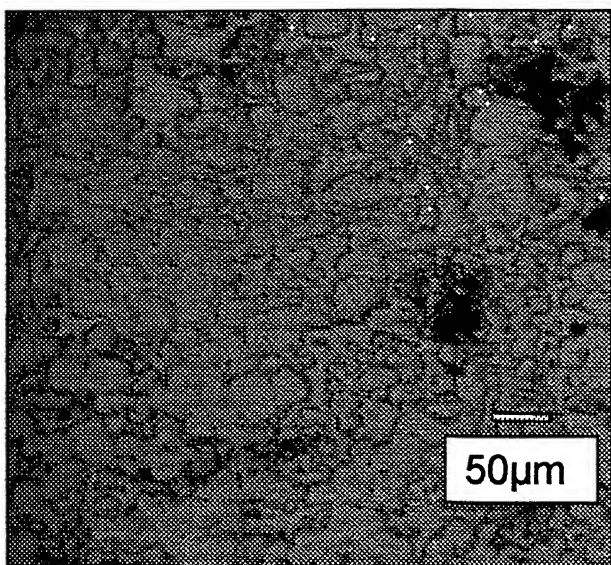


(a)

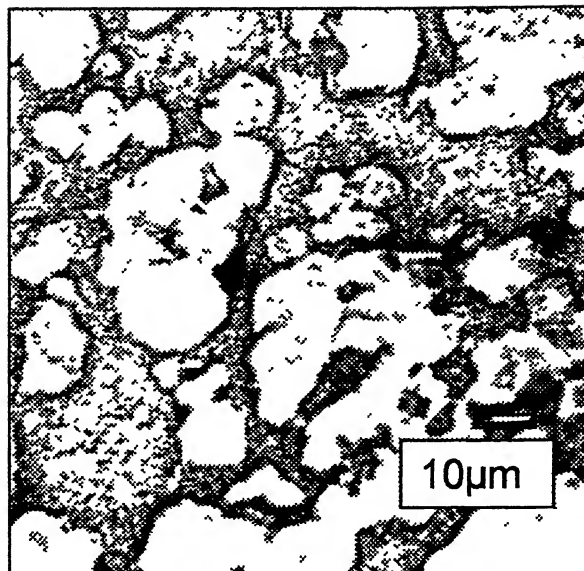


(b)

**Figure 5.17:** Optical micrographs of uncoated W-40Cu with Ni activator, sintered at 1400°C (a) 100×; (b) 500× magnification.

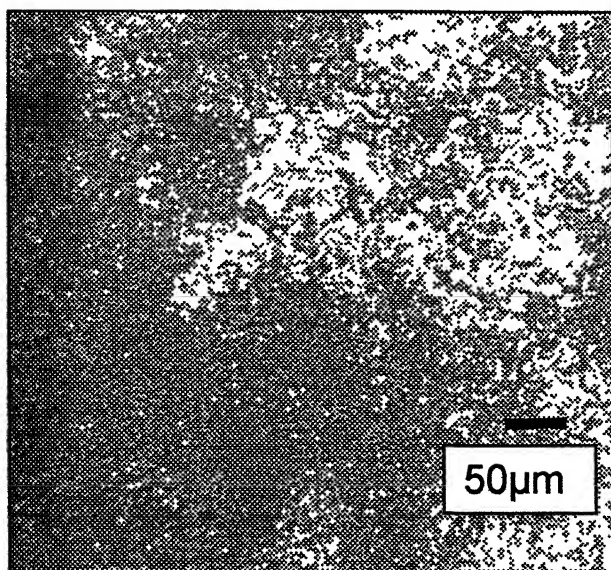


(a)

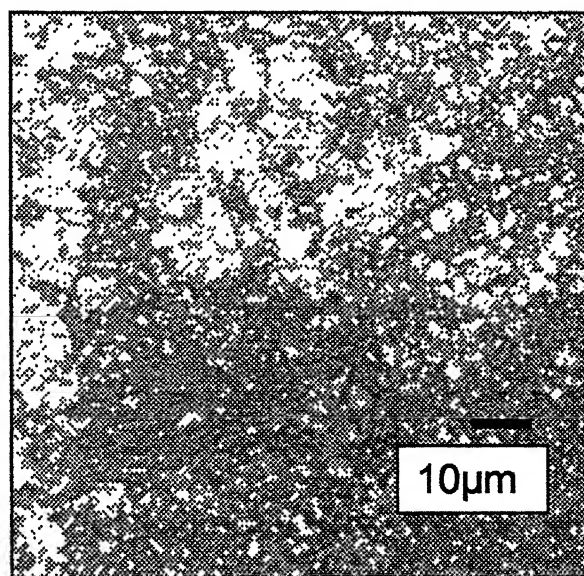


(b)

**Figure 5.18:** Optical micrographs of coated W-40Cu with Co activator, sintered at 1400°C (a) 100×; (b) 500× magnification.



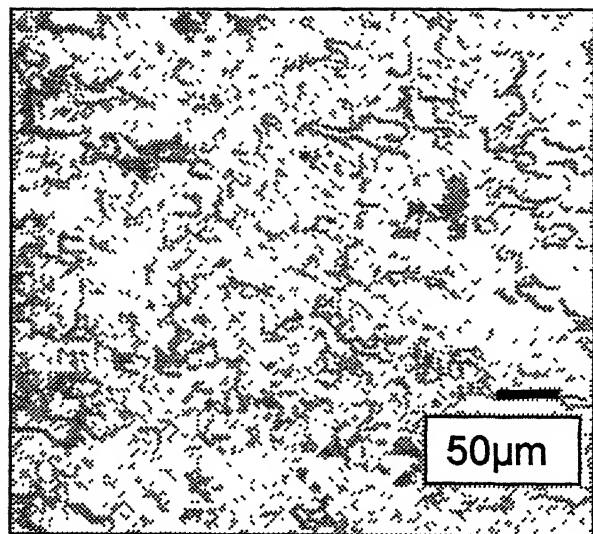
(a)



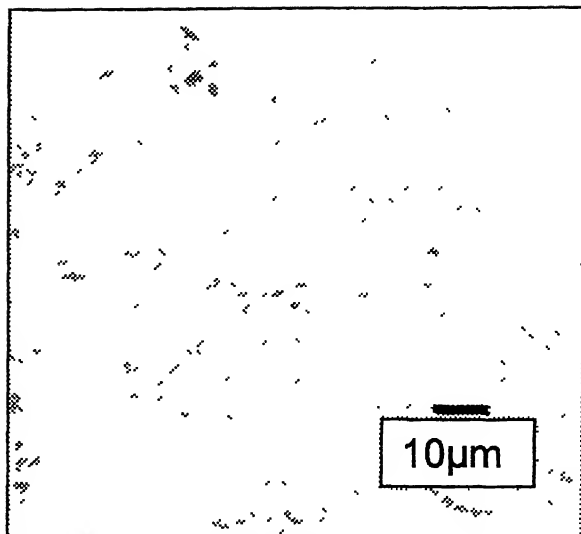
(b)

**Figure 5.19:** Optical micrographs of uncoated W-40Cu with Co activator, sintered at 1400°C (a) 100×; (b) 500× magnification.



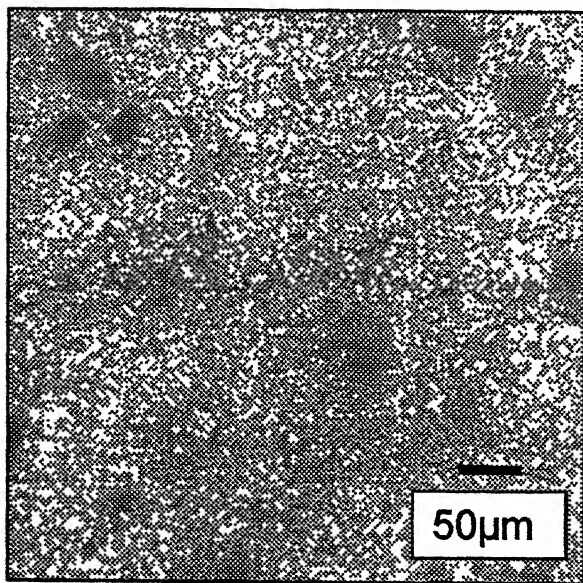


(a)

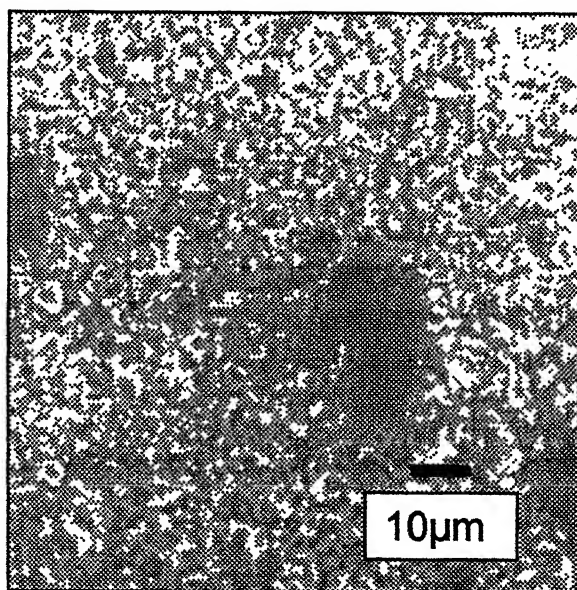


(b)

**Figure 5.20:** Optical micrographs of coated W-40Cu with Fe activator, sintered at 1400°C (a) 100×; (b) 500× magnification



(a)



(b)

**Figure 5.21:** Optical micrographs of uncoated W-40Cu with Fe activator, sintered at 1400°C (a) 100×; (b) 500× magnification.



## 5.4 SEM microscopy

Figure 5.22 shows the SEM micrographs of the coated W-10Cu samples. The samples are sintered at 1000°C. Figure 5.23 shows the same microstructure of the uncoated samples. The presence of pore is more in the second case than that of the first one. The black portions in the microstructure are the possible positions of the pores. The distribution of Cu is more homogeneous in coated samples than that of the uncoated one.

Figure 5.24 shows the micrographs of the W-10Cu compacts, sintered at 1400°C, without any activator addition. The pores are more in the uncoated samples compared to coated one.

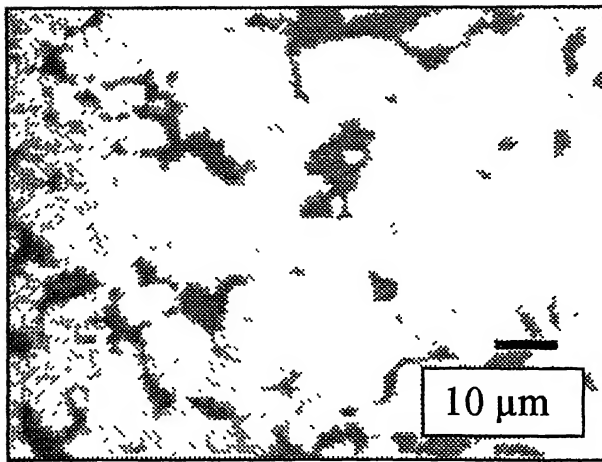
Figure 5.25 shows the micrographs of the W-10Cu compacts, sintered at 1400°C, with Ni activator addition. The pores are more in the uncoated samples compared to coated one.

Figure 5.26 shows the micrographs of the W-10Cu compacts, sintered at 1400°C, with Co activator addition. The pores are more in the uncoated samples compared to coated one.

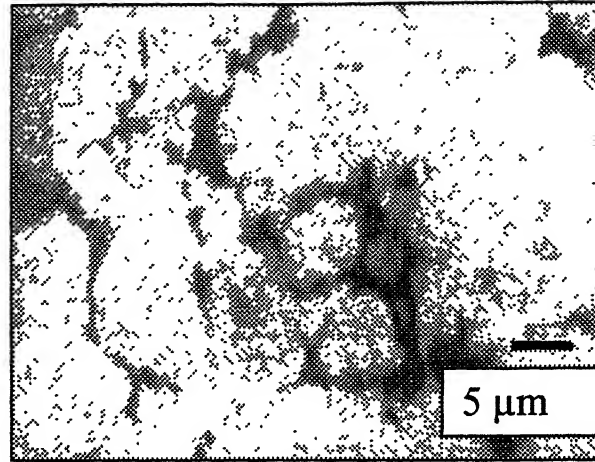
Figure 5.27 shows the micrographs of the W-10Cu compacts, sintered at 1400°C, with Fe activator addition. The pores are more in the uncoated samples compared to coated one.

Figure 5.28 shows the micrographs of the W-40Cu compacts, sintered at 1400°C, without activator addition. Here the amount of Cu melt is more than the W-10Cu compacts. Clearly the W-W grain contacts are visible in the microstructure.

Figure 5.29 shows the micrographs of the W-40Cu compacts, sintered at 1400°C, with Ni activator addition. Here the amount of Cu melt is more than the W-10Cu compacts. Clearly, the W-W grain contacts are visible in the microstructure.

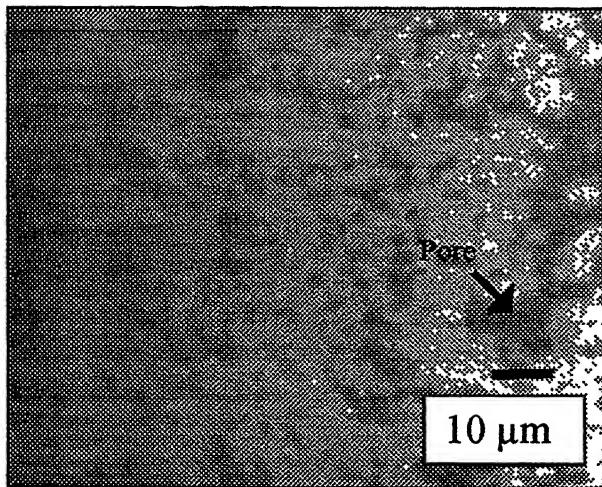


(a)

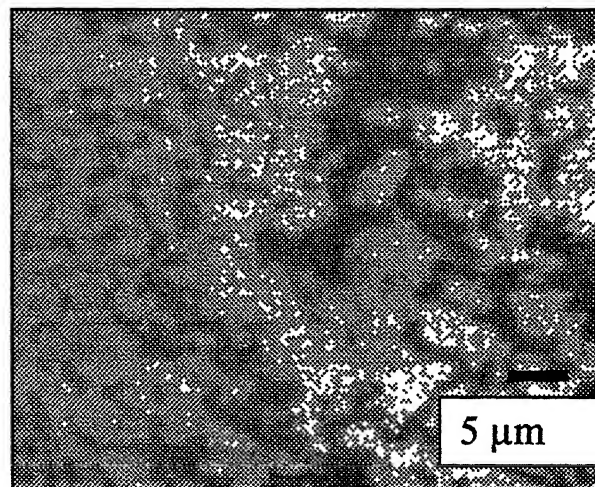


(b)

**Figure 5.22:** SEM micrographs of W-10Cu (C) without activator, sintered at 1000°C (a) 1000×; (b) 3000× magnification.



(a)



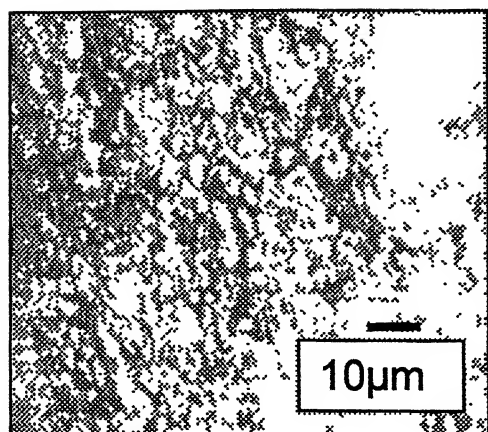
(b)

**Figure 5.23:** SEM micrographs of W-10Cu (UC) without activator, sintered at 1000°C (a) 1000×; (b) 3000× magnification.

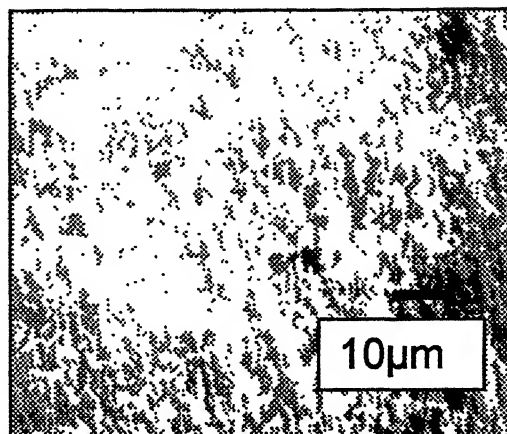
## W-10Cu, no activator

Coated

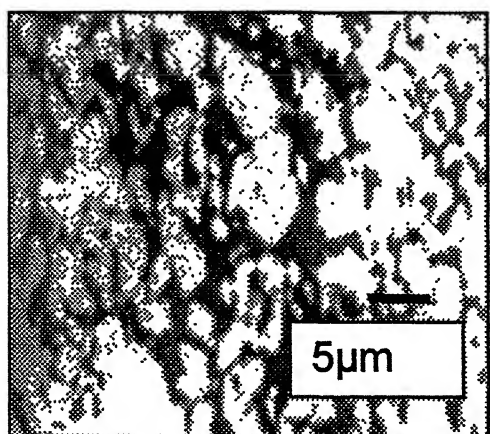
Uncoated



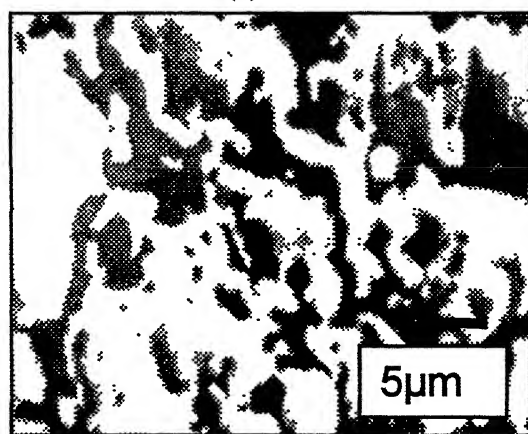
(a)



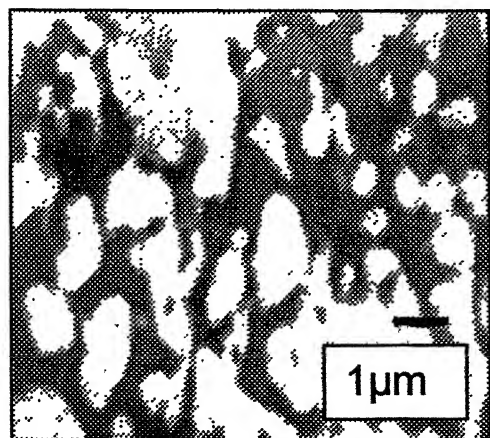
(b)



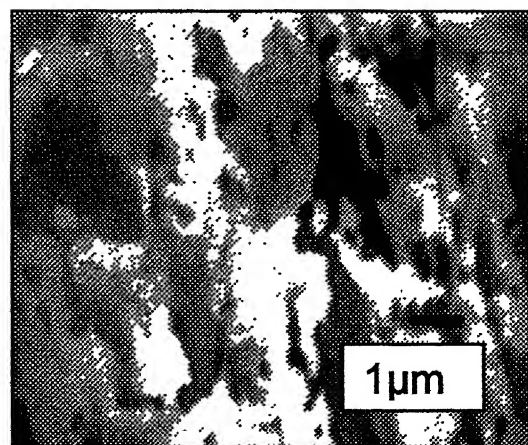
(c)



(d)



(e)



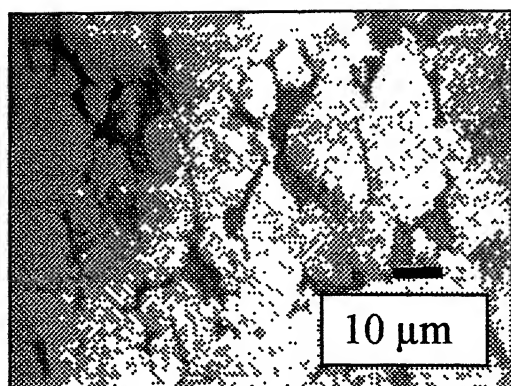
(f)

**Figure 5.24:** SEM micrographs of W-10Cu without activator, sintered at 1400°C (a) and (b) 1000×; (c) and (d) 3000×; (e) and (f) 6000× magnification

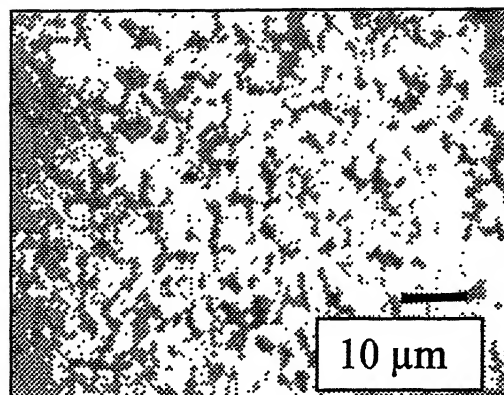
## W-10Cu, Ni activator

Coated

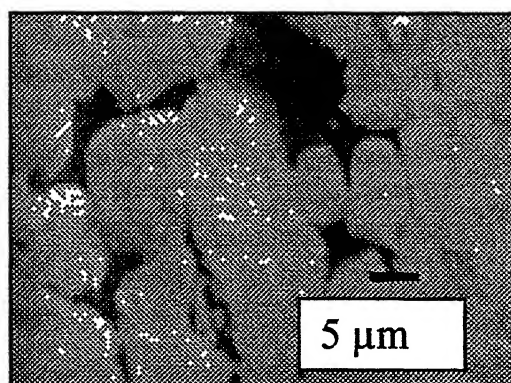
Uncoated



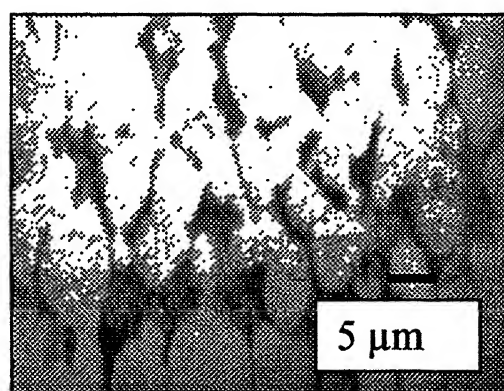
(a)



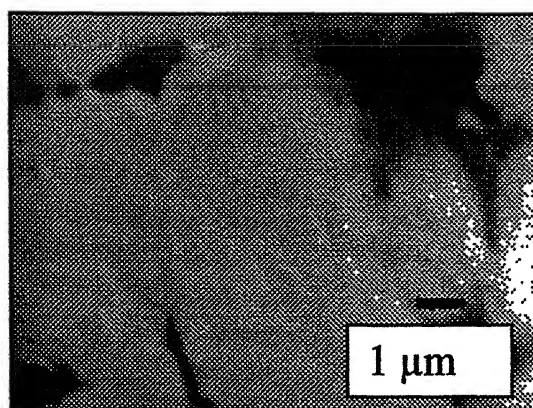
(b)



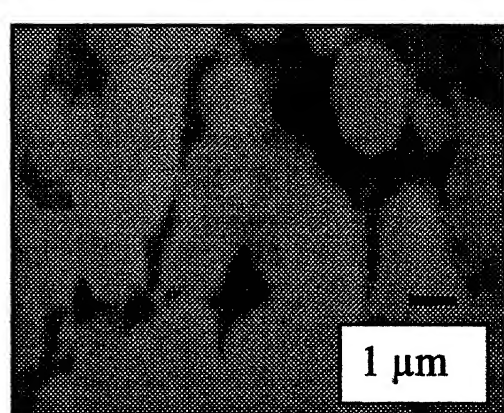
(c)



(d)



(e)

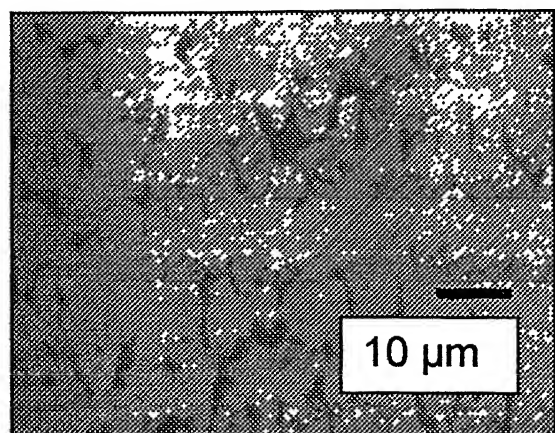


(f)

**Figure 5.25:** SEM micrographs of W-10Cu with Ni activator, sintered at 1400°C (a) and (b) 1000×; (c) and (d) 3000×; (e) and (f) 6000× magnification.

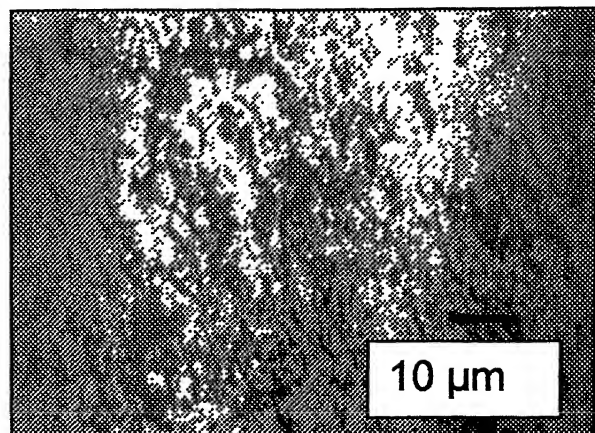
## W-10Cu, Co activator

Coated

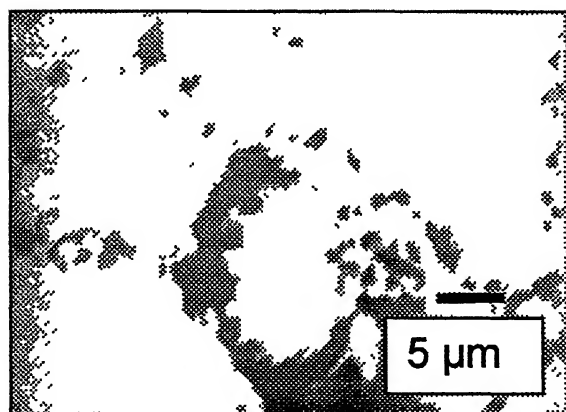


(a)

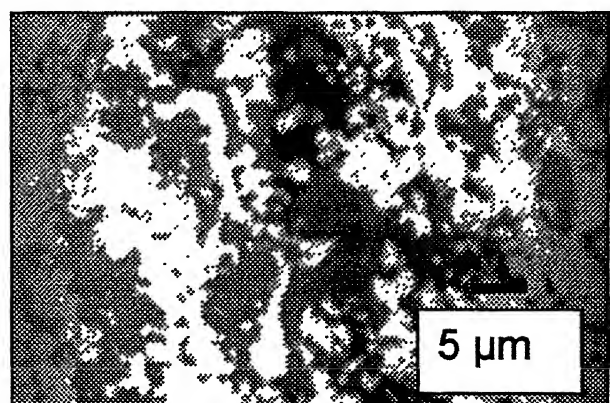
Uncoated



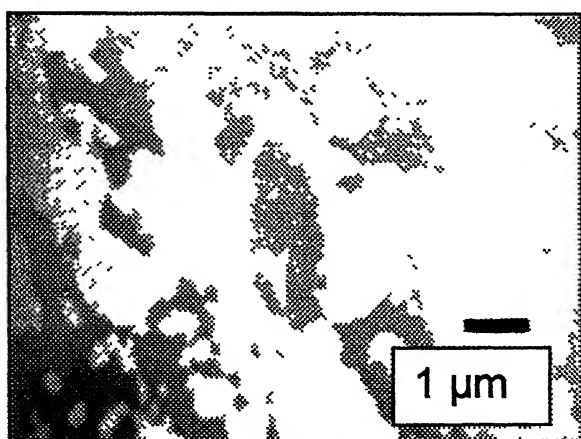
(b)



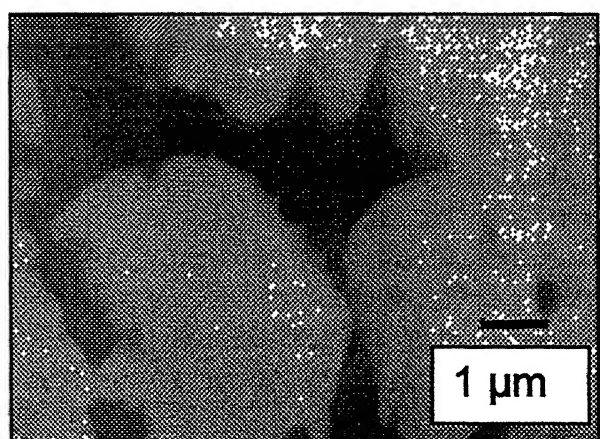
(c)



(d)



(e)



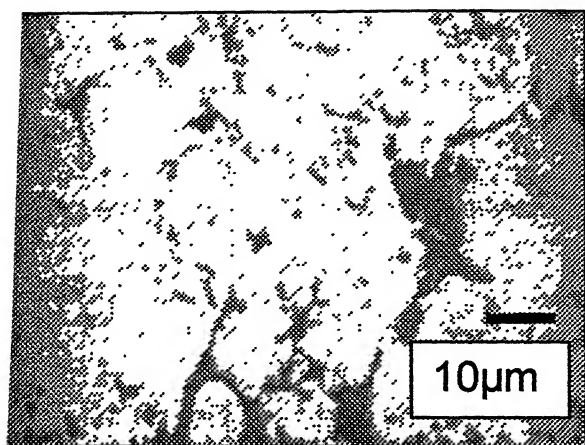
(f)

**Figure 5.26:** SEM micrographs of W-10Cu with Co activator, sintered at 1400°C (a)



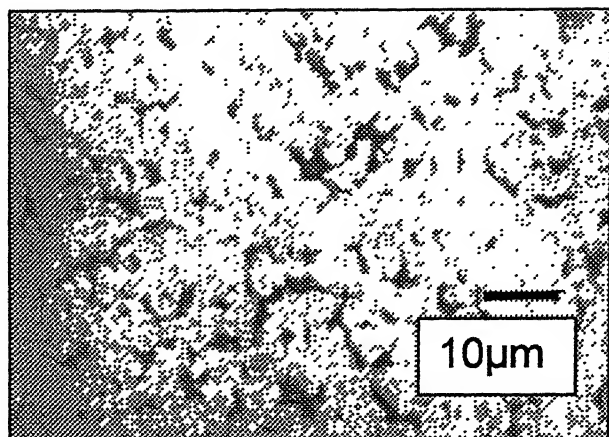
## W-10Cu, Fe activator

Coated

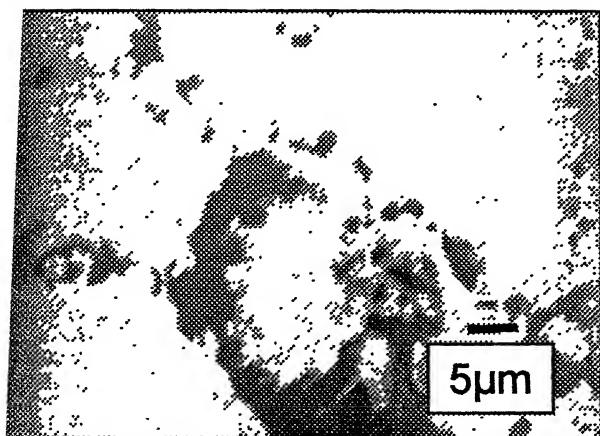


(a)

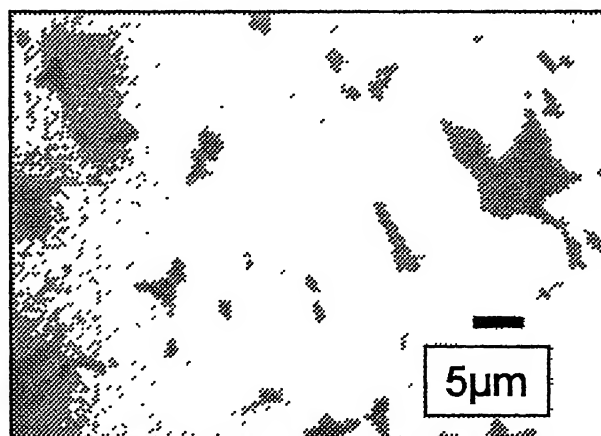
Uncoated



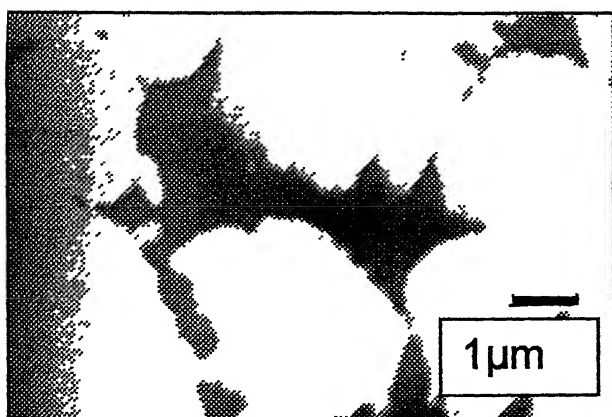
(b)



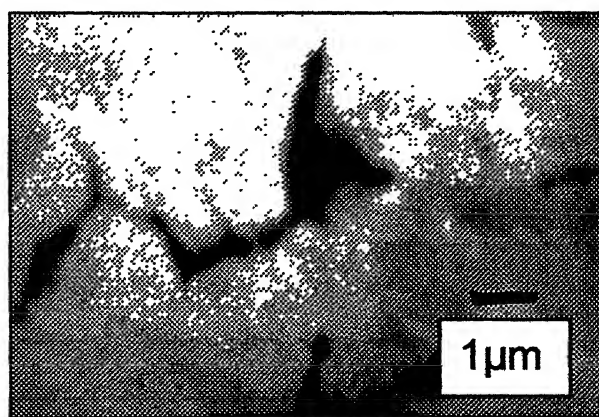
(c)



(d)



(e)



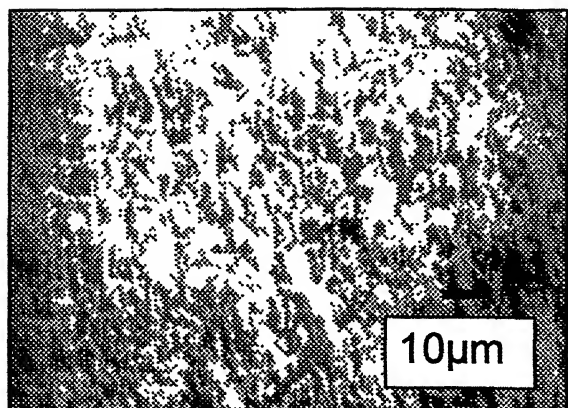
(f)

**Figure 5.27:** SEM micrographs of W-10Cu with Fe activator, sintered at 1400°C (a) and (b) 1000×; (c) and (d) 3000×; (e) and (f) 6000× magnification.

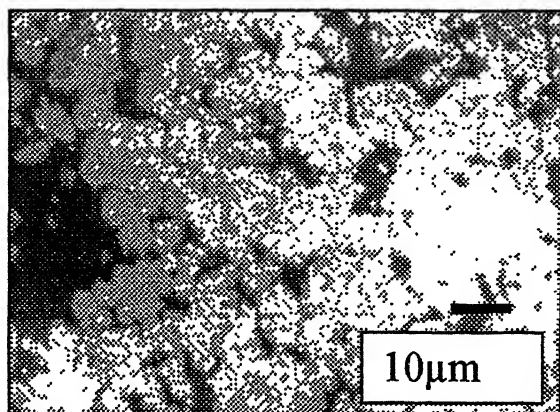
## W-40Cu, no activator

Coated

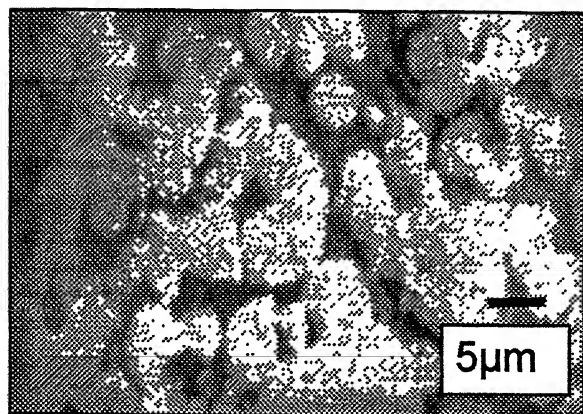
Uncoated



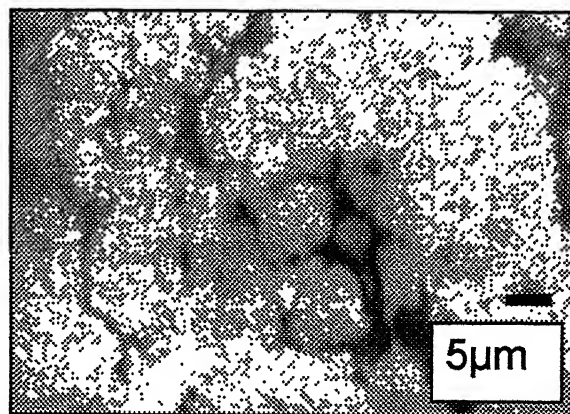
(a)



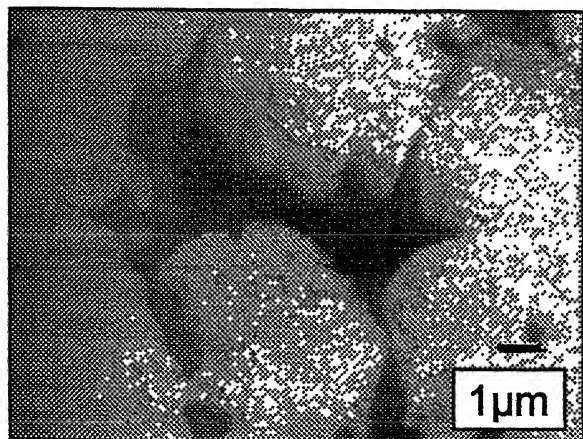
(b)



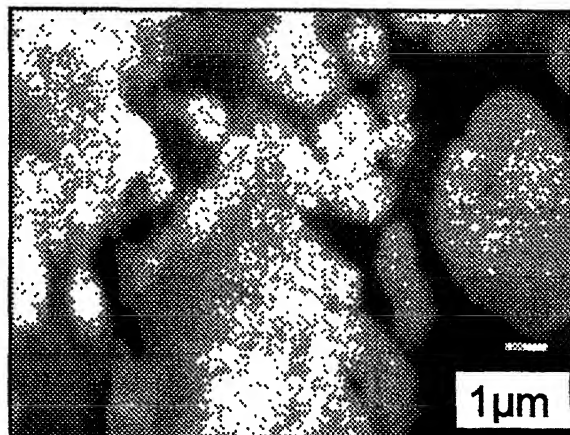
(c)



(d)



(e)

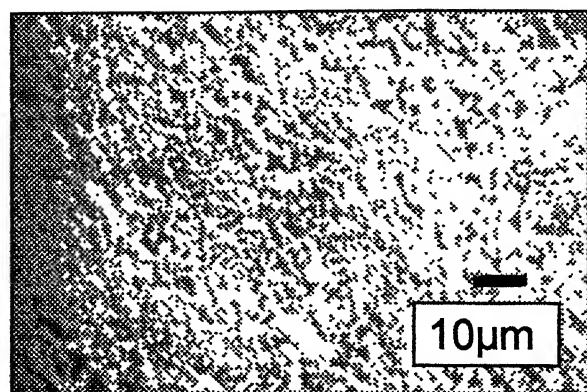


(f)

Figure 5.28: SEM micrographs of W-40Cu with Fe activator, sintered at 1400°C (a)

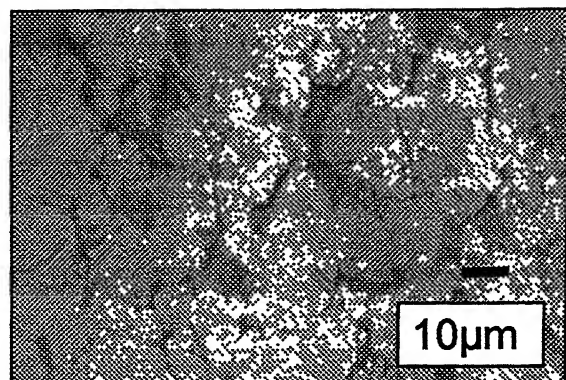
## W-40Cu, Ni activator

Coated

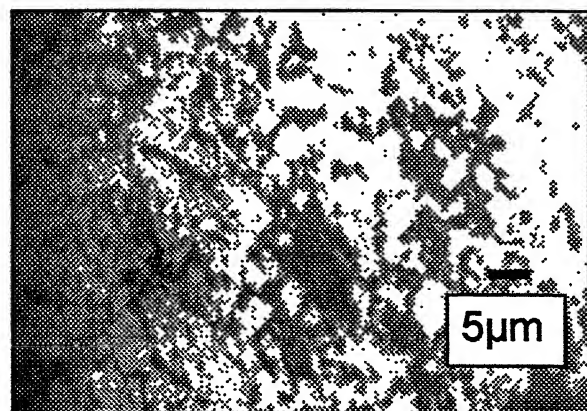


(a)

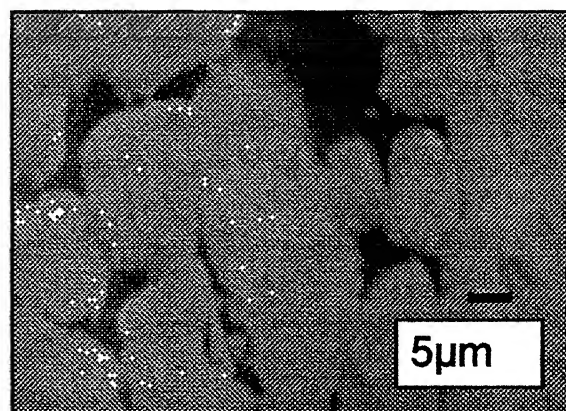
Uncoated



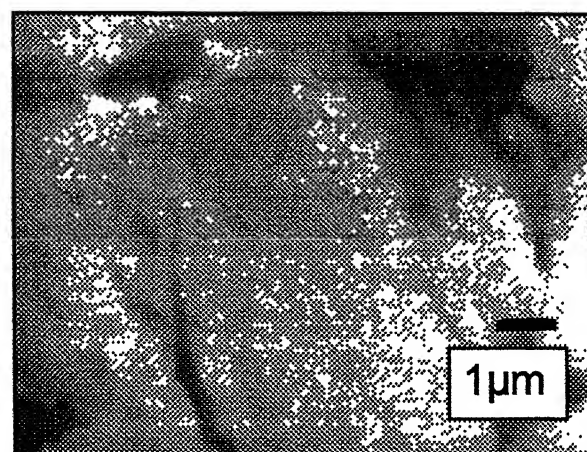
(b)



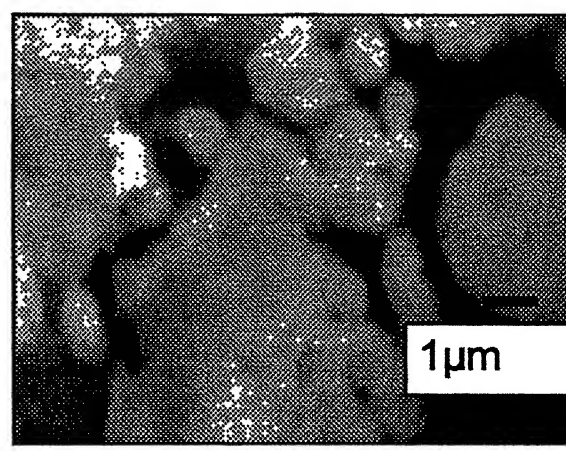
(c)



(d)



(e)



(f)

**Figure 5.29:** SEM micrographs of W-40Cu with Ni activator, sintered at 1400°C (a) and (b) 1000×; (c) and (d) 3000×; (e) and (f) 6000× magnification.



Figure 5.30 shows the micrographs of the W-40Cu compacts, sintered at 1400°C, with Co activator addition

Figure 5.31 shows the micrographs of the W-40Cu compacts, sintered at 1400°C, with Fe activator addition.

## 5.5 Hardness

The hardness values are given in the Appendix IV. Figures 5.32a to 5.32c compare the effect of activator addition on W-Cu alloys with varying Cu contents on the hardness at 1000°C, 1200°, and 1400°C, respectively. For all compositions, the hardness of the compacts increases with increasing temperature. However, for a particular sintering temperature, the hardness decreases as the Cu content is increased, irrespective of the activator addition. As compared to the uncoated samples, the coated samples in general have a marginally higher hardness. It is interesting to note that for both coated and uncoated samples, addition of activators enhances the hardness. The positive role of activators in hardness enhancement is more pronounced during liquid phase sintering (1200° and 1400°C).

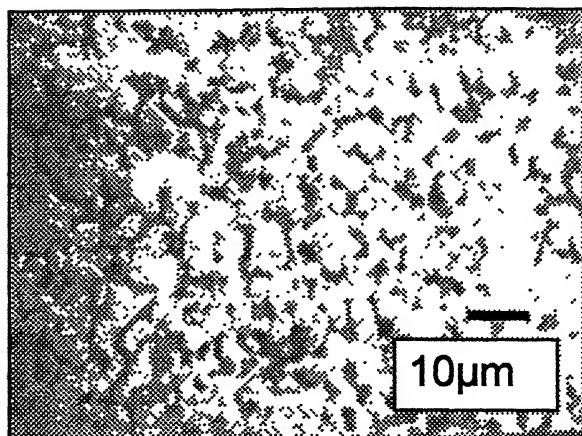
## 5.6 Compressive test

The compressive strength for some of the selective samples is taken. All the coppers are dissolved first and then the compressive strengths are measured. So it essentially gives the W-W skeleton strength. The compressive strength values are shown in Figure 5.33.

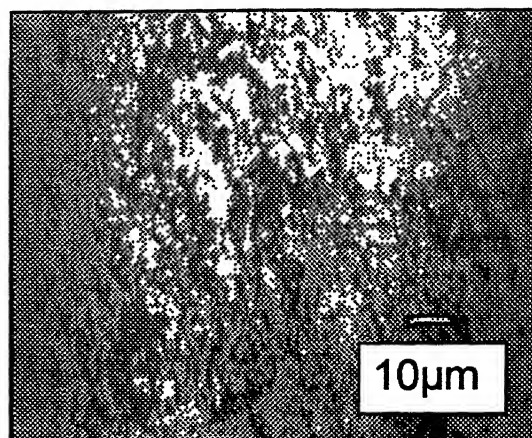
## W-40Cu, Co activator

Coated

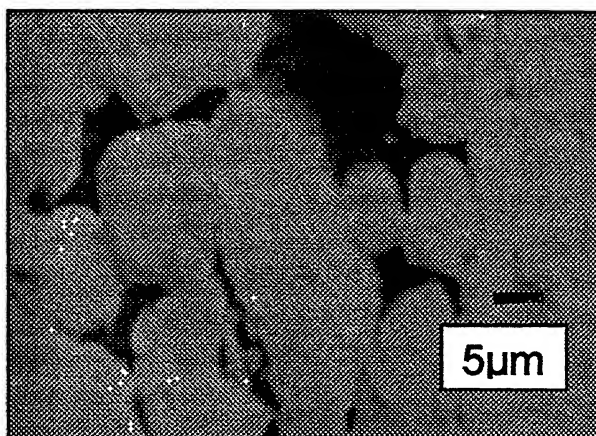
Uncoated



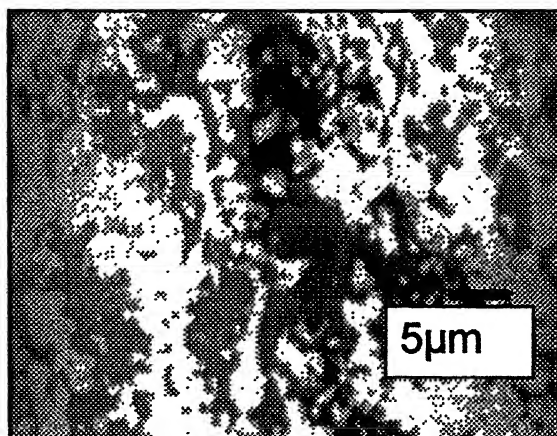
(a)



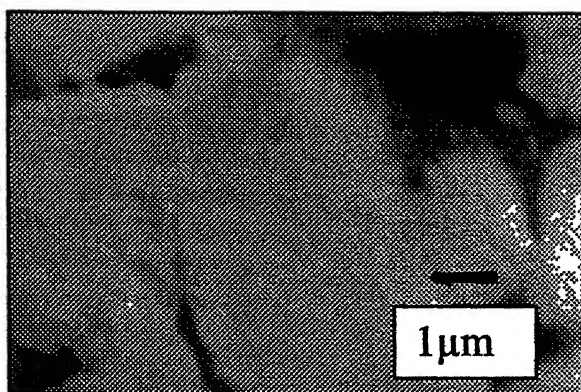
(b)



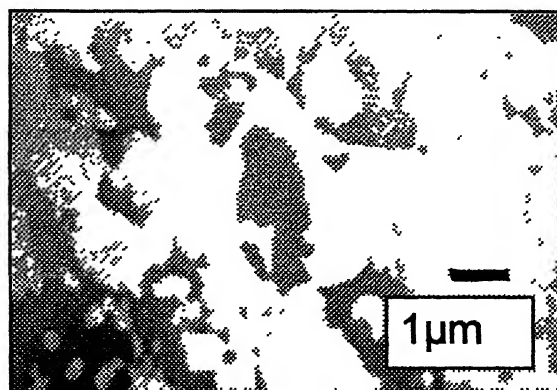
(c)



(d)



(e)



(f)

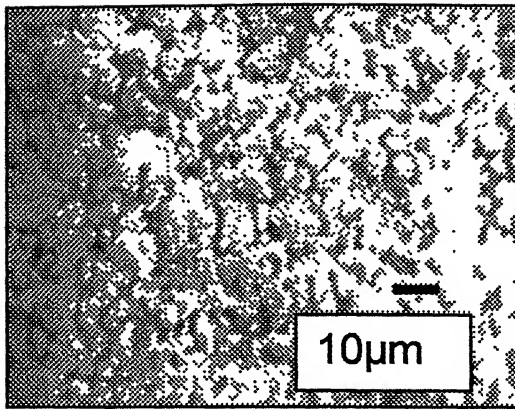
**Figure 5.30:** SEM micrographs of W-40Cu with Co activator, sintered at 1400°C (a)

and (b) 1000×; (c) and (d) 2000×; (e) and (f) 5000× magnification

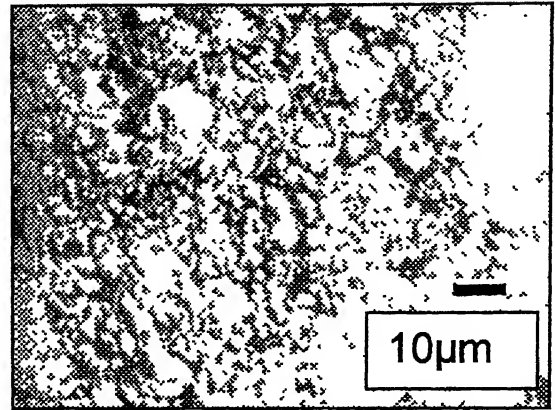
## W-40Cu, Fe activator

Coated

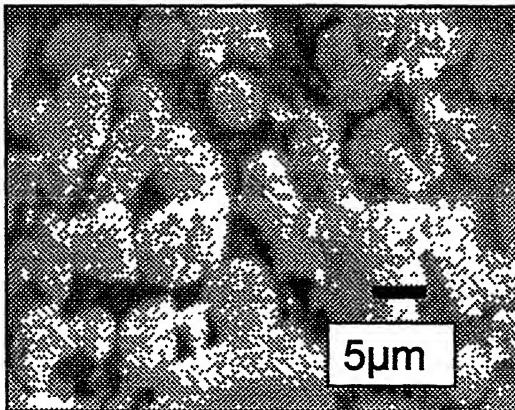
Uncoated



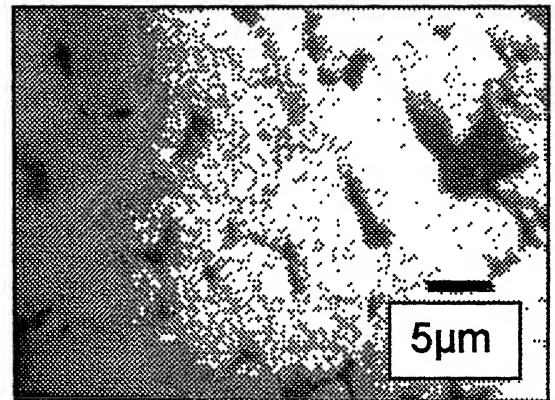
(a)



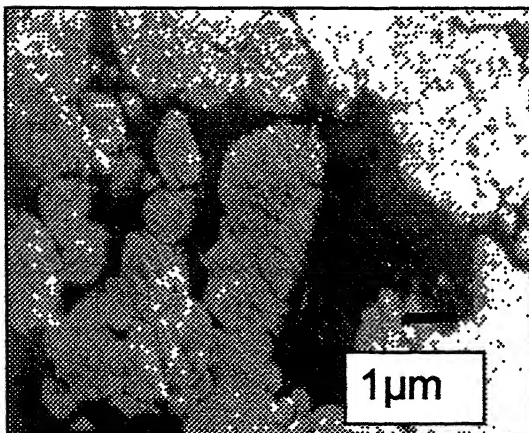
(b)



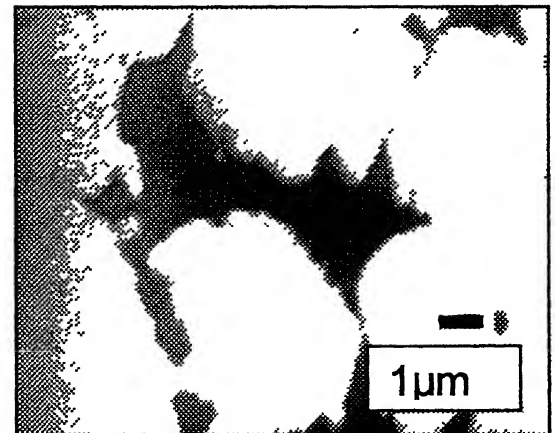
(c)



(d)

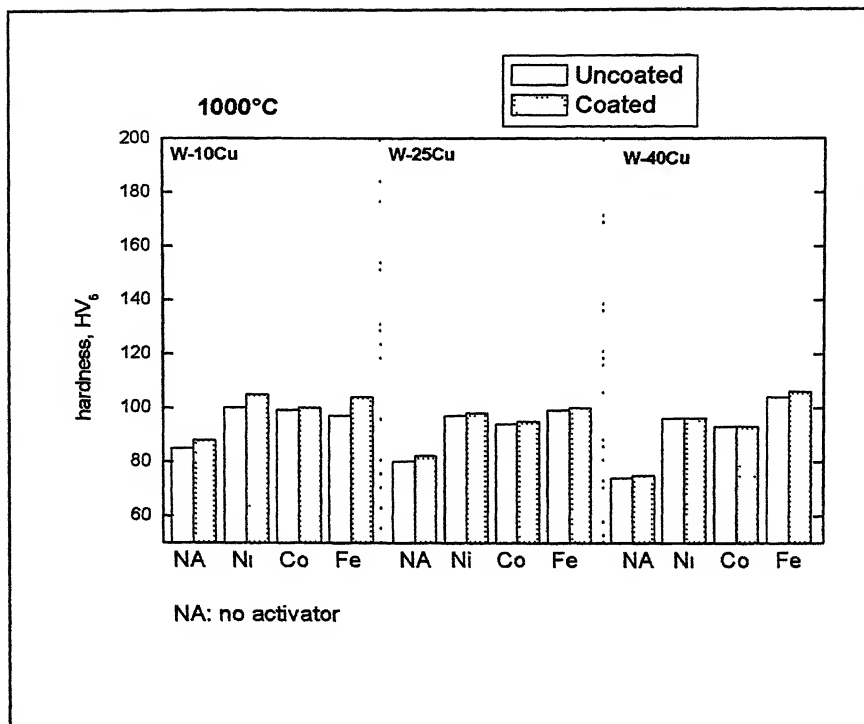


(e)

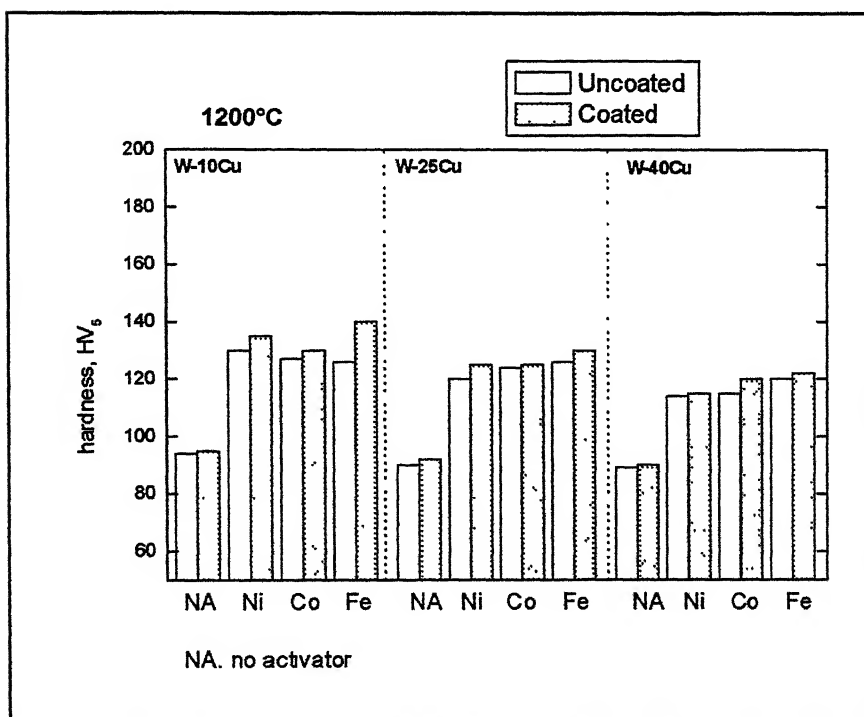


(f)

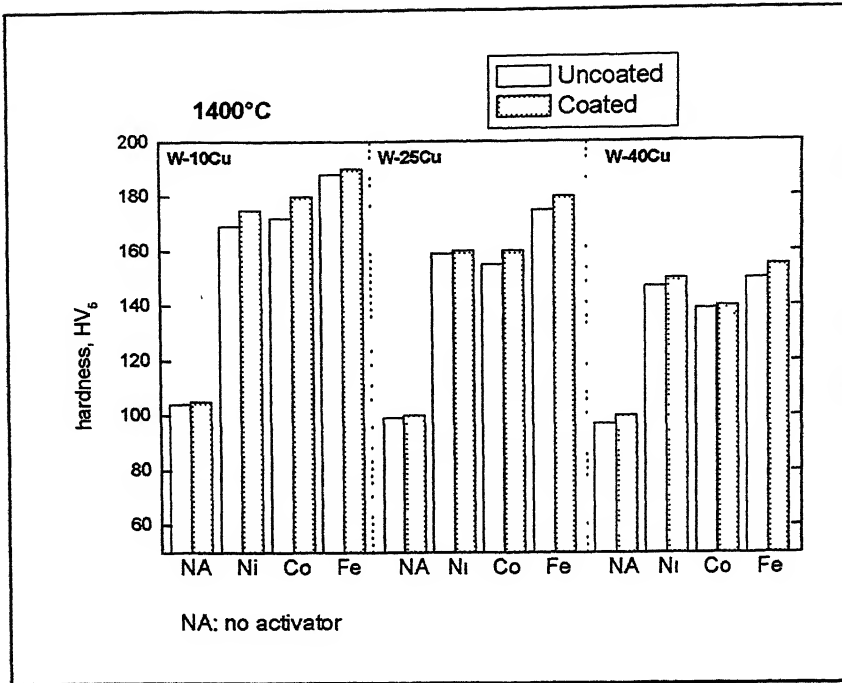
**Figure 5.31:** SEM micrographs of W-40Cu with Co activator, sintered at 1400°C (a) and (b) 1000 $\times$ ; (c) and (d) 3000 $\times$ ; (e) and (f) 6000 $\times$  magnification



(a)



(b)



(c)

**Figure 5.32:** Effect of Cu content, coating, and activator addition on the hardness of W-Cu alloys sintered at (a) 1000°C, (b) 1200°C, and (c) 1400°C.

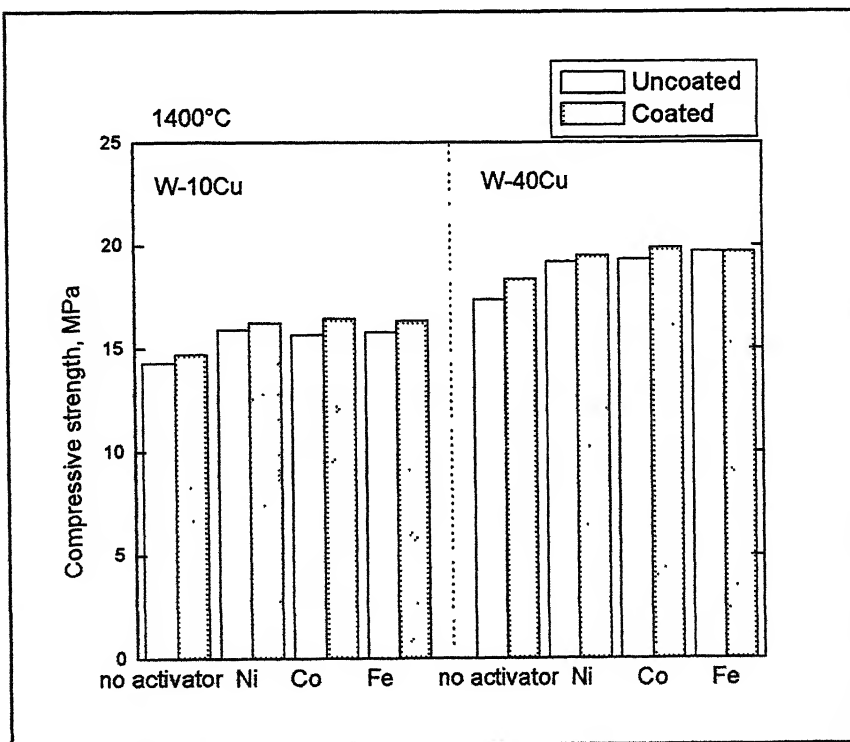


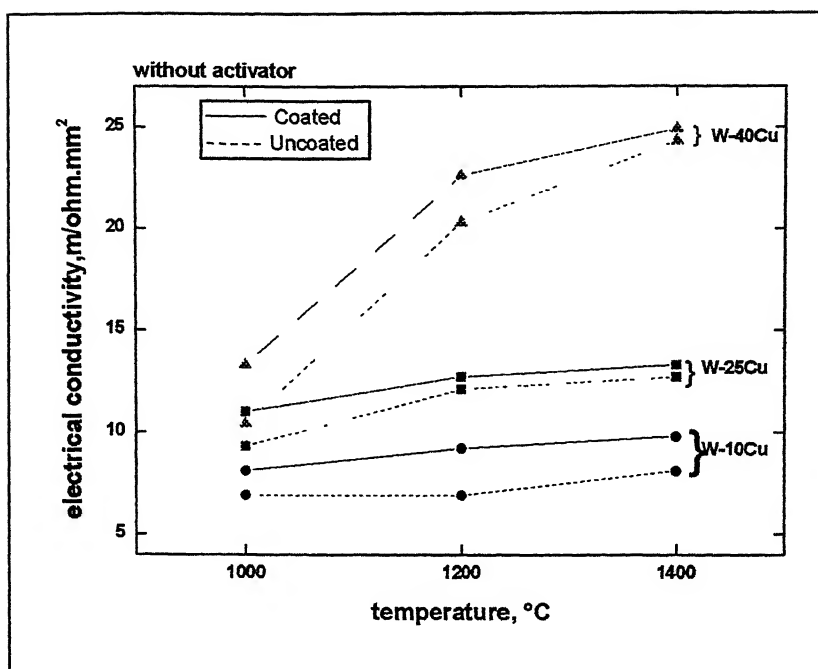
**Figure 5.33:** Effect of Cu content, coating, and activator addition on the compressive strength of W-Cu alloys sintered at 1400°C.

## 5.7 Electrical Conductivity

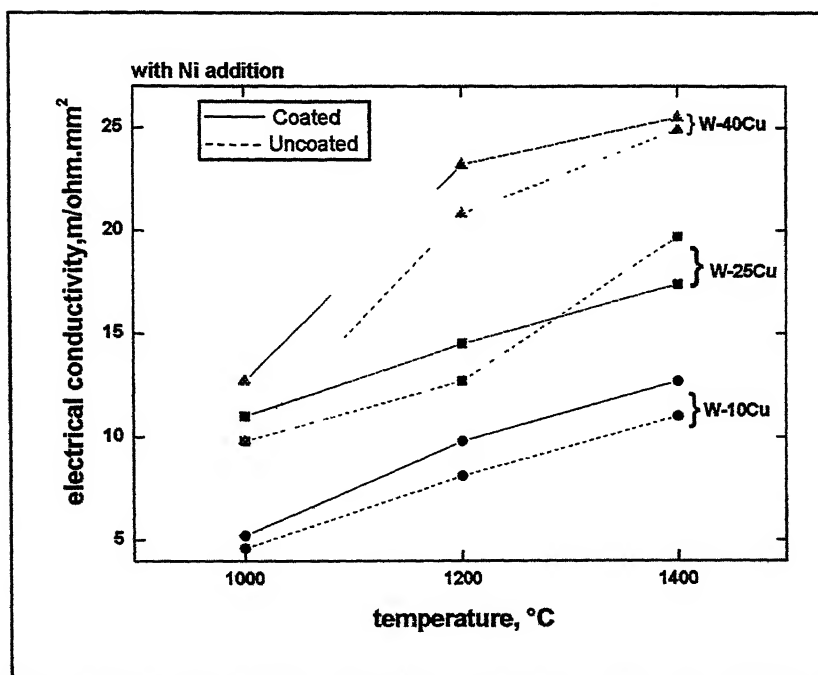
Electrical conductivity data of the sintered compacts is listed in Appendix V. Figures 5.34a to 5.34d compare the effect of activator addition on the electrical conductivity on W-Cu alloys sintered at 1000°C, 1200°C, and 1400°C. For all conditions, the conductivity of the coated samples is higher than the uncoated ones. The electrical conductivity of both coated and uncoated W-Cu compact increases with increasing Cu content and sintering temperature. As compared to the uncoated W-Cu alloys, no discernible trend in conductivity was observed by the additions of Ni, Co, and Fe activators.

## 5.8 Thermal Conductivity

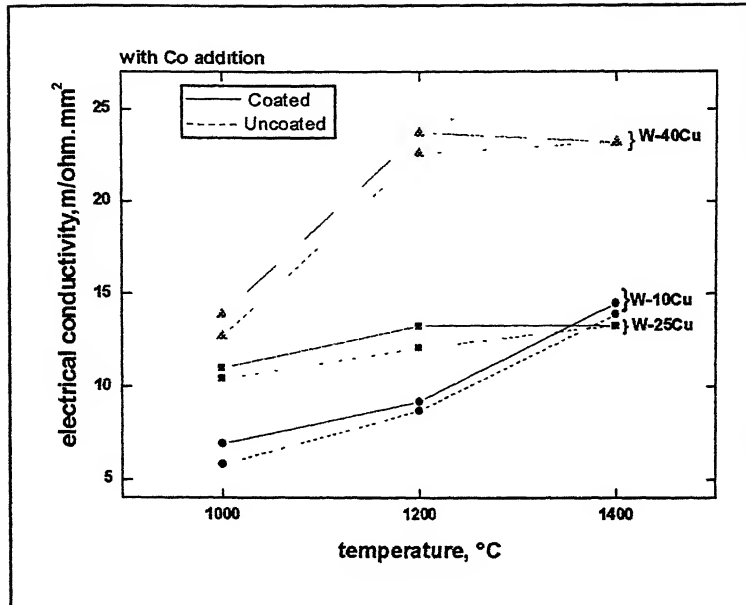
Appendix VI represents the thermal conductivity data of various sintered compacts. Figures 5.35a to 5.35d compare the effect of activator addition on the thermal conductivity of W-Cu alloys sintered at 1000°C, 1200°C, and 1400°C. In the present work the thermal conductivity is not measured directly. It is derived from the value of the electrical conductivity by using the Wiedemann-Franz Law [72]. The law states that the ratio of the thermal to electrical conductivity is:  $(\pi^2/3) * ((k/e)^2) * T$ , where  $k$  is the Boltzman constant,  $e$  is the charge of an electron, and  $T$  is temperature. Here also as like the electrical conductivity, the coated samples are showing higher thermal conductivity than that of the uncoated ones.



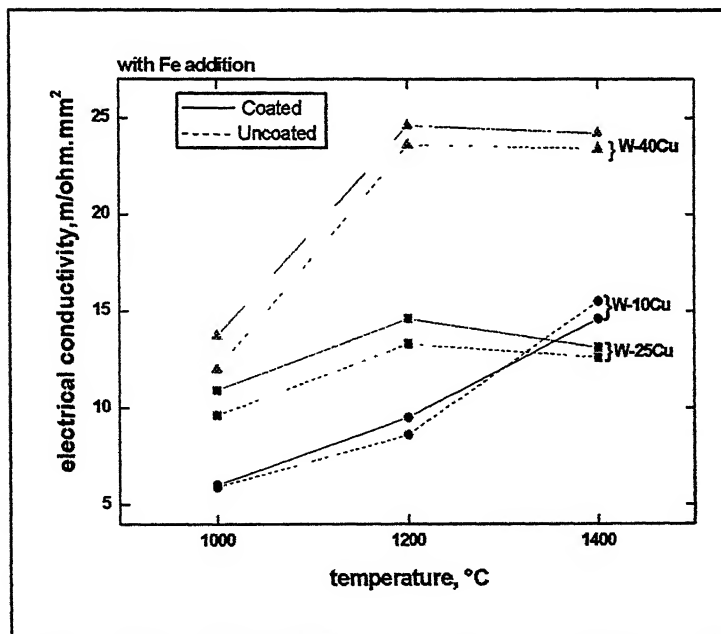
(a)



(b)



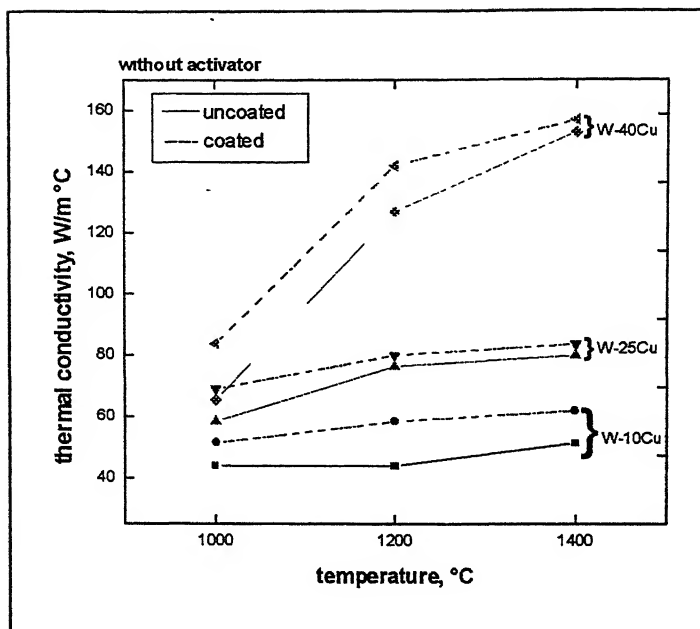
(c)



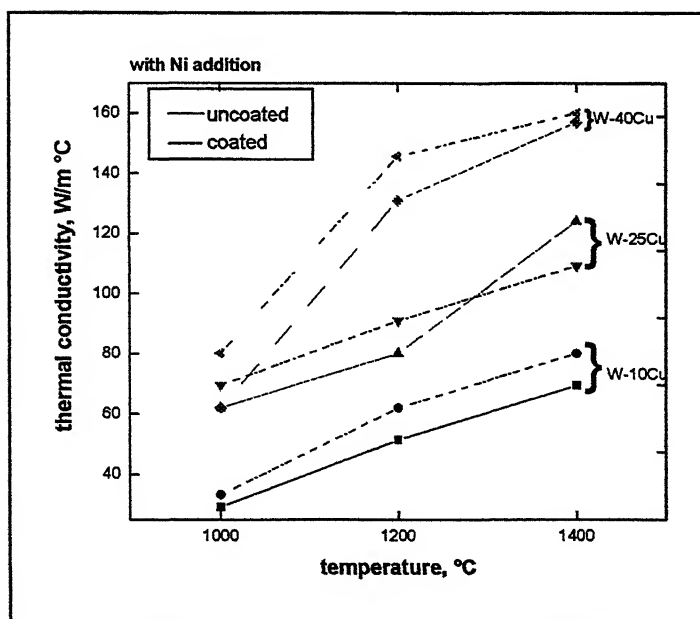
(d)

**Figure 5.34:** Effect of Cu content, sintering temperature, and coating on the electrical conductivity of W-Cu alloys (a) without activator; (b) with Ni addition; (c) with Co addition; and (d) with Fe addition.

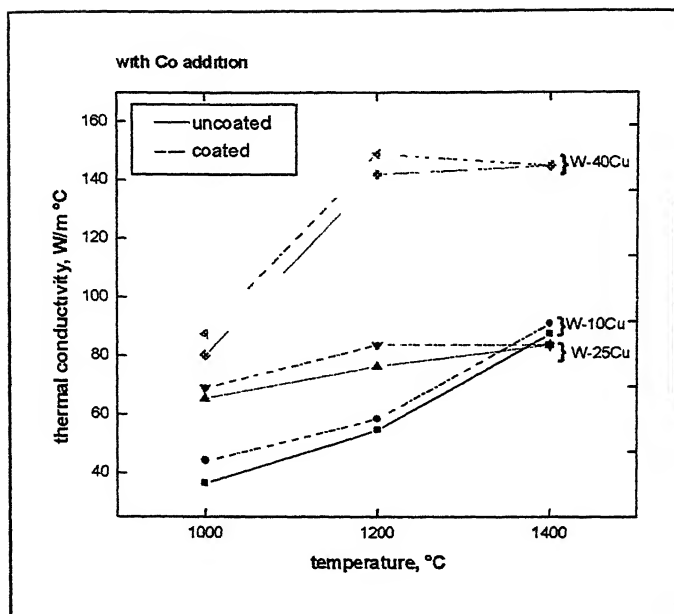




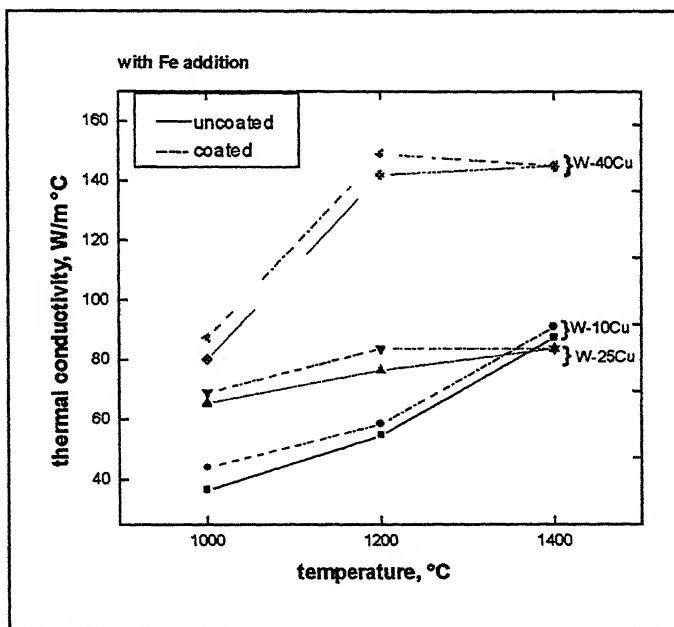
(a)



(b)



(c)



(d)

**Figure 5.35:** Effect of Cu content, coating, and sintering temperature on the thermal conductivity of W-Cu alloys sintered at (a) without activator (b) with Ni addition, (c) with Co addition, and (d) with Fe addition.

## **Chapter 6**

### **DISCUSSION**

The results obtained in the present investigation are discussed in this chapter. The following chapter is presented in five sections. The first section summarizes the changes in densification behavior of the coated and the uncoated W-Cu compacts as a function of sintering temperature, Cu content, and addition of transition metal activators. Radial and axial shrinkage aspects of the coated and uncoated samples are discussed in second section. Microstructural features observed in optical and scanning electron microscopy are discussed in section three. Section four discusses about the Hardness measurement and its variations. Electrical and thermal conductivity behaviors are discussed in subsequent sections

#### **6.1 Densification Behavior**

The average W powder size used for the present investigation varied between 5 to 10  $\mu\text{m}$ . For such sizes, W-Cu compacts normally do not undergo much densification in either coated or uncoated forms, even when sintered up to 1400°C. In fact, there is not much difference in the sintered density of W-Cu compacts when sintered at solid state (1000°C) and liquid phase (1200 and 1400°C) conditions (Figure 5.1). This is in line with the reported observations in the literature [7,64]. The negligible solubility of W in Cu obviates solution reprecipitation as densification mechanism. Hence, densification occurs predominantly by solid state sintering and capillary induced rearrangement of W grains during liquid phase sintering [20]. The rearrangement will be more pronounced in case of coated alloys because of homogeneous melt distribution. As indicated in Figures 5.1 and 5.2, coated W-Cu

samples always yield higher sintered density as compared to their uncoated counter parts. Elsewhere, Ozkal *et. al.* too has reported similar observation [10].

Coated W-Cu alloys result in higher sintered density even with Ni, Co, and Fe activator addition. Figure 6.1 compares the effect of activator addition and coating on the density of W-10Cu and W-40Cu compacts solid state sintered at 1000°C. For lower Cu content the coated sample with activator gives higher sintered density as compared to uncoated ones. For W-10Cu, activators do not really contribute towards densification at 1000°C. On the other hand, the uncoated W-10Cu samples show significant density enhancement by Ni, Co, and Fe addition. This can be inferred by the interaction mechanism of activators with the W-Cu system. Cobalt and iron do not have so significant solubility in Cu or in W. Consequently, they enhance the density of W compacts by segregating at the W-W interface and by forming an intermetallic phase ( $W_6Fe_7/W_6Co_7$ ) which provides short circuit diffusion path [27]. Figures 3.1, 3.2, 3.3, 3.4, 3.5, and 3.6 show the phase diagrams for Co-Cu, Fe-Cu, Cu-Ni, Co-W, Fe-W, and Ni-W system, respectively. In case of coated samples, Fe or Co does not come in direct contact with W and there effect on densification is restricted. Addition of less than 1 wt. % Ni has shown to result in full densification of W compacts even when sintered below 1500°C [7]. This has been attributed due to solubility of Ni in W. Thus, Ni remains segregated at the W-W particle interface provides a short circuit path for enhanced diffusion during sintering. For W-Cu alloys though, the mechanism of densification enhancement by Ni addition is different. Nickel has complete solid solubility with Cu. Figure 3.3 shows the phase diagram of Cu-Ni system. Hence, during sintering, rather than remaining segregated at the W-W interface, Ni preferentially forms solid solution with Cu [65]. At the sintering temperature, W has limited solubility in the Cu-Ni matrix, which depends on the Ni content [66]. This

leads to solution reprecipitation mechanism during sintering which enhances densification. In case of uncoated samples, it is likely that there are some W-Co, W-Fe, and W-Ni contact surfaces initially which contribute to densification enhancement. Of course, as the sintering progresses, Ni dissolves into Cu, whereas Fe and Co remain segregated. This explains the highest sintered density with Co/Fe addition in uncoated W-10Cu as compared to Ni addition.

The probability of W-Ni or W-Fe and W-Co contacts being formed is reduced as the Cu content increases. Consequently, at 1000°C, there is no significant effect of either activator in both coated as well as uncoated W-40Cu alloy, as shown in Figure 6.1. Figures 6.2 and 6.3 schematically show the effect of Fe, Co, and Ni addition, respectively, on the microstructural evolution in both coated and uncoated W-Cu alloys.

Figure 6.4 compares the effect of activator addition and coating on the sintered density of W-10Cu alloys liquid phase sintered at 1200°C and 1400°C. As shown in Figure 6.4, when liquid phase sintered at 1200°C, activators significantly enhance densification in both coated as well as uncoated compacts. For coated W-10Cu compacts, Fe or Co is a better activator, whereas, Ni addition leads to more densification enhancement for uncoated once at 1200°C. At 1400°C, the potency of the activators becomes even more pronounce with Ni being a better activator in both coated as well as uncoated conditions.

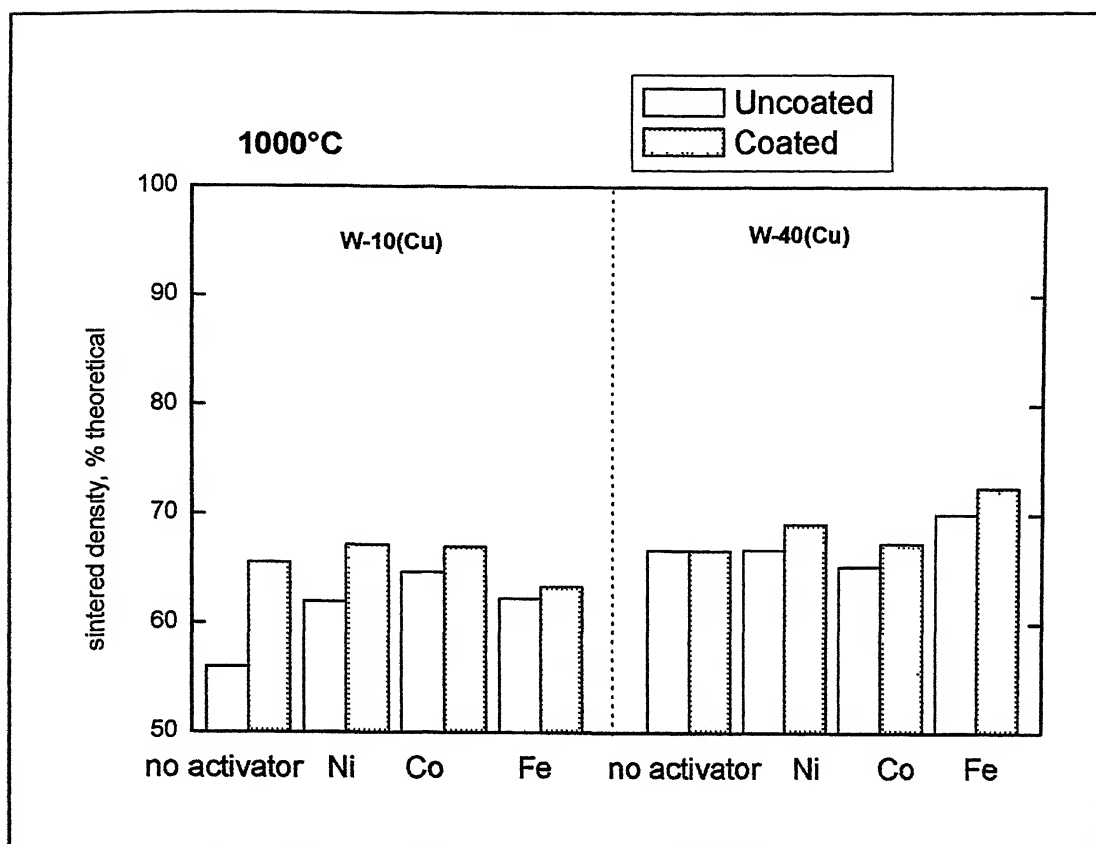


**Figure 6.1:** Effect of activator addition on the sintered density of coated and uncoated W-10Cu and W-40Cu alloys sintered at 1000°C.

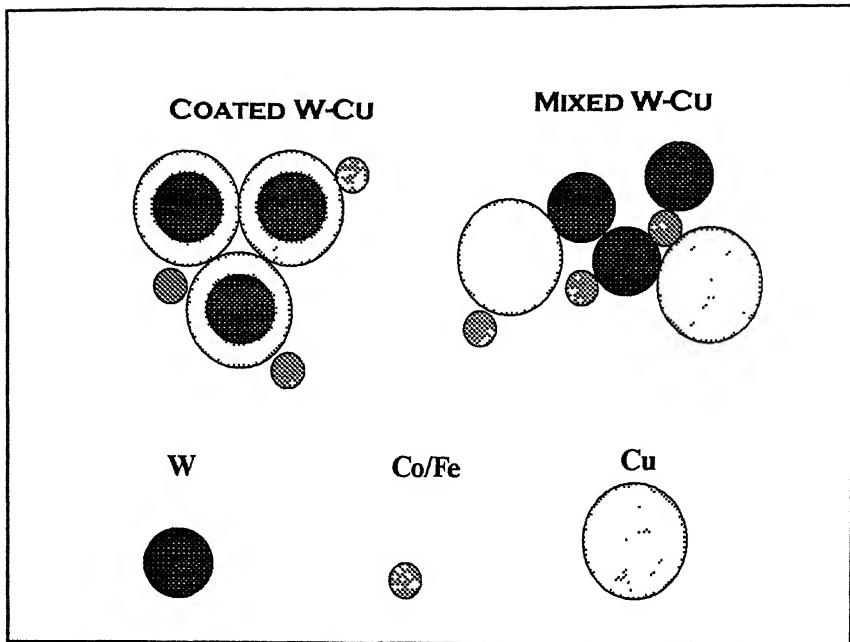


**Figure 6.2:** Schematic representation of the effect of Fe/Co activator addition on the coated and uncoated W-Cu alloy.

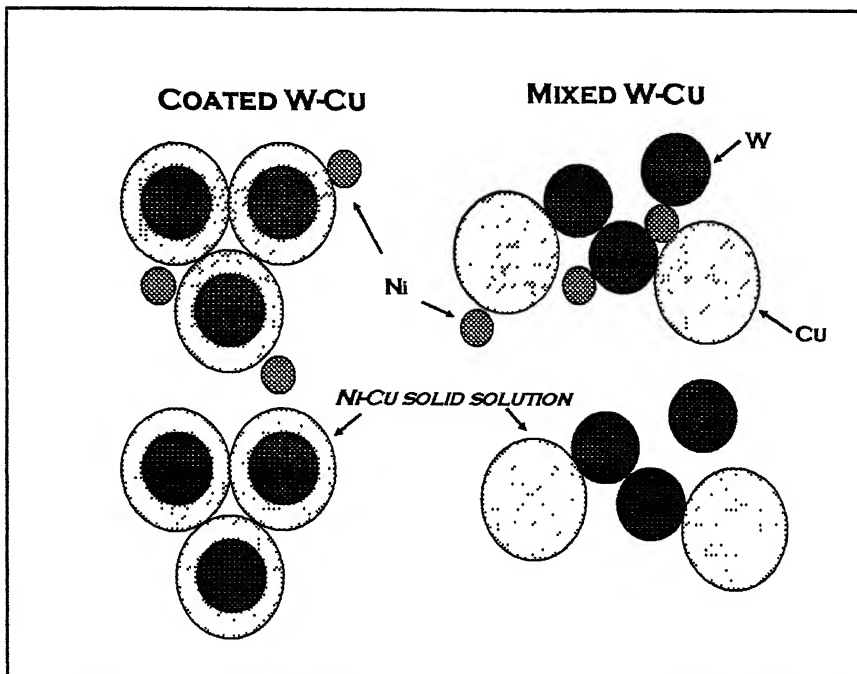


**Figure 6.3:** Schematic representation of the effect of Ni activator addition on the coated and uncoated W-Cu alloy

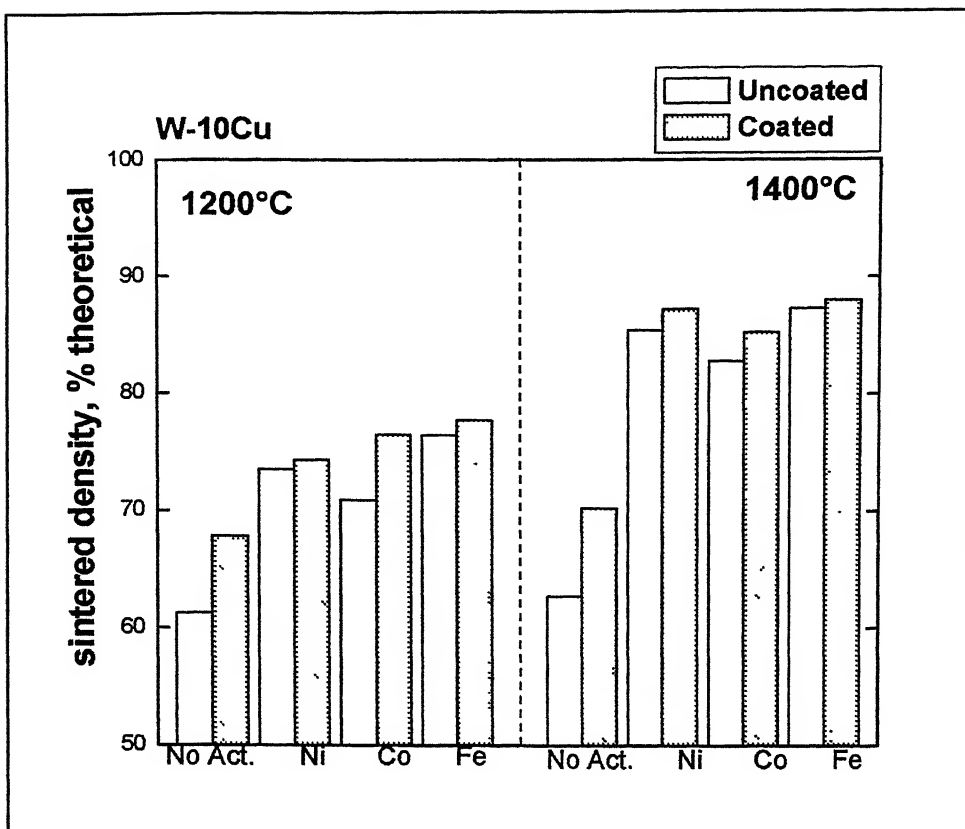


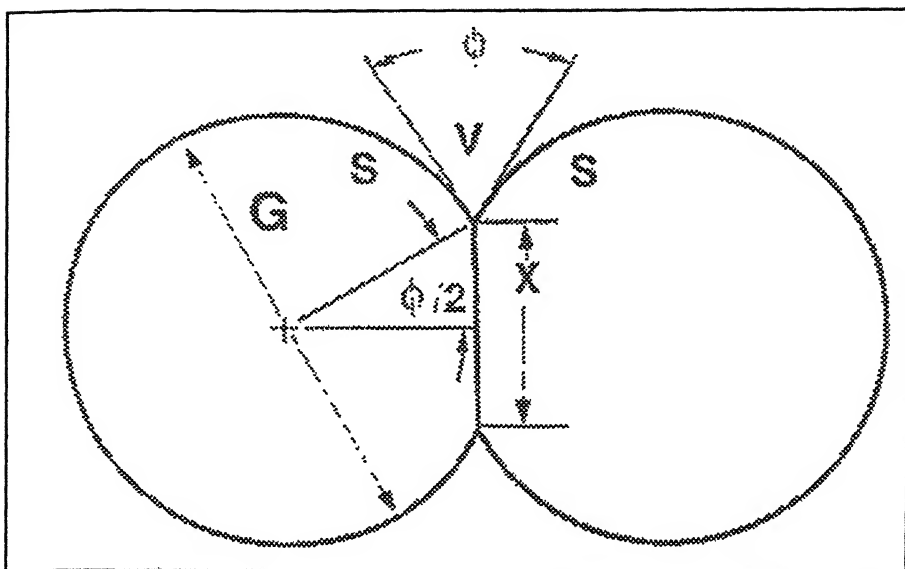
**Figure 6.4:** Effect of activator addition on the sintered density of coated and uncoated W-10Cu alloys sintered at 1200°C and 1400°C.



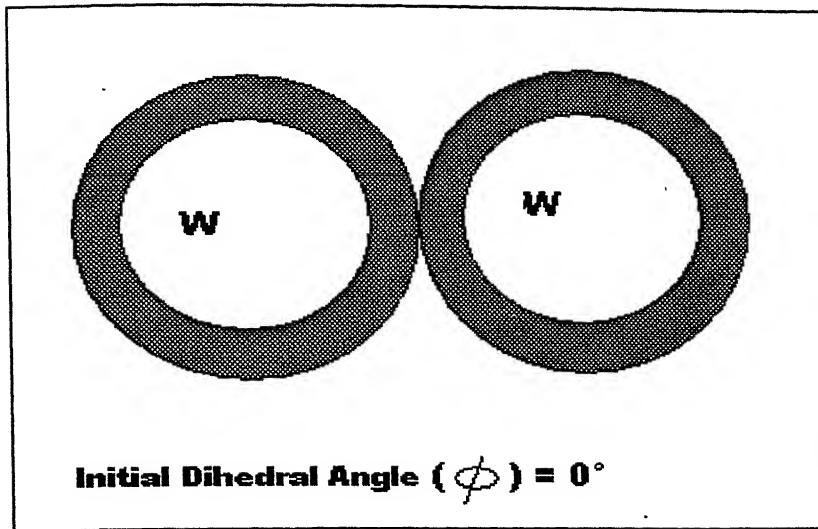
Besides the wetting angle, dihedral angle is another parameter that influences the densification behavior during liquid phase sintering [67]. Dihedral angle is defined as the angle between the liquid-liquid and solid-solid interface. In the Figure 6.5,  $\Phi$  is the dihedral angle. The high dihedral angle represents the balance between the solid-solid and solid-liquid interfacial energies; and is also expressed as the interparticle neck size to the grain size ratio. So from the geometry of the Figure 6.5 we can say that  $X/G = \sin(\Phi/2)$ , where  $X$  is the interparticle neck size and  $G$  is the grain size. The higher the dihedral angle, the larger is the interparticle neck size that forms. It is well known that the W-Cu system has a high dihedral angle ranging between from 85 to 95° [68,69]. In case of uncoated W-Cu compacts prepared by the mixing of the constituent powders, prior to Cu melt formation, the W-W particle contacts will form by the solid state sintering. Because of the high dihedral angle the network of W-W interparticle contacts remain stable even on Cu melt formation. After the Cu melt formation, it selectively dissolved chemically to reveal the interconnected W-W skeletal structure. The network of W grains forms a contiguous structure. It has been shown that because of the high dihedral angle the W-Cu compacts with up to 80 vol. % of Cu can be liquid phase sintered without distortion [70]. However, the conditions that promote structural rigidity hinder densification through capillary induced rearrangement.

Figure 6.6 shows the schematic microstructure of coated W-Cu alloys in unsintered and liquid phase sintered conditions. Initially, the Cu coated W powders correspond to a zero degree dihedral angle configuration. This condition persists till melt formation. When the coated W-Cu compacts are liquid phase sintered, the Cu melt will retract partially from the W surface in order to attain the non-zero dihedral angle configuration. Eventually, the microstructure of liquid phase sintered coated W-

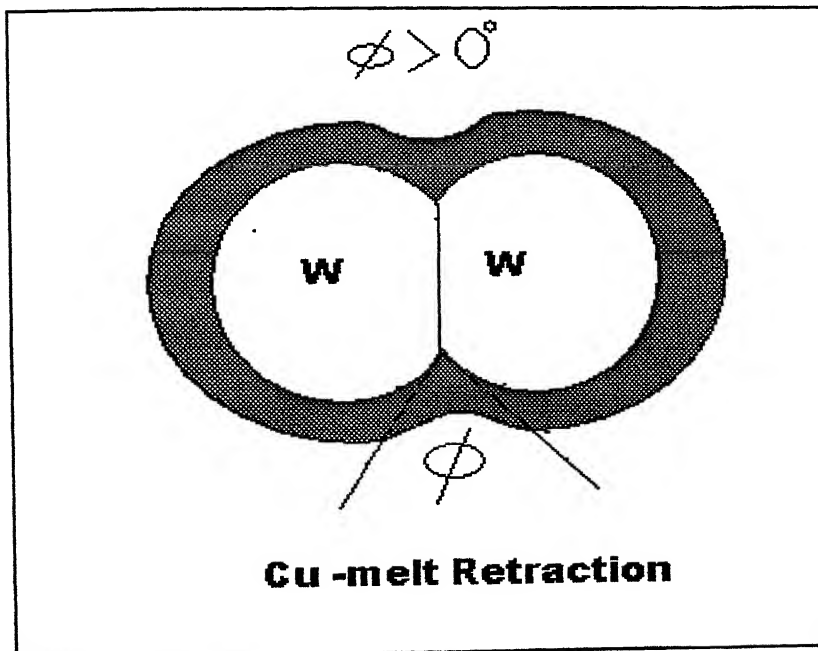
Cu compacts will become similar to that of uncoated (premixed) compacts. Nickel addition to the W-Cu system reduces the dihedral angle [70]. However, the amount of Ni relative to Cu is too low to cause any significant reduction in the dihedral angle. Unlike Ni, Fe or Co addition is not expected to have any effect on the dihedral angle as it is not soluble in either W or Cu. However, Fe/Co does indeed segregate at the W-W interface and forms an intermetallic phase ( $W_6Fe_7/W_6Co_7$ ) [27]. The critical content of Fe/Co required to form this intermetallic phase and whether or not  $W_6Fe_7/W_6Co_7$  – if it forms – occurs as a continuous thin layer will influence the dihedral angle of W-Cu system. Elsewhere, in hard metals, Henjered *et al.* has shown a continuous sub monolayer of Co segregated at the WC grain boundaries using high resolution micro analytical technique. Similar in depth studies are required to understand the nature of segregation of Co at the W-W interface and its effect thereof on the dihedral angle of the W-Cu system.



**Figure 6.5:** Schematic representation of the dihedral angle and its relationship with grain size and neck size [25].



(a)



(b)

**Figure 6.6:** Schematic representation of the microstructure of coated W-Cu system (a) prior to sintering, and (b) after liquid phase sintering. The high dihedral angle in W-Cu system favors Cu melt retraction, thereby reducing the effect coverage of Cu on to w grains and favoring W-W contacts.

The lower sintered density of uncoated W-Cu sample can also be attributed to the disparity in size and size distribution of Cu powder relative to W, which causes inhomogeneous melt formation. During liquid phase sintering, the Cu melt diffuses in to the smaller pore regions and leaves behind large pores corresponding to the prior location of coarse Cu powders. Consequently, the larger pores will be more difficult to eliminate by further sintering. Panichkina and Filipov [64]; and Upadhyaya and German [20] have reported an increase in the pore size in W-Cu compacts during sintering. Elsewhere, similar result has been shown by Debata and Upadhyaya [71] on W-Cu system containing Sn.

## 6.2 Variation in Radial and Axial shrinkage

Figure 5.3 compares the axial versus radial shrinkage of the coated and uncoated compacts, compacted at 200MPa pressure. From the Figure it is clear that all the compacts undergo shrinkage, neither of the compacts show swelling. In the plot a line is drawn diagonally which indicates the ideal case, which means that any point on this line indicates uniform shrinkage in both the directions i.e. the compact aspect ratio is maintained during sintering. In other words the compact undergone isotropic dimensional change. In practice however it is often difficult to achieve isotropic shrinkage during sintering. Because we know that the shrinkage or expansion will occur under the influence of two factors, namely, chemically induced shrinkage and stress induced factor. Stress induced factor will play an important role in case of cylindrical compacted sample. As the samples are compacted in a single acting press there will be a density gradient from the top to bottom. Moreover from the radial direction no stresses are offered. In general terms, the sample grows or shrinks less in the radial direction compared to the axial direction. This could possibly be tied up

with the direction of applied stress and locked-in elastic stresses. This can very well be supported from the experimental data of present study.

As the sintering temperature increases the shrinkage in both the directions also get increased. Whenever we increased the temperature above 1083°C, essentially liquid phase sintering occurred. As the liquid formed, it helped in rearrangement of the particles. So, shrinkage is expected. It is to be remembered that too much of liquid could distort the compact. But in the present case no distortion or swelling was observed. So it can be concluded that the volume fraction of the liquid formed was sufficient to fill all the pores.

### 6.3 Microstructural Evolution

In this study, optical microscopy and SEM of uncoated and coated samples sintered at different conditions show significant difference in microstructural evolution. In general, in case of solid state sintering of W-Cu samples (sintered at 1000°C), coalescence of W-W grains is less compare to liquid state sintering of the same (sintered at 1200 and 1400°C). This is because of the fact that at higher temperature, the diffusivity of W increases and thus the densification. With addition of activators (Ni, Fe, and Co), there is further increase of densification for both solid state and liquid phase sintering of the samples. But the increment of density in case of solid state is much less (only 10 to 12%) than that of liquid phase sintering (almost 40%) due to higher diffusivity in the latter case. The addition of Fe/Co forms intermetallic phases ( $W_6Fe_7/W_6Co_7$ ) at the surface of W grains which provide short circuit path for enhanced diffusion during sintering, thus shows better coalescence in the microstructure of samples with activator addition. However, addition of Ni as an activator, acts differently. During sintering, rather than segregated at the W-W interface, Ni preferentially forms solid solution with Cu and this leads to solution

reprecipitation mechanism which enhance densification and can be clearly shown by the better coalescence in the microstructure. Microstructures show that the coalescence, i.e. densification, is much better in case coated samples than that of uncoated ones. It is due to the fact that the Cu melt which has been formed is homogeneously distributed in case of coated samples, so the porosity is much less and also the pore size and they are homogeneously distributed. Whereas, in case of uncoated ones, the Cu melt is inhomogeneously distributed, thus porosity become much higher, inhomogeneously distributed and also very big pores can be seen in the microstructure. From the microstructure it can also be observed that, coalescence is better in case of Ni added samples than that of Fe/Co added ones when sintered at higher temperature. This can be explained in the following manner. During liquid phase sintering (above the melting point of Cu), Ni forms a solid solution with Cu, which leads to solution reprecipitation and thus enhance the densification, whereas, Fe/Co enhance densification by intermetallic formation. So at higher temperature, the solubility of W in Ni-Cu solid solution increases, this leads to the enhancement of the solution reprecipitation mechanism and as a result the overall densification increases.

The average W-powder size used for the present study varied between 5 to 8  $\mu\text{m}$ . Other than coating the homogeneity also depends on the powder particle size and morphology. If the powder particles are coarser then some of the largest particles were not broken up. The formation of the intermetallic phases with the addition of Co/Fe at the surface of the W grains could not be confirmed due to the fine grain size. The SEM micrographs show the higher contiguity observed with the addition of activators. This leads to the higher mechanical strength in the compacts with the addition of activators.

A higher copper concentration results in a larger volume fraction of liquid during sintering, which alters the densification behavior of the compacts. With the increase in the liquid volume fraction rearrangement will be more. So densification increases. The thermal and the electrical conductivity also increase with the increase of the melt.

## **6.4 Variation in Hardness**

The hardness of W-Cu alloys decreases with increasing Cu content which is the softer phase as compared to W. Alternatively, for a particular composition, hardness increases with increasing sintering temperature and coating, both of which result in lower porosity. Figure 6.7 shows the hardness of the W-Cu alloys both with and without activators, sintered at various temperatures, as a function of the sintered density. As shown in Figure 6.7, the hardness increases with increasing sintered density. Thus conditions that lead to an increase in sintered density, such as activator addition and sintering temperature increase, enhance the hardness. It is interesting to note that the W-Cu alloys without any activator addition have very little difference between their hardness. However, there is significant enhancement in the hardness with activator addition, particularly at 1200°C and 1400°C. Furthermore, irrespective of activator addition, the hardness is higher for high W-Cu alloys with lower Cu contents.

## **6.5 Variation in Compressive Strength**

The variation in compressive strength is a bit reverse to that of the hardness values. The strength value increases with the increase in Cu content. Also the strength increases with the activator addition. It is being evident from the Figure 5.33. In this experiment we try to measure the strength of the W-W skeleton structure. We know that with the increase in the ductile phase in a composite increases its compressive



strength. In fact, for a purely ductile material the compressive strength is said to be infinite. For a brittle material also the compressive strength is always higher than that of its tensile strength. In the presently investigated system W is a brittle phase and Cu is ductile phase. So with the increase in Cu content the increase in the strength value of the composite is quite obviate. The microstructures of the compressed samples are shown in Figure 6.8 and 6.9. The grains are elongated in the perpendicular directions of loading.

## **6.6 Variation in Electrical conductivity and Thermal conductivity**

Just like hardness, the electrical conductivity too increases as the conditions that decrease porosity prevail. In general, the electrical conductivity is directly proportion to the thermal conductivity (Wiedemann-Franz law) and the same has been shown to be valid for sintered W-Cu system as well. In coated W-Cu alloys, there is a relatively more contiguous path of Cu-Cu contact which results in slightly higher conductivity as compared to the uncoated alloys. It has been reported that the addition of transition metal activators drastically reduces the conductivity of W-Cu alloys. However in the present study, no such trend was observed. It is likely that the decrease in conductivity is proportionately compensated by the corresponding increase in the sintered density by activator addition. This is evident by re-plotting the conductivity data against the sintered density. As shown in Figure 6.10, the electrical conductivity increases with increasing sintered density. Also, there seem to be three distinct regions, with the W-40Cu alloys lying in the top most regions (highest conductivity) and W-10Cu alloys being in the region with lowest conductivity. Furthermore, addition of activator only shifts the sintered density and does not result in much variation in the electrical conductivity.

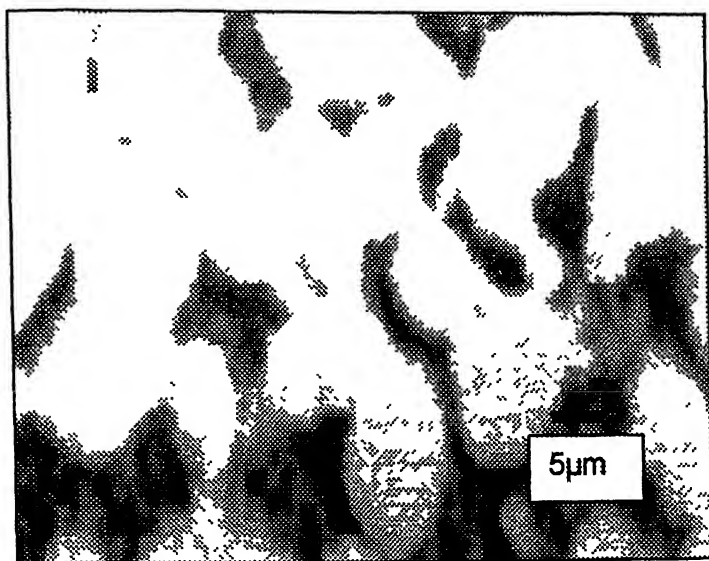


**Figure 6.8:** SEM micrograph of W-10Cu compact sintered at 1400°C with Ni activator after compression testing.

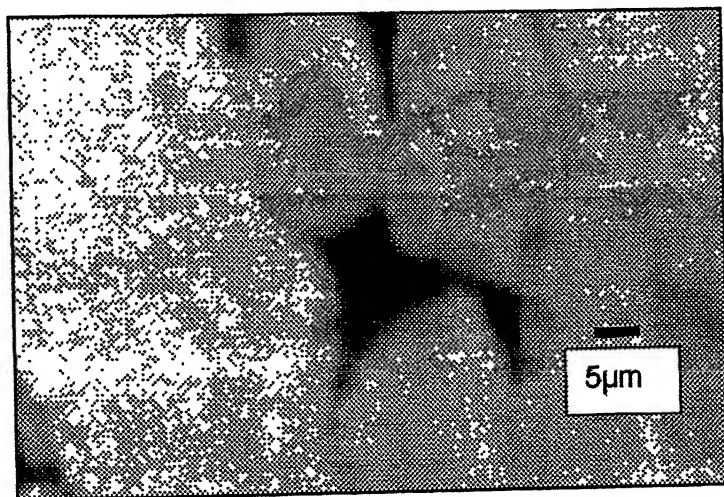


**Figure 6.9:** SEM micrograph of W-40Cu compact sintered at 1400°C with Ni activator after compression testing.

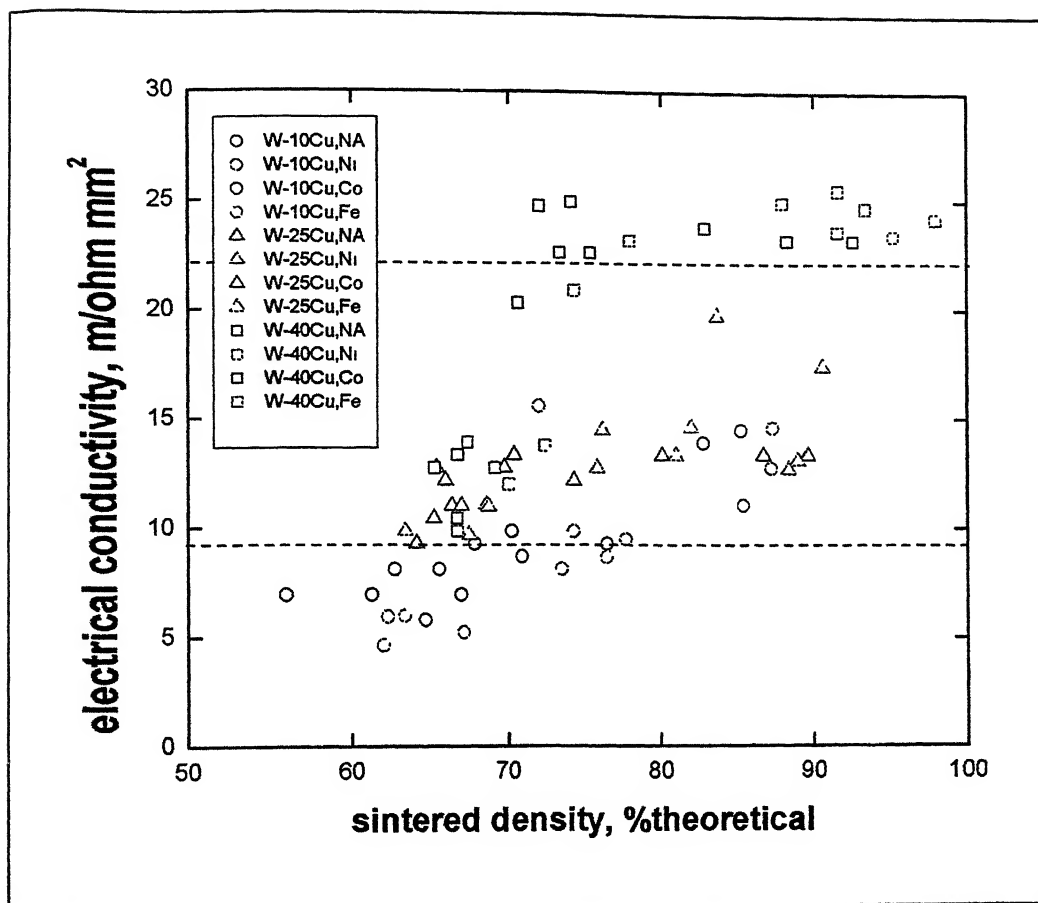


**Figure 6.10:** Variation in the electrical conductivity of W-Cu alloys with and without activator addition plotted against the sintered density.

## Chapter 7

### CONCLUSIONS

Multiple transport mechanisms are responsible for the densification behaviour of liquid phase sintered materials. This study shows that densification in W-Cu alloys increases with increase in Cu content and with powder modification by coating Cu on to W. But this enhancement is not too much. This is due to the fact that in W-Cu system in liquid phase sintered condition the main two densification mechanisms are absent, namely solution reprecipitation and rearrangement. The density enhancement can be greatly accomplished by the additions of transition metal activators. They can alter the dihedral angle of the system and thus rearrangement phenomena can take place by particle fragmentation. The W-Cu system sinters predominantly by a solid state mechanism, and there is not much density enhancement even when the alloys are liquid phase sintered at 1200° and 1400°C. Ni additions to W-Cu decrease the solid-liquid surface energy and increase the solubility of W in the liquid phase. As the solubility increases, the dominant densification mechanism changes from solid state diffusion to mass transport through the liquid phase. The required solubility to achieve full density is directly related to the particle size. In the absence of sufficient solubility for densification via liquid phase sintering mechanisms, high sintered densities can still be achieved by enhancing solid state diffusion. This can be accomplished by a reduction in particle size or by the addition of elements like Fe and Co that form an activated layer at the W grain boundaries in the presence of Cu.

For all the cases, the coated W-Cu alloy yield higher sinter density, mechanical properties, and electrical properties than the uncoated one. This is mainly due to the homogeneous melt formation in the coated samples as opposed to that of

the uncoated one. The choice of the activators depend on the Cu content, state of the powder (coated vs. uncoated), and the sintering temperature.

## REFERENCES

- 1 R.M. German, K.F. Hens, and J.L. Johnson, "Powder Metallurgy Processing of Thermal Management Materials for Microelectronic Applications," *International Journal of Powder Metallurgy*, 1994, v. 30, n. 2, pp 205-214.
- 2 T.W. Kirk, S G. Caldwell, and J J Oakes, "Mo-Cu Composites for Electronic Packaging Applications," Advances in Powder Metallurgy and Particulate Materials, Metal Powder Industries Federation, Princeton, NJ, USA, 1992, v. 9, pp. 115-122.
- 3 R.M. German, Powder Injection Molding, Metal Powder Industries Federation, Princeton, NJ, USA, 1990.
- 4 A. Upadhyaya, "Tungsten Heavy Alloys for Ordnance and Thermal Management Applications," *Transactions Indian Institute of Metals*, 2002, v. 55, n. 1-2, pp. 51-69.
- 5 A. Upadhyaya, "Processing Strategy for Consolidating Tungsten Heavy Alloys for Ordnance Applications," *Journal of Material Chemistry and Physics*, 2001, v. 67, pp. 101-110.
- 6 Anonymous, "Low Thermal Expansion High Thermal Conductivity Refractory Metal Alloys for Heat Sinks," *International Journal of Refractory and Hard Metals*, 1988, v. 7, pp.134.
- 7 J.L. Johnson, "Densification, Micro structural Evolution and Thermal Properties of Liquid Phase Sintered Composites," Ph.D. Thesis, The Pennsylvania State University, University Park, PA, USA 1994.
- 8 High Performance Heat Sink Substrate Materials, Brush Wellman Engineered Materials, Tucson, Arizona, USA ([www.brushwellman.com](http://www.brushwellman.com)).

- 9 J. L. Johnson and R. M. German, "Factors Affecting Thermal Conductivity of W-Cu Composites," Advances in Powder Metallurgy and Particulate Materials, Metal Powder Industries Federation, Princeton, NJ, USA, 1993, v. 4, pp. 201-213.
- 10 B. Özkal, A. Upadhyaya, M. L. Ovecoglu, and R. M. German, "Comparative Effects of Coated Powders on the Sintering Behavior of W-Cu Alloys," Proceedings 2<sup>nd</sup> Turkish National Powder Metallurgy Conference, S. Saritas (ed.), Türk Toz Metalurjisi Derneği, Ankara, Turkey 2000, pp 185-191.
- 11 J. L. Johnson and R. M. German, "Powder Metallurgy Processing of Mo-Cu for Thermal Management Applications," *International Journal of Powder Metallurgy*, 1999, v.35, n 8, pp. 39-48.
- 12 J. Lezanski and W. Rutkowski, "Infiltration of a Liquid in Sintered Tungsten-Three Stages of Infiltration," *Powder Metallurgy International*, 1987, v.19, n. 2, pp. 29-31.
- 13 W. S. Wang and K. S. Hwang, "The Effect of Tungsten Particle Size on Processing and Properties of Infiltrated W-Cu Compacts," *Metallurgical and Materials Transactions A*, 1998, v. 29A, pp. 1509-1515.
- 14 B. Yang and R. M. German, "Infiltrated Sintering of Powder Injection Molded W-Cu Alloys with Ni Additions," Advances in Powder Metallurgy and Particulate Materials, Metal Powder Industries Federation, Princeton, NJ, USA, 1993, v. 5, pp. 105-119.
- 15 J. L. Johnson and R. M. German, "A Theory of Activated Liquid Phase Sintering and Its Application to the W-Cu System," Advances in Powder Metallurgy and Particulate Materials, Metal Powder Industries Federation, Princeton, NJ, USA, 1992, v. 3, pp. 35-46.

- 16 B. Yang and R M German, "The Effect of Tungsten Particle Size and Powder Treating Techniques on the Sintered Properties of W-15Cu," Advances in Powder Metallurgy and Particulate Materials, Metal Powder Industries Federation, Princeton, NJ, USA, 1993, v. 2, pp 203-216
- 17 R.M. German and J.L Johnson, "Chemically Activated Liquid Phase Sintering of W-Cu," *International Journal of Powder Metallurgy*, 1994, v. 30, n. 1, pp. 91-102.
- 18 P.R. Subramaniam and D.E. Laughlin, Phase Diagrams of Binary Copper Alloys, The Materials Information Society, Materials Park, ASM International, 2<sup>nd</sup> ed., v. 2, 1990.
- 19 W.J. Huppmann and H. Reigger, "Modelling of Rearrangement Processes in Liquid Phase Sintering," *Acta Metallurgica*, 1975, v. 23, pp. 965-971.
- 20 A. Upadhyaya and R.M. German, "Densification and Dilation of Sintered W-Cu Alloys," *International Journal of Powder Metallurgy*, 1998, v. 34, n. 2, pp. 43-55.
- 21 T.B. Massalski, Barrelet, and C. Sanborn, Binary Alloy Phase Diagram, The Materials Information Society, Materials Park, ASM International, 2<sup>nd</sup> ed., v. 2, 1990.
- 22 V.V. Panichkina, M.M. Sirotyuk, and V.V. Skorokhod, *Soviet Powder Metallurgy and Metal Ceramics*, 1982, v. 21, pp. 447.
- 23 J.S. Lee and T.H. Kim, "Synthesis and Consolidation of Nano-Composite Metal Powder," Proceedings of Fourth Nisshin Engineering Particle Technology International Seminar NEPTIS IV, K. Niihara (ed.), Nisshin Engineering Co., Osaka, Japan, 1995, pp. 59-65.



- 24 K.V Sebastian and G S. Tendulkar, "High Density Tungsten Copper Liquid phase Sintered Composites from co-reduced oxide Powders," *International Journal of Powder Metallurgy and Powder Technology*, 1979, v 15, pp. 45-53
- 25 R.M German, Sintering Theory and Practice, Plenum Press, New York, USA, 1996.
- 26 R.M. German and V. Ham, "The Effect of Ni and Pd additions on the Activated Sintering of Tungsten," *International Journal of Powder Metallurgy and Powder Technology*, 1976, v. 12, pp. 115-125.
- 27 T.H. Ihn, S.W Lee, and S.K. Joo, "Effect of Transition Metal Addition on Liquid Phase Sintering of W-Cu," *Powder Metallurgy*, 1994, v. 37, n. 4, pp. 283-288.
- 28 A. Belhadjhamida and R.M. German, "Tungsten and Tungsten Alloys by Powder Metallurgy- A Status Review," Tungsten and Tungsten Alloys-Recent Advances, Andrew Crowson, and Edward S. Chen (eds.), The Minerals, Metals & Materials Society, 1991, pp. 3-19.
- 29 T.H. Kim, J. Byeon, and J.S. Lee, "A New Production Route for Near-Net Shaped Full Density W-Cu Materials," Advances in Powder Metallurgy and Particulate Materials, Metal Powder Industries Federation, Princeton, NJ, USA, 1992, v. 2, pp. 431-437.
- 30 A.M. Popa, J.M. Missiaen, J.M. Chaix, "Solid State Sintering in W-Cu Composites: From Microstructure to Densification," Proceedings of 2000 Powder Metallurgy World Congress, K Kosuge and H. Nagoi (eds.), Japan Society of Powder and Powder Metallurgy, Japan 2000, pp. 96-98.
- 31 J.S. Lee, W.A. Kaysser, and G. Petzow, Modern Developments in Powder Metallurgy, Metal Powder Industries Federation, Princeton, NJ, USA, 1985, v. 15, pp. 489.

- 32 J.S. Lee, T.H. Kim, and T.G. Kang, Proceedings of Powder Metallurgy World Congress PM94, Société Française Métallurgie et de Matériaux, Paris, France, 1994, v. 2, pp. 1501-1504.
- 33 P.R. Subramaniam and D.E. Laughlin, Phase Diagrams of Binary Copper Alloys, The Materials Information Society, Materials Park, ASM International, 2<sup>nd</sup> ed., v. 2, 1994, pp. 475-477.
- 34 Y.D. Kim, J.C. Kim, S.S. Ryu, and I.H. Moon, Proceedings of Powder Metallurgy World Congress PM98, European Powder Metallurgy Association, Shrewsbury, UK, 1998, pp. 579-582.
- 35 K. Wojtasik and S. Stolarz, "Micro-Composite Tungsten-Copper Contact Materials," Proceedings of Powder Metallurgy World Congress PM98, European Powder Metallurgy Association, Shrewsbury, UK, pp. 573-578.
- 36 J.S. Lee, E.S. Yoon, and J.H. Yu, Proceedings of Powder Metallurgy World Congress PM98, European Powder Metallurgy Association, Shrewsbury, UK, pp. 57.
- 37 K.V. Sebastian and G.S. Tendulkar, *Planseeberichte Pulvermetallurgie*, 1977, v. 25, pp. 84-87.
- 38 N.C. Kothari, "Effects of Particle Size on the Sintering Kinetics in Tungsten Powder," *Powder Metallurgy International*, 1964, v. 7, pp. 251-260.
- 39 J. Kurtz, "Sintered High Density Tungsten and Tungsten Alloys," Proceedings Second Annual Spring Meeting, Metal Powder Association, NY, USA, 1946, pp. 40-52.
- 40 V.J. Vacek, "Über die Beeinflussung des Sinterverhaltens von Wolfram," *Planseeberichte für Pulvermetallurgie*, 1959, v. 7, pp. 6-17.

- 41 J H Brophy, H.W Hayden, and J Wulff, "The Final Stages of Densification in Ni-W Compacts," *Transactions AIME*, 1962, v. 224, pp 797-803.
- 42 G.H. Gessinger and H F. Fischmeister, "A Modified Model for the Sintering of Tungsten with Nickel Additions," *Journal of Less Common Metals*, 1972, v. 27, pp. 129-141.
- 43 W.E Gurwell, "A Review of Embrittlement Mechanisms in Tungsten Heavy Alloys," Report PNL-SA-13645, Pacific Northwest Laboratory, Richland, WA, USA, April 1986.
- 44 R.M German and Z.A Munir, "Enhanced Low Temperature Sintering of Tungsten," *Metallurgical Transactions*, 1976, v. 7A, pp. 1873-1879
- 45 T. Kaneko, "Effect of Microstructure on the Mechanical Properties of Sintered W-Based Alloys," *Journal of Japan Society Powder Metallurgy*, 1990, v. 37, pp. 885-892.
- 46 J.S. Lee, H.H. Hwang, and H. Shin, "Influence of Ni-P Alloy Addition in the Formation of W-Skeleton," *International Journal of Refractory and Hard Metals*, 1990, v. 9, pp. 46-49.
- 47 I.H. Moon and J.S. Lee, "Activated Sintering of Tungsten-Copper Contact Materials," *Powder Metallurgy International*, 1979, v. 22, pp. 5-7.
- 48 R.M. German and K.S. Churn, "Sintering Atmosphere Effects on the Ductility of W-Ni-Fe Heavy Metals," *Metallurgical Transactions*, 1984, v. 15A, pp. 747-754.
- 49 H. Hofmann, and G. Petzow, "Influence of Sintering Atmosphere on Mechanical Properties of Tungsten Based Heavy Alloys," Modern Development in Powder Metallurgy, 1985, v. 8, pp. 17-31.
- 50 S. Farooq, P.B. Kemp, A. Bose, and R.M. German, "Effect of Initial Oxygen Content and Sintering Atmosphere Dew Point on the Properties of Tungsten

- Based Heavy Alloys," *International Journal of Refractory and Hard Metals*, 1989, v 8, pp. 236-243.
- 51 W.J. Huppmann and H. Riegger, "Liquid Phase Sintering of the Model System W-Ni," *International Journal of Powder Technology*, 1977, v. 13, pp. 242-247.
  - 52 B.H. Rabin and R.M. German, "Microstructure Effects on Tensile Properties of W-Ni-Fe," *Metallurgical Transactions*, 1988, v. 19, pp. 1523-1532.
  - 53 R.M. German, J.E. Hanafee, and S.L. DiGiallonardo, "Toughness Variation with Test Temperature and Cooling Rate for Liquid Phase Sintered W-3.5Ni-1.5Fe," *Metallurgical Transactions*, 1984, v. 15A, pp. 121-128.
  - 54 W.D. Kingery, "Densification during Sintering in The Presence of a Liquid Phase 1. Theory," *Journal of Applied Physics*, 1959, v. 30, pp. 301-306.
  - 55 C. Ghosh and A. Upadhyaya, "Sintering of Coated W-Cu Alloys," *Transactions PMAI*, 2002, v. 28, p. 84-91
  - 56 L.B. Ekbom, Tungsten Heavy Metals, "Liquid Phase Sintering and Mechanical Properties," Technical Report, Department of Physical Metallurgy, Royal Institute of Technology, Stockholm, Sweden, 1990.
  - 57 V. Smolej, S. Pejovnic, and W.A. Kaysser, "Rearrangement during Liquid Phase Sintering of Large Particles," *Powder Metallurgy International*, 1982, v. 14, pp. 34-36.
  - 58 W.A. Kaysser, O.J. Kwon, and G. Petzow, "Pore Formation and Pore Elimination during Liquid Phase Sintering," Proceedings of International Powder Metallurgy Conference, Associazione Italiana di Metallurgia, Florence, Italy, 1982, v. 6, pp. 23-30.
  - 59 S. Farooq, A. Bose, and R.M. German, "Theory of Liquid Phase Sintering: Modern Experiments on W-Ni-Fe Heavy Alloy System," Progresses in Powder

Metallurgy, Metal Powder Industries Federation, Princeton, NJ, USA, 1987, v. 43, pp. 65-77

- 60 R.M. German and S. Farooq, "An Update on the Theory of Liquid Phase Sintering," Sintering 87, Applied Science Pub., London, UK, 1988, v. 1, pp. 459-464.
- 61 W. Schatt, S. Rolle, A. Sibilla, and E. Friedrich, "Effect of Dislocation Density during Liquid Phase Sintering," *Science of Sintering*, 1986, v. 18, pp. 3-20.
- 62 G.H. Gessinger, H.F. Fishmeister, and H.L. Lukas, "A Model for Second Stage Liquid Phase Sintering with a Partially Wetting Liquid," *Acta Metallurgica*, 1973, v. 21, pp. 715-724.
- 63 W.A. Kaysser, M. Zivcovic, and G. Petzow, "Shape Accommodation during Grain Growth in the Presence of a Liquid Phase," *Journal of Material Science*, 1985, v. 20, pp. 578-584.
- 64 V.V. Panichkina and N.I. Filipov, "Structure Formation Processes in The sintering of Dispersed Copper-Tungsten Pseudo-Alloys," *Science of Sintering*, 1994, v. 20, n. 3, pp. 269-275.
- 65 J.L. Johnson and R.M. German, "The Solubility Criterion for Liquid Phase Sintering," Advances in Powder Metallurgy and Particulate Materials, Metal Powder Industries Federation, Princeton, NJ, USA, 1994, v. 3, pp. 267-279.
- 66 C. Ghosh and A. Upadhyaya, "Effect of Coating and Activators on Sintering of W-Cu Alloys," *Powder Metallurgy Progress*, 2002, v. 2, n. 2, pp. 98-110.
- 67 R.M. German, Liquid Phase Sintering, Plenum Press, New York, USA, 1985.
- 68 A. Upadhyaya, "Distortion in Liquid Phase Sintered Tungsten Heavy Alloys," M.S. Thesis, The Pennsylvania State University, University Park, PA, USA 1996.

- 69 A. Upadhyaya, "A Microstructure Based Model for Shape Distortion During Liquid Phase Sintering," Ph D. Thesis, The Pennsylvania State University, University Park, PA, USA 1998
- 70 A Upadhyaya and R M German, Advances in Powder Metallurgy and Particulate Materials, Metal Powder Industries Federation, Princeton, NJ, USA, 1996, v. 5, pp. 107.
- 71 M. Debata and A. Upadhyaya, "Effect of Transition Metal Additives on Activated Sintering of Tungsten-Bronze," *Transactions of PMAI*, 2002, v. 28, pp. 92-101.
- 72 [www.hyperphysics.phy-astr.gsu.edu/hbase/thermo/thercond](http://www.hyperphysics.phy-astr.gsu.edu/hbase/thermo/thercond).

## Appendix I

### Experimental data for the green samples

*Activator used: Nil; Compaction Pressure: 200 MPa; Initial Diameter of the Compact: 1.27 cm; Sintering Temperature: 1000°C.*

Composition	State*	Green Compacts				
		Weight (g)	Height (cm.)	Volume (cm <sup>3</sup> )	Density (g/cm <sup>3</sup> )	Density (% theo.)
W-10Cu	UC	4.915	0.400	0.510	9.610	55.740
	C	4.153	0.290	0.370	11.310	65.610
W-25Cu	UC	2.717	0.230	0.290	9.330	62.530
	C	3.536	0.290	0.370	9.630	64.550
W-40Cu	UC	3.871	0.350	0.450	8.640	65.630
	C	2.860	0.260	0.330	8.690	66.010

*Activator used: Nil; Compaction Pressure: 200 MPa; Initial Diameter of the Compact: 1.27 cm; Sintering Temperature: 1200°C.*

Composition	State*	Green Compacts				
		Weight (g)	Height (cm.)	Volume (cm <sup>3</sup> )	Density (g/cm <sup>3</sup> )	Density (% theo.)
W-10Cu	UC	3.753	0.290	0.360	10.360	60.120
	C	4.673	0.320	0.400	11.610	67.330
W-25Cu	UC	4.851	0.400	0.510	9.580	64.200
	C	3.136	0.240	0.300	10.230	69.170
W-40Cu	UC	3.270	0.300	0.380	8.610	65.420
	C	3.307	0.300	0.380	8.710	66.160

*Activator used: Nil; Compaction Pressure: 200 MPa; Initial Diameter of the Compact: 1.27 cm; Sintering Temperature: 1400°C.*

Composition	State*	Green Compacts				
		Weight (g)	Height (cm.)	Volume (cm <sup>3</sup> )	Density (g/cm <sup>3</sup> )	Density (% theo.)
W-10Cu	UC	3.689	0.280	0.350	10.480	60.780
	C	2.845	0.210	0.260	10.800	62.660
W-25Cu	UC	3.076	0.260	0.330	9.340	62.660
	C	5.108	0.400	0.510	9.990	66.930
W-40Cu	UC	2.906	0.300	0.380	7.650	58.140
	C	4.249	0.370	0.470	8.970	68.180

*Activator used: Ni; Compaction Pressure: 200 MPa; Initial Diameter of the Compact: 1.27 cm; Sintering Temperature: 1000°C.*

Composition	State*	Green Compacts				
		Weight (g)	Height (cm.)	Volume (cm <sup>3</sup> )	Density (g/cm <sup>3</sup> )	Density (% theo.)
W-10Cu	UC	5.649	0.450	0.560	10.000	58.430
	C	3.250	0.240	0.300	10.880	63.520
W-25Cu	UC	4.926	0.430	0.540	9.290	60.970
	C	4.586	0.390	0.490	9.050	62.590
W-40Cu	UC	5.440	0.530	0.670	8.170	62.350
	C	2.684	0.260	0.320	8.280	63.220



*Activator used: Ni; Compaction Pressure: 200 MPa; Initial Diameter of the Compact: 1.27 cm; Sintering Temperature: 1200°C.*

Composition	State*	Green Compacts				
		Weight (g)	Height (cm.)	Volume (cm <sup>3</sup> )	Density (g/cm <sup>3</sup> )	Density (% theo.)
W-10Cu	UC	4.673	0.370	0.470	9.870	57.650
	C	4.791	0.350	0.450	10.690	62.430
W-25Cu	UC	5.838	0.520	0.660	8.870	59.750
	C	3.798	0.330	0.420	9.150	61.630
W-40Cu	UC	4.493	0.440	0.560	8.030	61.280
	C	3.489	0.330	0.410	8.450	64.530

*Activator used: Ni; Compaction Pressure: 200 MPa; Initial Diameter of the Compact: 1.27 cm; Sintering Temperature: 1400°C.*

Composition	State*	Green Compacts				
		Weight (g)	Height (cm.)	Volume (cm <sup>3</sup> )	Density (g/cm <sup>3</sup> )	Density (% theo.)
W-10Cu	UC	6.126	0.500	0.630	9.680	56.520
	C	4.894	0.360	0.450	10.800	63.070
W-25Cu	UC	4.827	0.430	0.550	8.820	59.460
	C	4.313	0.360	0.460	9.460	63.770
W-40Cu	UC	6.449	0.580	0.730	8.780	67.040
	C	4.641	0.410	0.520	8.850	67.580

*Activator used: Co; Compaction Pressure: 200 MPa; Initial Diameter of the Compact: 1.27 cm; Sintering Temperature: 1000°C.*

Composition	State*	Green Compacts				
		Weight (g)	Height (cm.)	Volume (cm <sup>3</sup> )	Density (g/cm <sup>3</sup> )	Density (% theo.)
W-10Cu	UC	4.243	0.340	0.430	9.860	57.570
	C	8.978	0.740	0.940	9.580	55.970
W-25Cu	UC	5.076	0.440	0.560	9.030	60.850
	C	5.335	0.450	0.570	9.410	63.380
W-40Cu	UC	4.998	0.480	0.610	8.210	62.650
	C	4.183	0.400	0.510	8.260	63.050

*Activator used: Co; Compaction Pressure: 200 MPa; Initial Diameter of the Compact: 1.27 cm; Sintering Temperature: 1200°C.*

Composition	State*	Green Compacts				
		Weight (g)	Height (cm.)	Volume (cm <sup>3</sup> )	Density (g/cm <sup>3</sup> )	Density (% theo.)
W-10Cu	UC	4.688	0.390	0.490	9.590	56.030
	C	5.996	0.450	0.570	10.520	61.470
W-25Cu	UC	5.444	0.480	0.610	8.990	60.610
	C	6.089	0.510	0.650	9.360	63.050
W-40Cu	UC	4.104	0.410	0.520	7.900	60.340
	C	5.456	0.510	0.650	8.450	64.500

*Activator used: Co; Compaction Pressure: 200 MPa; Initial Diameter of the Compact: 1.27 cm; Sintering Temperature: 1400°C.*

Composition	State*	Green Compacts				
		Weight (g)	Height (cm.)	Volume (cm <sup>3</sup> )	Density (g/cm <sup>3</sup> )	Density (% theo.)
W-10Cu	UC	5.635	0.440	0.560	10.020	58.550
	C	6.945	0.510	0.650	10.750	62.820
W-25Cu	UC	4.543	0.400	0.510	8.880	59.850
	C	5.241	0.420	0.530	9.860	66.410
W-40Cu	UC	4.680	0.440	0.560	8.360	63.840
	C	4.468	0.410	0.520	8.610	65.700

*Activator used: Fe; Compaction Pressure: 200 MPa; Initial Diameter of the Compact: 1.27 cm; Sintering Temperature: 1000°C.*

Composition	State*	Green Compacts				
		Weight (g)	Height (cm.)	Volume (cm <sup>3</sup> )	Density (g/cm <sup>3</sup> )	Density (% theo.)
W-10Cu	UC	4.560	0.340	0.430	10.590	62.020
	C	8.900	0.740	0.940	9.500	55.620
W-25Cu	UC	5.200	0.440	0.560	9.250	62.460
	C	4.326	0.450	0.570	9.410	63.510
W-40Cu	UC	4.855	0.480	0.610	7.990	61.120
	C	4.326	0.400	0.510	8.540	65.350

*Activator used: Fe; Compaction Pressure: 200 MPa; Initial Diameter of the Compact: 1.27 cm; Sintering Temperature: 1200°C.*

Composition	State*	Green Compacts				
		Weight (g)	Height (cm.)	Volume (cm <sup>3</sup> )	Density (g/cm <sup>3</sup> )	Density (% theo.)
W-10Cu	UC	4 392	0.330	0.420	10.510	61.540
	C	3 212	0.230	0.290	11.030	64.580
W-25Cu	UC	3 872	0.320	0.410	9.560	64.530
	C	4.950	0.400	0.510	9.770	66.000
W-40Cu	UC	2.216	0.220	0.280	7.960	60.870
	C	3 299	0.310	0.390	8.410	64.310

*Activator used: Fe; Compaction Pressure: 200 MPa; Initial Diameter of the Compact: 1.27 cm; Sintering Temperature: 1400°C.*

Composition	State*	Green Compacts				
		Weight (g)	Height (cm.)	Volume (cm <sup>3</sup> )	Density (g/cm <sup>3</sup> )	Density (% theo.)
W-10Cu	UC	4.673	0.370	0.470	9.980	58.400
	C	4.791	0.350	0.440	10.810	63.300
W-25Cu	UC	5.838	0.520	0.660	8.870	59.870
	C	3.798	0.330	0.420	9.090	61.380
W-40Cu	UC	4.493	0.440	0.560	8.070	61.710
	C	3.489	0.330	0.420	8.350	63.890

\* UC: uncoated; C: Cu-coated W

## Appendix II

### Experimental data for the sintered samples

*Activator used: Nil; Compaction Pressure: 200 MPa; Initial Diameter of the Compact: 1.27 cm; Sintering Temperature: 1000°C.*

Composition	State*	Sintered Compacts						
		Weight (g)	Height (cm.)	Diameter (cm.)	Volume (cm <sup>3</sup> )	Density (g/cm <sup>3</sup> )	Density (% theo.)	D.P.
W-10Cu	UC	4.910	0.402	1.270	0.510	9.640	55.940	0.000
	C	4.120	0.288	1.270	0.360	11.300	65.540	0.000
W-25Cu	UC	2.710	0.224	1.270	0.280	9.560	64.090	0.040
	C	3.510	0.280	1.270	0.350	9.900	66.360	0.050
W-40Cu	UC	3.870	0.350	1.266	0.440	8.780	66.700	0.030
	C	2.850	0.258	1.266	0.320	8.780	66.100	0.020

*Activator used: Nil; Compaction Pressure: 200 MPa; Initial Diameter of the Compact: 1.27 cm; Sintering Temperature: 1200°C.*

Composition	State*	Sintered Compacts						
		Weight (g)	Height (cm.)	Diameter (cm.)	Volume (cm <sup>3</sup> )	Density (g/cm <sup>3</sup> )	Density (% theo.)	D.P.
W-10Cu	UC	3.750	0.282	1.266	0.350	10.560	61.250	0.030
	C	4.660	0.316	1.268	0.400	11.700	67.840	0.020
W-25Cu	UC	4.830	0.398	1.254	0.490	9.840	65.930	0.050
	C	3.120	0.238	1.266	0.300	10.410	69.770	0.020
W-40Cu	UC	3.250	0.290	1.240	0.350	9.300	70.660	0.150
	C	3.280	0.268	1.270	0.340	9.660	73.380	0.210

*Activator used: Nil; Compaction Pressure: 200 MPa; Initial Diameter of the Compact: 1.27 cm; Sintering Temperature: 1400°C.*

Composition	State*	Sintered Compacts						
		Weight (g)	Height (cm.)	Diameter (cm.)	Volume (cm <sup>3</sup> )	Density (g/cm <sup>3</sup> )	Density (% theo.)	D.P.
W-10Cu	UC	3.670	0.274	1.256	0.340	10.810	62.700	0.050
	C	2.820	0.206	1.200	0.230	12.110	70.230	0.200
W-25Cu	UC	3.040	0.254	1.250	0.310	9.760	65.390	0.070
	C	5.070	0.440	1.240	0.480	10.500	70.390	0.100
W-40Cu	UC	2.880	0.260	1.220	0.300	9.480	72.040	0.330
	C	4.170	0.354	1.240	0.430	9.750	74.120	0.190

*Activator used: Ni; Compaction Pressure: 200 MPa; Initial Diameter of the Compact: 1.27 cm; Sintering Temperature: 1000°C.*

Composition	State*	Sintered Compacts						
		Weight (g)	Height (cm.)	Diameter (cm.)	Volume (cm <sup>3</sup> )	Density (g/cm <sup>3</sup> )	Density (% theo.)	D.P.
W-10Cu	UC	5.640	0.440	1.240	0.530	10.610	61.990	0.090
	C	3.250	0.234	1.240	0.280	11.490	67.120	0.100
W-25Cu	UC	4.920	0.426	1.250	0.520	9.410	63.390	0.060
	C	4.570	0.378	1.230	0.450	10.170	68.560	0.160
W-40Cu	UC	5.430	0.500	1.258	0.620	8.740	66.720	0.120
	C	2.670	0.240	1.250	0.290	9.060	69.120	0.160

*Activator used: Ni; Compaction Pressure: 200 MPa; Initial Diameter of the Compact: 1.27 cm; Sintering Temperature: 1200°C.*

Composition	State*	Sintered Compacts						
		Weight (g)	Height (cm.)	Diameter (cm.)	Volume (cm <sup>3</sup> )	Density (g/cm <sup>3</sup> )	Density (% theo.)	D.P
W-10Cu	UC	4.650	0.350	1.160	0.370	12.580	73.500	0.370
	C	4.780	0.300	1.264	0.380	12.720	74.270	0.320
W-25Cu	UC	5.820	0.420	1.252	0.520	11.260	75.850	0.400
	C	3.780	0.270	1.256	0.330	11.310	76.190	0.380
W-40Cu	UC	4.480	0.370	1.258	0.460	9.740	74.350	0.340
	C	3.460	0.300	1.200	0.340	10.210	77.970	0.380

*Activator used: Ni; Compaction Pressure: 200 MPa; Initial Diameter of the Compact: 1.27 cm; Sintering Temperature: 1400°C.*

Composition	State*	Sintered Compacts						
		Weight (g)	Height (cm.)	Diameter (cm.)	Volume (cm <sup>3</sup> )	Density (g/cm <sup>3</sup> )	Density (% theo.)	D.P.
W-10Cu	UC	6.110	0.492	1.040	0.420	14.630	85.440	0.660
	C	4.870	0.356	1.080	0.330	14.940	87.270	0.660
W-25Cu	UC	4.800	0.422	1.080	0.390	12.420	83.710	0.600
	C	4.310	0.350	1.080	0.320	13.450	90.600	0.740
W-40Cu	UC	6.450	0.568	1.120	0.560	11.530	88.000	0.640
	C	4.610	0.390	1.120	0.380	12.000	91.610	0.740

*Activator used: Co; Compaction Pressure: 200 MPa; Initial Diameter of the Compact: 1.27 cm; Sintering Temperature: 1000°C.*

Composition	State*	- Sintered Compacts						
		Weight (g)	Height (cm.)	Diameter (cm)	Volume (cm <sup>3</sup> )	Density (g/cm <sup>3</sup> )	Density (% theo.)	D.P.
W-10Cu	UC	4.230	0.338	1.200	0.380	11.070	64.660	0.170
	C	8.960	0.669	1.220	0.780	11.460	66.950	0.250
W-25Cu	UC	5.060	0.420	1.260	0.520	9.680	65.200	0.110
	C	5.310	0.450	1.230	0.530	9.940	66.970	0.100
W-40Cu	UC	4.980	0.460	1.270	0.580	8.550	65.250	0.070
	C	4.150	0.390	1.240	0.470	8.820	67.360	0.120

*Activator used: Co; Compaction Pressure: 200 MPa; Initial Diameter of the Compact: 1.27 cm; Sintering Temperature: 1200°C.*

Composition	State*	Sintered Compacts						
		Weight (g)	Height (cm.)	Diameter (cm.)	Volume (cm <sup>3</sup> )	Density (g/cm <sup>3</sup> )	Density (% theo.)	D.P.
W-10Cu	UC	4.670	0.364	1.160	0.380	12.140	70.900	0.340
	C	5.980	0.448	1.140	0.460	13.090	76.480	0.390
W-25Cu	UC	5.430	0.466	1.160	0.490	11.030	74.310	0.350
	C	6.060	0.500	1.140	0.510	11.880	80.070	0.460
W-40Cu	UC	4.080	0.378	1.180	0.410	9.880	75.400	0.380
	C	5.410	0.472	1.160	0.500	10.860	82.880	0.520



*Activator used: Co; Compaction Pressure: 200 MPa; Initial Diameter of the Compact: 1.27 cm; Sintering Temperature: 1400°C.*

Composition	State*	Sintered Compacts						
		Weight (g)	Height (cm.)	Diameter (cm.)	Volume (cm <sup>3</sup> )	Density (g/cm <sup>3</sup> )	Density (% theo )	D P
W-10Cu	UC	5.630	0.434	1.080	0.400	14.180	82.800	0.590
	C	6.930	0.500	1.110	0.470	14.600	85.280	0.600
W-25Cu	UC	4.540	0.400	1.060	0.350	12.870	86.740	0.670
	C	5.230	0.414	1.110	0.390	13.300	89.650	0.690
W-40Cu	UC	4.660	0.440	1.080	0.400	11.570	88.300	0.680
	C	4.440	0.400	1.080	0.370	12.130	92.610	0.780

*Activator used: Fe; Compaction Pressure: 200 MPa; Initial Diameter of the Compact: 1.27 cm; Sintering Temperature: 1000°C.*

Composition	State*	Sintered Compacts						
		Weight (g)	Height (cm.)	Diameter (cm.)	Volume (cm <sup>3</sup> )	Density (g/cm <sup>3</sup> )	Density (% theo.)	D.P.
W-10Cu	UC	4.520	0.341	1.260	0.430	10.630	62.240	0.010
	C	8.890	0.670	1.250	0.820	10.820	63.340	0.170
W-25Cu	UC	5.160	0.421	1.251	0.520	9.980	67.480	0.130
	C	5.310	0.450	1.215	0.520	10.190	68.730	0.140
W-40Cu	UC	4.830	0.460	1.209	0.530	9.150	70.040	0.220
	C	4.290	0.390	1.217	0.450	9.460	72.420	0.200

*Activator used: Fe; Compaction Pressure: 200 MPa; Initial Diameter of the Compact: 1.27 cm; Sintering Temperature: 1200°C.*

Composition	State*	Sintered Compacts						
		Weight (g)	Height (cm.)	Diameter (cm.)	Volume (cm <sup>3</sup> )	Density (g/cm <sup>3</sup> )	Density (% theo.)	D.P.
W-10Cu	UC	4.360	0.328	1.140	0.330	13.030	76.450	0.370
	C	3.200	0.226	1.166	0.240	13.270	77.710	0.360
W-25Cu	UC	3.860	0.310	1.150	0.320	11.990	81.000	0.450
	C	4.930	0.380	1.167	0.410	12.150	82.000	0.460
W-40Cu	UC	2.210	0.194	1.100	0.180	11.980	91.600	0.770
	C	3.280	0.274	1.118	0.270	12.200	93.410	0.800

*Activator used: Fe; Compaction Pressure: 200 MPa; Initial Diameter of the Compact: 1.27 cm; Sintering Temperature: 1400°C.*

Composition	State*	Sintered Compacts						
		Weight (g)	Height (cm )	Diameter (cm.)	Volume (cm <sup>3</sup> )	Density (g/cm <sup>3</sup> )	Density (% theo.)	D.P.
W-10Cu	UC	4.650	0.350	1.180	0.380	12.150	71.000	0.300
	C	4.780	0.306	1.270	0.390	12.340	72.000	0.240
W-25Cu	UC	5.820	0.420	1.161	0.440	13.100	88.400	0.700
	C	3.780	0.270	1.162	0.290	13.210	89.000	0.710
W-40Cu	UC	4.480	0.372	1.110	0.360	12.450	95.240	0.860
	C	3.460	0.295	1.080	0.270	12.810	98.000	0.930

\* UC: uncoated; C: Cu-coated W

### Appendix III

#### Axial and radial dimensions of the samples

*Activator used: Nil; Initial Diameter of the Compact: 1.27 cm; Sintering Temperature: 1000°C.*

Composition	State*	Before Sintering		After Sintering		Axial Shrinkage %	Radial Shrinkage %
		Ht (cm.)	Dia (cm.)	Ht. (cm.)	Dia (cm )		
W-10Cu	UC	0.400	1.270	0.400	1.270	0	0
	C	0.290	1.270	0.288	1.270	0.689	0
W-25Cu	UC	0.230	1.270	0.224	1.270	2.608	0
	C	0.290	1.270	0.280	1.270	3.448	0
W-40Cu	UC	0.350	1.270	0.350	1.266	0	0.315
	C	0.260	1.270	0.258	1.266	0.769	0.315

*Activator used: Nil; Initial Diameter of the Compact: 1.27 cm; Sintering Temperature: 1200°C.*

Composition	State*	Before Sintering		After Sintering		Axial Shrinkage %	Radial Shrinkage %
		Ht. (cm.)	Dia (cm.)	Ht. (cm.)	Dia (cm.)		
W-10Cu	UC	0.290	1.270	0.282	1.266	2.758	0.314
	C	0.320	1.270	0.316	1.268	1.250	0.157
W-25Cu	UC	0.400	1.270	0.398	1.254	0.500	1.259
	C	0.240	1.270	0.238	1.266	0.833	0.314
W-40Cu	UC	0.300	1.270	0.290	1.240	3.333	2.362
	C	0.300	1.270	0.268	1.270	10.667	0

*Activator used: Nil; Initial Diameter of the Compact: 1.27 cm; Sintering Temperature: 1400°C.*

Composition	State*	Before Sintering		After Sintering		Axial	Radial
		Ht (cm.)	Dia (cm.)	Ht. (cm )	Dia (cm )	Shrinkage %	Shrinkage %
W-10Cu	UC	0.280	1.270	0.274	1.256	2.143	1.102
	C	0.210	1.270	0.206	1.200	1.904	5.511
W-25Cu	UC	0.260	1.270	0.254	1.250	2.307	1.574
	C	0.400	1.270	0.400	1.240	0	2.362
W-40Cu	UC	0.300	1.270	0.260	1.220	13.333	3.937
	C	0.370	1.270	0.354	1.240	4.324	2.362

*Activator used: Ni; Initial Diameter of the Compact: 1.27 cm; Sintering Temperature: 1000°C.*

Composition	State*	Before Sintering		After Sintering		Axial	Radial
		Ht. (cm.)	Dia (cm.)	Ht. (cm.)	Dia (cm.)	Shrinkage %	Shrinkage %
W-10Cu	UC	0.450	1.270	0.440	1.240	2.222	2.362
	C	0.240	1.270	0.234	1.240	2.500	2.362
W-25Cu	UC	0.430	1.270	0.426	1.250	0.930	1.574
	C	0.390	1.270	0.378	1.230	3.076	3.149
W-40Cu	UC	0.530	1.270	0.500	1.258	5.660	0.944
	C	0.260	1.270	0.240	1.250	7.692	1.574

*Activator used: Ni; Initial Diameter of the Compact: 1.27 cm; Sintering Temperature: 1200°C*

Composition	State*	Before Sintering		After Sintering		Axial Shrinkage %	Radial Shrinkage %
		Ht. (cm.)	Dia (cm.)	Ht. (cm.)	Dia (cm.)		
W-10Cu	UC	0.370	1.270	0.350	1.160	5.405	8.670
	C	0.350	1.270	0.300	1.264	14.285	0.472
W-25Cu	UC	0.520	1.270	0.420	1.254	19.231	1.259
	C	0.330	1.270	0.270	1.256	18.182	1.102
W-40Cu	UC	0.440	1.270	0.370	1.258	15.909	0.944
	C	0.330	1.270	0.300	1.200	9.090	5.511

*Activator used: Ni; Initial Diameter of the Compact: 1.27 cm; Sintering Temperature: 1400°C*

Composition	State*	Before Sintering		After Sintering		Axial Shrinkage %	Radial Shrinkage %
		Ht. (cm.)	Dia (cm.)	Ht. (cm.)	Dia (cm.)		
W-10Cu	UC	0.500	1.270	0.492	1.040	1.600	18.110
	C	0.360	1.270	0.356	1.080	1.11	14.960
W-25Cu	UC	0.430	1.270	0.422	1.080	1.860	14.960
	C	0.360	1.270	0.350	1.080	2.777	14.960
W-40Cu	UC	0.580	1.270	0.568	1.120	2.068	11.811
	C	0.410	1.270	0.390	1.120	4.878	11.811

*Activator used: Co; Initial Diameter of the Compact: 1.27 cm; Sintering Temperature: 1000°C.*

Composition	State*	Before Sintering		After Sintering		Axial	Radial
		Ht. (cm.)	Dia (cm.)	Ht (cm.)	Dia (cm.)	Shrinkage %	Shrinkage %
W-10Cu	UC	0.340	1.270	0.338	1.200	0.588	5.511
	C	0.740	1.270	0.669	1.220	9.594	3.937
W-25Cu	UC	0.440	1.270	0.420	1.260	4.545	0.787
	C	0.450	1.270	0.450	1.230	0	3.149
W-40Cu	UC	0.480	1.270	0.460	1.270	4.167	0
	C	0.400	1.270	0.390	1.240	2.500	2.362

*Activator used: Co; Initial Diameter of the Compact: 1.27 cm; Sintering Temperature: 1200°C.*

Composition	State*	Before Sintering		After Sintering		Axial	Radial
		Ht. (cm )	Dia (cm.)	Ht. (cm )	Dia (cm.)	Shrinkage %	Shrinkage %
W-10Cu	UC	0.390	1.270	0.364	1.160	6.667	8.661
	C	0.450	1.270	0.448	1.140	0.444	10.236
W-25Cu	UC	0.480	1.270	0.466	1.160	2.917	8.661
	C	0.510	1.270	0.500	1.140	1.961	10.236
W-40Cu	UC	0.410	1.270	0.378	1.180	7.805	7.087
	C	0.510	1.270	0.472	1.160	7.451	8.661

*Activator used: Co; Initial Diameter of the Compact: 1.27 cm; Sintering Temperature: 1400°C.*

Composition	State*	Before Sintering		After Sintering		Axial	Radial
		Ht. (cm.)	Dia (cm.)	Ht. (cm.)	Dia (cm.)	Shrinkage %	Shrinkage %
W-10Cu	UC	0.440	1.270	0.434	1.080	14.960	1.363
	C	0.510	1.270	0.500	1.100	13.385	1.960
W-25Cu	UC	0.400	1.270	0.400	1.060	16.534	0
	C	0.420	1.270	0.414	1.100	13.385	1.429
W-40Cu	UC	0.440	1.270	0.440	1.080	14.960	0
	C	0.410	1.270	0.400	1.080	14.960	2.439

*Activator used: Fe; Initial Diameter of the Compact: 1.27 cm; Sintering Temperature: 1000°C.*

Composition	State*	Before Sintering		After Sintering		Axial	Radial
		Ht. (cm.)	Dia (cm.)	Ht. (cm.)	Dia (cm.)	Shrinkage %	Shrinkage %
W-10Cu	UC	0.340	1.270	0.340	1.260	0	0.787
	C	0.740	1.270	0.670	1.250	9.459	1.154
W-25Cu	UC	0.440	1.270	0.421	1.251	4.318	1.496
	C	0.450	1.270	0.450	1.215	0	4.330
W-40Cu	UC	0.480	1.270	0.460	1.209	4.167	4.803
	C	0.400	1.270	0.390	1.217	2.500	4.173

*Activator used: Fe; Initial Diameter of the Compact: 1.27 cm; Sintering Temperature: 1200°C.*

Composition	State*	Before Sintering		After Sintering		Axial	Radial
		Ht (cm.)	Dia (cm.)	Ht (cm.)	Dia (cm.)	Shrinkage %	Shrinkage %
W-10Cu	UC	0.330	1.270	0.328	1.140	0.606	10.236
	C	0.230	1.270	0.226	1.666	1.739	8.189
W-25Cu	UC	0.320	1.270	0.310	1.150	3.125	9.449
	C	0.400	1.270	0.380	1.166	5.000	8.189
W-40Cu	UC	0.220	1.270	0.194	1.100	11.727	13.385
	C	0.310	1.270	0.274	1.118	11.613	11.969

*Activator used: Fe; Initial Diameter of the Compact: 1.27 cm; Sintering Temperature: 1400°C.*

Composition	State*	Before Sintering		After Sintering		Axial	Radial
		Ht. (cm.)	Dia (cm.)	Ht (cm.)	Dia (cm.)	Shrinkage %	Shrinkage %
W-10Cu	UC	0.370	1.270	0.350	1.180	5.405	7.086
	C	0.350	1.270	0.306	1.270	12.571	0
W-25Cu	UC	0.520	1.270	0.420	1.161	19.231	8.582
	C	0.330	1.270	0.270	1.162	18.181	8.504
W-40Cu	UC	0.440	1.270	0.372	1.110	15.454	12.598
	C	0.330	1.270	0.295	1.108	10.606	14.960

\* UC: uncoated; C: Cu-coated W



## Appendix IV

### Hardness values of the samples, HV<sub>5</sub>.

#### *No activator*

Composition	State*	Sintering Temperature					
		@1000°C		@1200°C		@1400°C	
		Average value	Standard deviation	Average value	Standard deviation	Average value	Standard deviation
W-10Cu	UC	85	0.34	94	0.77	104	0.63
	C	88	0.49	95	0.69	105	0.75
W-25Cu	UC	80	0.52	90	0.46	99	0.52
	C	82	0.21	92	0.23	100	0.65
W-40Cu	UC	74	0.89	89	0.48	97	0.78
	C	75	0.63	90	0.54	100	0.65

#### *Ni activator*

Composition	State*	Sintering Temperature					
		@1000°C		@1200°C		@1400°C	
		Average value	Standard deviation	Average value	Standard deviation	Average value	Standard deviation
W-10Cu	UC	100	0.12	130	0.65	169	0.23
	C	105	0.23	135	0.29	170	0.28
W-25Cu	UC	97	0.34	120	0.34	159	0.48
	C	98	0.49	125	0.26	160	0.56
W-40Cu	UC	96	0.66	114	0.64	147	0.65
	C	96	0.79	115	0.79	150	0.79

*Co activator*

Composition	State*	Sintering Temperature					
		@1000°C		@1200°C		@1400°C	
		Average value	Standard deviation	Average value	Standard deviation	Average value	Standard deviation
W-10Cu	UC	99	0.23	127	0.46	172	0.64
	C	100	0.85	130	0.22	180	0.72
W-25Cu	UC	94	0.69	124	0.13	155	0.64
	C	95	0.79	125	0.89	160	0.23
W-40Cu	UC	93	0.89	115	0.86	139	0.45
	C	93	0.64	120	0.65	140	0.48

*Fe activator*

Composition	State*	Sintering Temperature					
		@1000°C		@1200°C		@1400°C	
		Average value	Standard deviation	Average value	Standard deviation	Average value	Standard deviation
W-10Cu	UC	97	0.07	126	0.56	188	0.35
	C	104	0.65	140	0.26	190	0.39
W-25Cu	UC	99	0.29	126	0.46	175	0.44
	C	100	0.63	130	0.26	180	0.12
W-40Cu	UC	104	0.45	120	0.49	150	0.46
	C	106	0.79	122	0.23	155	0.46

\* UC: uncoated; C: Cu-coated W

## Appendix V

### Electrical conductivity of the sintered samples.

*Sintering temperature: 1000°C*

Composition	State*	Electrical Conductivity							
		No activator		Ni		Co		Fe	
		% I.A.C.S	m/ohm.mm <sup>2</sup>	% I.A.C.S	m/ohm.mm <sup>2</sup>	% I.A.C.S	m/ohm.mm <sup>2</sup>	% I.A.C.S	m/ohm.mm <sup>2</sup>
W-10Cu	UC	12.000	6.900	8.000	4.600	10.000	5.800	10.000	5.800
	C	14.000	8.100	9.000	5.200	12.000	6.900	11.000	6.380
W-25Cu	UC	16.000	9.300	17.000	9.800	18.000	10.400	17.000	9.860
	C	19.000	11.000	20.000	11.000	19.000	11.000	18.000	10.440
W-40Cu	UC	18.000	10.400	17.000	9.800	22.000	12.700	21.000	12.180
	C	23.000	13.300	22.000	12.700	24.000	13.900	24.000	13.920

*Sintering temperature: 1200°C*

Composition	State*	Electrical Conductivity							
		No activator		Ni		Co		Fe	
		% I.A.C.S	m/ohm.mm <sup>2</sup>	% I.A.C.S	m/ohm.mm <sup>2</sup>	% I.A.C.S	m/ohm.mm <sup>2</sup>	% I.A.C.S	m/ohm.mm <sup>2</sup>
W-10Cu	UC	12.000	6.960	14.000	8.120	15.000	8.700	15.000	8.700
	C	16.000	9.280	17.000	9.860	16.000	9.280	17.000	9.860
W-25Cu	UC	21.000	12.180	22.000	12.760	21.000	12.180	23.000	13.340
	C	22.000	12.760	25.000	14.500	23.000	13.340	25.000	14.500
W-40Cu	UC	35.000	20.300	36.000	20.880	39.000	22.620	41.000	23.780
	C	39.000	22.620	40.000	23.200	41.000	23.780	43.000	24.940

*Sintering temperature: 1400°C*

Composition	State*	Electrical Conductivity							
		No activator		Ni		Co		Fe	
		% I.A.C.S	m/ohm mm <sup>2</sup>	% I.A.C.S	m/ohm.mm <sup>2</sup>	% I.A.C.S	m/ohm.mm <sup>2</sup>	% I.A.C.S	m/ohm.mm <sup>2</sup>
W-10Cu	UC	14 000	8 120	20.000	11.060	24 000	13.920	25.000	14 500
	C	17.000	9.860	22 000	12 760	25.000	14 500	27 000	15.660
W-25Cu	UC	22 000	12.760	34.000	19 720	23 000	13 340	22 000	12.690
	C	23.000	13.340	30.000	17 400	23 000	13 340	23 000	13.120
W-40Cu	UC	42.000	24.360	43.000	24.940	40 000	23 200	40.000	23 200
	C	43.000	24.940	44.000	25 520	40 000	23.200	42 000	24 360

\* UC *uncoated*; C: *Cu-coated W*

## Appendix VI

### Thermal conductivity of the sintered samples.

*Sintering temperature: 1000°C*

Composition	State*	Thermal Conductivity (W/ m.°C)			
		No activator	Ni	Co	Fe
W-10Cu	UC	44.000	29.130	36.400	36.400
	C	51.480	33.270	44.000	44.000
W-25Cu	UC	58.390	62.000	65.500	65.500
	C	69.000	69.400	69.000	69.000
W-40Cu	UC	65.500	62.000	80.120	80.120
	C	83.760	80.120	87.400	87.400

*Sintering temperature: 1200°C*

Composition	State*	Thermal Conductivity (W/ m.°C)			
		No activator	Ni	Co	Fe
W-10Cu	UC	44.000	51.480	54.630	54.630
	C	58.390	62.000	58.390	58.390
W-25Cu	UC	76.480	80.120	76.480	76.480
	C	80.120	91.000	83.760	83.760
W-40Cu	UC	127.000	131.000	142.000	142.000
	C	142.000	145.670	149.000	149.000

*Sintering temperature: 1400°C*

Composition	State*	Thermal Conductivity (W/ m.°C)			
		No activator	Ni	Co	Fe
W-10Cu	UC	51.480	69.400	87 400	87 400
	C	62.000	80.120	91.000	91.000
W-25Cu	UC	80.120	124.000	83.760	83.760
	C	83.760	109.250	83.760	83 760
W-40Cu	UC	153.000	157 000	145.000	145.000
	C	157.000	160.000	145.000	145.000

\* UC: uncoated; C: Cu-coated W

A 143513



A143513